THE STRUCTURE AND OSCILLATION OF RAPIDLY ROTATING STARS

William Thorne
TRINITY COLLEGE
UNIVERSITY OF CAMBRIDGE

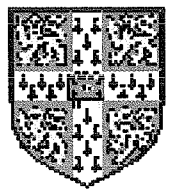

A DISSERTATION
SUBMITTED FOR THE DEGREE
OF DOCTOR OF PHILOSOPHY AT THE
UNIVERSITY OF CAMBRIDGE
2004

This dissertation is the result of my own work and includes nothing which is the outcome of work done in collaboration, except where mentioned.

8/12/04

Contents

Contents

THE STRUCTURE AND OSCILLATION OF RAPIDLY ROTATING STARS

Preface

This dissertation does not exceed 60,000 words in length.

Some of the work contained in this dissertation has been published, or is due to be published in refereed scientific journals or conference proceedings.

Material from chapter 2 is prepared for submission in:

Thorne, W. A. & Gough, D. O., 2005, MNRAS

Material from chapters 3, 4 and 7 is prepared for submission in:

Thorne, W. A. & Gough, D. O., 2005, MNRAS

A summary of material from chapters 2–5 has been published in:

Thorne, W. A., *Rotation: Distorted Co-Ordinate Systems and a Generalization of the Traditional Approximation* in *Helio- and Asteroseismology: Towards a Golden Future*, USA. Ed: D. Danesy

An overview of this work also has been published in:

The Observatory, **124**, 348, October 2004

Summary

The study of how rotation affects the pulsations of stars dates back many years. It has often been achieved by using a perturbative approach. This approach is often acceptable, as in the case of the Sun, because the Sun rotates slowly. Problems then arise when rotation is not "small" enough to be treated as a perturbation.

For considering rotation, there are two immediate scalings that define "small" – either scaling by the natural frequency of the star, or by scaling by the observed pulsational frequency. Quite large values of rotation scaled in the latter way have been dealt with in geophysics by use of the "Traditional Approximation" without conflicting with observed data. This approximation has recently been transferred over to Astronomy, in a direct way without explicit, thorough, testing.

In this thesis, the Traditional Approximation as defined in geophysics is extensively tested, and generalized to the oblate orthogonal co-ordinates that will form a natural basis for a star distorted by the centrifugal effects of rotation. The method of finding these co-ordinates, and further calculating their effect on the pulsations, is presented, and several examples are given.

By use of this method, we are able to define accurately the effects of rotation upon the structure and pulsations of a star, when the method is valid, *regardless of the ratio of the rotation rate to the pulsational frequency.* This has opened up a new realm of stars to our future study.

As a use of this method in fitting asteroseismic data, genetic algorithms, optimizers that have become increasingly popular in recent times, are also investigated, and methods of increasing their efficiency are discussed.

Acknowledgments

"...God....my mom....I have so many people that I know I need to thank...." - Halle Berry, 24 March 2002

It is only on coming to write and think about this section that I am less mocking of Oscar acceptance speeches. There are too many people to thank by name. Hopefully they know my gratitude, but I shall force myself to mention only four individuals. The first two are in the quotation; the third is Douglas, my supervisor. His patience and help are ineffable, and I hope I get close to communicating my thankfulness and respect by saying that even over a number of years the level of my respect for him has never reached a plateau. The fourth is Pascale for, in particular, one comment she made six months into my PhD.

In terms of groups, the members of the helioseismology group have been wonderful over the past few years for all their help and interesting discussions. There are a number of people who have kept me sane and on the right tracks and need to be mentioned: my family, the Winchester crowd, the O14 massive, Travs and leaders, my year group, the folk of First and Third and all my other friends.

Chapter 1

INTRODUCTION

"He also made the stars." – Genesis 1:16b

1.1 THE SUN AND OTHER STARS

From the dawn of time, mankind has wondered about the Sun and stars – as is evinced from ancient monuments such as Stonehenge to the plethora of references in the Biblical psalms, our fascination with these sources of light (although we now know them to be much more) is possibly matched only by the difficulty which we have classically encountered when trying to study them. The ancient concept of "as high as the heavens" to express vast distances remains with us, as can be seen in the use of the term "astronomical" in everyday life.

It is only relatively recently that the Sun has actually been viewed as a star, or, to invert the problem, that other stars are viewed as being like the Sun. The case of Galileo's suggestion that there might be better theoretical starting points than the model of the celestial spheres is well known.

The rotation of the Sun, or at least its surface, is probably the first well-measured solar parameter; returning to Galileo, his use of the newly invented telescope found sunspots, which rotated around the Sun about once every month, showing the rotation of the Sun and giving it a rough rotational period that would be further refined. By comparison, it was not until 1752 that Lacaille, using a transit of Venus, managed to obtain a reasonably

accurate measure of distance to the Sun, and hence its radius. Measuring the mass of the Sun was then possible with Newton's theory of gravitation and the determination of the gravitational constant G by Cavendish.

The identification of the source of energy for the light that man had so long enjoyed took even longer: it was realised that this amount of energy could not be produced by chemical reactions; so the onus fell upon gravitational energy to provide. Kelvin and Helmholtz calculated that the system could radiate for 10^7 years, and all seemed fine[1]. However Eddington realised, and stated, that the energy was generated by the nuclear burning of hydrogen into helium; this, to some extent, completed the foundations of the problem of solar and stellar modelling.

Eddington also acknowledged the previously referred to difficulty in studying the stars in yet another way - that of being certain of the makeup of the interior of stars. Beginning his work, *The internal constitution of the stars* (1926), he famously writes: *At first sight it would seem that the deep interior of the sun and stars is less accessible to scientific investigation than any other region of the universe. Our telescopes may probe farther and farther into the depths of space; but how can we ever obtain certain knowledge of that which is hidden behind substantial barriers? What appliance can piece through the outer layers of a star and test the conditions within?*

He would then go on to show a way of modelling that would not actively "probe", suggesting that we learn "*by awaiting and interpreting the messages dispatched to us by the objects of nature*" which we still do, but in a more direct route than he foresaw. We now have the joy of knowing of such an appliance that Eddington wondered whether would exist: the tool of asteroseis-

[1] Although it is interesting to note that evolutionary theories had no problem in fitting into this time scale; the phrase "real bronx cheer" was not invented by this stage.

mology.

1.2 HELIO- AND ASTEROSEISMOLOGY

In 1960, a study of the Doppler shift of the spectral line of Ba II showed oscillatory motion, with a dominant period of about five minutes. The frequency spectrum was found to be discrete, and is was concluded that the oscillations are waves trapped in the resonant cavity of the Sun. It was soon realised that these oscillations, and in particular their frequencies, could tell us about the interior of the Sun. Traditionally in helio- and asteroseismology, the frequencies measured are those of normal modes, viewed as standing waves. This is different to the use of seismology as usually practised by geophysicists, where usually individual waves are traced back to a single exciting event, as the excitation of stellar waves is not caused by an event at a fixed point in space and time, but rather by a type of event, such as stochastic excitation by the convection, which occurs continually throughout the outer layers of the star.

1.2.1 A BRIEF PRIMER ON SEISMOLOGY

Before we proceed to study perturbations, we must look at the equations that govern the structure of the star (in this case the Sun). These fall into five categories:

1. The equation of hydrostatic support:

$$\nabla p = -\rho \nabla \Phi + \boldsymbol{F} , \tag{1.1}$$

where p, ρ and Φ are the hydrostatic pressure, density and gravitational potential respectively, and $\boldsymbol{F}$ represents non-gravitational body forces. This equation comes from the

momentum equation, with time derivatives set to zero (although these time derivatives will re-appear when this equation is perturbed later).

2. Poisson's equation:

$$\nabla^2\Phi = 4\pi G\rho \,, \tag{1.2}$$

with G the gravitational constant.

3. An equation of energy transport, whose r component (in spherical polar co-ordinates) is

$$\frac{L}{4\pi r^2} = F_{\rm rad} + F_{\rm conv} \,, \tag{1.3}$$

in which L is the luminosity, and $F_{\rm rad}$ and $F_{\rm conv}$ are the radiative and convective fluxes respectively, given by equations such as

$$F_{\rm rad} = \frac{-4\sigma T^3}{3\kappa\rho}\frac{{\rm d}T}{{\rm d}r} \,, \tag{1.4}$$

$$F_{\rm conv} = \rho c_p \left(\frac{Gm}{Tr^2}\right)^{1/2} (\Delta\nabla T)^{3/2} \lambda_{\rm ml}^2 \,, \tag{1.5}$$

with σ, T, κ, c_p, m, $\Delta\nabla T$, $\lambda_{\rm ml}$ are the Stefan-Boltzmann constant, temperature, Rosseland mean opacity, heat capacity at constant pressure, interior mass, superadiabatic temperature gradient, and the mixing-length parameter, respectively. The opacity is obtained from quantum effects, and is a large study in its own right, with stellar theorists often using tabulated values, such as those provided by the OPAL project. Examples of opacity formulae include

$$\kappa = \kappa_0 \rho T^{-3.5} \tag{1.6}$$

for Kramer's opacity (when the opacity is dominated by bound-free and free-free absorption), and $\kappa = \kappa_e$ for when opacity is dominated by electron scattering.

4. Energy generation, again in spherical polar co-ordinates:

$$\frac{\partial L}{\partial r} = 4\pi r^2 \rho \left(\epsilon - T \frac{\partial s}{\partial t} \right) , \tag{1.7}$$

where s is the specific entropy, and ϵ is the nuclear energy generation rate per unit mass, which is a function of the thermodynamic state and of the chemical composition:

$$\epsilon = \epsilon(\rho, T, X, Y, Z, ...) , \tag{1.8}$$

and is obtained from nuclear physics. X, Y, and Z are the abundances per unit mass of hydrogen, helium and metals (other elements) respectively.

5. An equation of state:

$$p = p(\rho, T, X, Y, Z, ...) . \tag{1.9}$$

In helioseismology, the measurements and their interpretations are so refined that one must take into account a number of physical factors such as relativistic effects, non-ideality of the gas (e.g., the effects of electron screening), turbulent motions and the ionization of elements.

There are also equations to follow the chemical evolution of a star, such as

$$\frac{\partial X_i}{\partial t} = \frac{m_i}{\rho}\left\{\sum_j r_{ji} - \sum_k r_{ik}\right\} + \text{mixing}\,, \tag{1.10}$$

where X_i denotes the abundance by mass of an element, m_i is the mass of element i, and r_{ij} denotes the reaction rate for the conversion of element i into element j, and t is the time. Mixing can be by diffusion or advection, the magnitude of which individually will strongly vary depending on the region of the star.

There are huge areas of ongoing research attached to the last three of these structure equations (energy transport, energy generation and the equation of state) and to the reaction rate calculations; for instance refining opacities and convective theories for the equation of energy transport, cross-section calculations to refine the formulae for the nuclear energy generation rate, and understanding some of the factors already listed for the equation of state. Many of these factors will only be touched upon here. For mathematical ease, a number of simplifications of the equation of state exist, in which the pressure is viewed as a function of density only. These are called *barotropic* equations of state, and will be adopted extensively in this work as they retain much of the physics whilst reducing the complexity.

Once we have a solution to these equations (i.e. a solar/stellar model), we can investigate its normal modes, which we do by perturbing the model, assuming our perturbations to be proportional to $e^{\Upsilon t}$ for some Υ. It is important to note when we consider this perturbation that hydrostatic equilibrium is instanteously satisfied inside the star, whilst a wave propagates over a dynamical timescale (of the order of an hour for the Sun); this satisfying of hydrostatics gives us $\Re(\Upsilon) = 0$, so our perturbations are proportional to $e^{-\mathrm{i}\omega t}$ for some real ω. Also the fact that we observe the Sun to be stable over this dynamical timescale encourages

us to view the perturbation as small enough to justify neglect of second-order terms in the perturbation. For an overview of seismology, see Gough (1993).

We shall first look at the case of no rotation; define $\boldsymbol{\xi}$ to be the displacement of a fluid element. Because we are ignoring quadratic terms and have no rotation, the velocity, $\boldsymbol{u}$, is given by

$$\boldsymbol{u} = \frac{D\boldsymbol{\xi}}{Dt} \approx \frac{\partial \boldsymbol{\xi}}{\partial t} = -\mathrm{i}\omega\boldsymbol{\xi} \; ; \tag{1.11}$$

for the other perturbations (such as to the density ρ and the pressure p), we shall denote Eulerian perturbations by primes, and Lagrangian perturbations by using a δ, so $\delta p = p' + \boldsymbol{\xi} \cdot \nabla p$, and similarly for other variables. Thus perturbing about our equilibrium state gives

$$-\omega^2 \rho \boldsymbol{\xi} = -\nabla p' - \rho' \nabla \Phi - \rho \nabla \Phi' \; , \tag{1.12}$$

$$\nabla^2 \Phi' = 4\pi G \rho' \; , \tag{1.13}$$

$$\rho' + \nabla.(\rho \boldsymbol{\xi}) = 0 \; , \tag{1.14}$$

$$\rho T \frac{Ds'}{Dt} = \rho \epsilon' - \nabla.\mathbf{F}' \; , \tag{1.15}$$

in which p, ρ, T and Φ now represent the unperturbed values associated with the equilibrium state. If we neglect heating, looking for *adiabatic* pulsations, we can greatly simplify the last of these equations, arriving at

$$\frac{\delta p}{p} = \gamma_1 \frac{\delta \rho}{\rho} \; , \tag{1.16}$$

$$\Leftrightarrow \frac{p'}{p} = \gamma_1 \left(\frac{\rho'}{\rho} + A\xi_r \right) \; , \tag{1.17}$$

where we have introduced an adiabatic exponent

$$\gamma_1 \equiv \left(\frac{\partial \ln p}{\partial \ln \rho}\right)_{\rm ad} \; ; \tag{1.18}$$

and ξ_r denotes the r component of $\boldsymbol{\xi}$ with respect to spherical polar coordinates. Equations (1.12), (1.13), (1.14) and (1.16) close the system, and we can solve for the perturbation. However, it will be useful to note some simplifications of the system:

1. We note that there is no coupling between the horizontal and vertical components of any of the equations that close the system. Hence we can look for separable solutions $f = f_{\rm v}(r) f_{\rm h}(\theta, \phi)$. Looking at equation (1.13), it is apparent that the sensible choice for the basis of horizontal functions $f_{\rm h}(\theta, \phi)$ is a set of eigenfunctions of the horizontal Laplace operator

$$\nabla_{\rm h}^2 f_{\rm h} = -\frac{L^2}{r^2} f_{\rm h} \; , \tag{1.19}$$

for some eigenvalue L^2. Further expanding this equation, we see that we can write

$$f_{\rm h}(\theta, \phi) = (-1)^m c_{lm} P_l^m(\cos\theta) e^{{\rm i}m\phi} \equiv Y_l^m \; , \tag{1.20}$$

where P_l^m is the associated Legendre function of the first kind, Y_l^m is a spherical harmonic, and c_{lm} is a normalization constant chosen such that

$$\begin{aligned} &\int_0^{\pi} \int_0^{2\pi} Y_{l'}^{m'*}(\cos\theta, \phi) Y_l^m(\cos\theta, \phi) \sin\theta {\rm d}\phi {\rm d}\theta \\ &\equiv \int_{-1}^{1} \int_0^{2\pi} Y_{l'}^{m'*}(\mu, \phi) Y_l^m(\mu, \phi) {\rm d}\phi {\rm d}\mu = \delta_{l\ l'} \delta_{m\ m'} \; , \end{aligned} \tag{1.21}$$

where we have used the notation (that will be assumed from now on) that $\mu = \cos\theta$ and that complex conjugates are denoted by an asterisk.

Y_l^m is characterized by the *degree*, l, and azimuthal order, m, both of which are integers; from the properties of spherical harmonics, we also know that

$$L^2 = l(l+1) \,, \tag{1.22}$$

and

$$|m| \leq l \,, \tag{1.23}$$

2. It is often possible to neglect the perturbation to the gravitational potential, Φ'; this is known as the Cowling Approximation. This has been well discussed in the literature (e.g. Christensen-Dalsgaard, 2003) and gives results in good agreement with the results for the full problem when either l is large, or the radial order, n, of the mode is large.

1.2.1.1 THE FIRST-ORDER EFFECTS OF ROTATION

If we now assume that the stellar system is rotating (and that rotation is the only zero-order velocity to consider) with an angular velocity, $\boldsymbol{\Omega}(r,\mu)$, which depends only on radius and latitude, obeying $\boldsymbol{\Omega}(r,\mu) = \Omega(r,\mu)\mathbf{e}_z$, then in the perturbed momentum equation the velocity we had denoted by $\boldsymbol{u}$ is replaced by $\boldsymbol{v} = \boldsymbol{u} + \boldsymbol{\Omega} \times \boldsymbol{r}$ (to save on confusion), and the displacement $\boldsymbol{\xi}$ must be determined relative to the moving equilibrium fluid:

$$\delta\boldsymbol{v} = \frac{D\boldsymbol{\xi}}{Dt} = \frac{\partial\boldsymbol{\xi}}{\partial t} + (\boldsymbol{v}\cdot\nabla)\boldsymbol{\xi} \tag{1.24}$$

$$= \frac{\partial \boldsymbol{\xi}}{\partial t} + \mathrm{i}m\Omega\boldsymbol{\xi} + \boldsymbol{\Omega} \times \boldsymbol{\xi} \ . \qquad (1.25)$$

Shifting to a co-ordinate frame rotating with uniform angular velocity Ω, our frequencies will change to $\tilde{\omega} = \omega - m\Omega$; this causes equation (1.12) to be modified to, to first order in Ω,[2]

$$-\tilde{\omega}^2\rho\boldsymbol{\xi} + 2\mathrm{i}\tilde{\omega}\rho[(\boldsymbol{\Omega} \times \boldsymbol{r}) \cdot \nabla]\boldsymbol{\xi} \ = -\nabla p' - \rho'\nabla\Phi - \rho\nabla\Phi' \ . \quad (1.26)$$

From this point onwards, we shall drop tildes in our equations, replacing $\tilde{\omega}$ by ω.

If Ω were small, then had we viewed our perturbation equation that described the spectrum of possible oscillations as

$$\omega^2\boldsymbol{\xi} \ = \mathcal{L}\boldsymbol{\xi} \ , \qquad (1.27)$$

rotation would have changed the operator $\mathcal{L}$ to $\mathcal{L} + \Delta\mathcal{L}$, with

$$\Delta\mathcal{L}(\boldsymbol{\xi}) \ = -2\mathrm{i}\omega\rho[(\boldsymbol{\Omega} \times \boldsymbol{r}) \cdot \nabla]\boldsymbol{\xi} \ , \qquad (1.28)$$

which would cause a frequency shift of (using the fact that the normal modes of pulsation form a complete set (Dyson & Schutz, 1979), $\mathcal{V}$ is the volume of the star)[3]:

$$\Delta\omega_{nlm} \ = -\mathrm{i}\frac{\int_{\mathcal{V}} 2\rho\boldsymbol{\xi}^* \cdot ([(\boldsymbol{\Omega} \times \boldsymbol{r}) \cdot \nabla]\boldsymbol{\xi})\,\mathrm{d}\mathcal{V}}{\int_{\mathcal{V}} \boldsymbol{\xi}^* \cdot \boldsymbol{\xi}\mathrm{d}\mathcal{V}} \ . \qquad (1.29)$$

We can also write this equation for the frequency splitting $\Delta\omega_{nlm}$ as

[2]Assuming $\boldsymbol{\Omega}$ is uniform and $\Omega = |\boldsymbol{\Omega}|$.

[3]The subscripts n, l and m classify the mode, with n being the radial order, and l and m classifying the spherical harmonic part of the mode.

$$\Delta\omega_{nlm} = \int_0^{r_*} \int_{-1}^{1} K_{nlm}(r,\mu)\Omega(r,\mu) r \mathrm{d}\mu \mathrm{d}r \ . \tag{1.30}$$

This method of getting a frequency shift from viewing the introduced rotation as a small change in the differential operator is an example of using a variational principle, which will be expanded upon later.

In equation (1.30), K_{nlm} is called a *kernel*, and the subject is well studied in helioseismology (e.g. Christensen-Dalsgaard, 2003); it is the case that $\Delta\omega_{nlm}$ is what is measured, whereas $\Omega(r,\mu)$ is what we desire to know. Returning to equation (1.29), we see that an individual $\Delta\omega_{nlm}$ will only be sensitive to the rotation in places where the accompanying $\boldsymbol{\xi}$ is appreciably non-zero. The region of points where $\boldsymbol{\xi}$ is appreciably non-zero (i.e. where it behaves in an oscillatory manner, rather than an exponentially decaying one) is known as the *region of propagation*, and the bounding points known as *upper* and *lower turning points*.

Because different $\Delta\omega_{nlm}$ are sensitive to different regions, we can use the differing shifts experienced to build up a map of the rotation inside the star. This method of building up a map of the interior properties (in this case rotation) is known as *inversion*; similar methods exist to calculate sound speeds and such like.

1.2.2 ASTEROSEISMOLOGY

It is not the case that the Sun is the only star to be seen to pulsate: in locations all over the H-R diagram, as shown in figure 1.1, we find pulsating stars. These range from white dwarfs to Mira variables, showing different types of pulsation, such as p modes (where the restoring force is pressure - comparable to acoustic waves in the air) and g modes (where the restoring force is gravity, via buoyancy). The Sun is a low-amplitude p-mode

pulsator, stochastically excited by its convection, whereas other stars, such as γ-Doradus stars, are g-mode pulsators. Likewise, the method of excitation also differs between types of pulsating star. We have reached an exciting time for asteroseismology (Gough, 1996), with space missions such as COROT, and MOST, and with current observations being able to detect, and exploit, solar-like oscillations in nearby stars (for example, Baglin et al. (2001) for COROT and Rucinski et al. (2003) for MOST). Inversion methods based on, for example, equation (1.30) can thus be used, but we must acknowledge that, as would be expected, there is no one method that will work for every star and its pulsations.

1.2.2.1 Observations & Their Restrictions

Inversion methods are very refined for *helio*seismology, and in the Sun we have immense spatial and temporal resolution. For instance, we can look at high-l p modes, and do inversions on them. This simply is not possible in other stars: we must use whole-disc integrated measurements.

It is the case that we shall need to work with modes of very low degree, l, or their equivalents. These are some of the most penetrating modes, and tell us things about the deep structure of stars. These modes do not give us as much information as having a raft of solar-like oscillations, but they are still very useful.

1.2.2.2 When does the perturbation method break down?

Whilst this method provides a simple way of determining the alteration of various modes by mild rotation, it is limited to just that: *mild* rotation. We have pulsating stars in locations all over the H-R diagram (see figure 1.1), many of which have much faster rotation, both in absolute terms and also, as will be defined shortly by the parameter ν, relative to its pulsational frequency, ω. Whilst the variational principle will give *an* answer, we desire

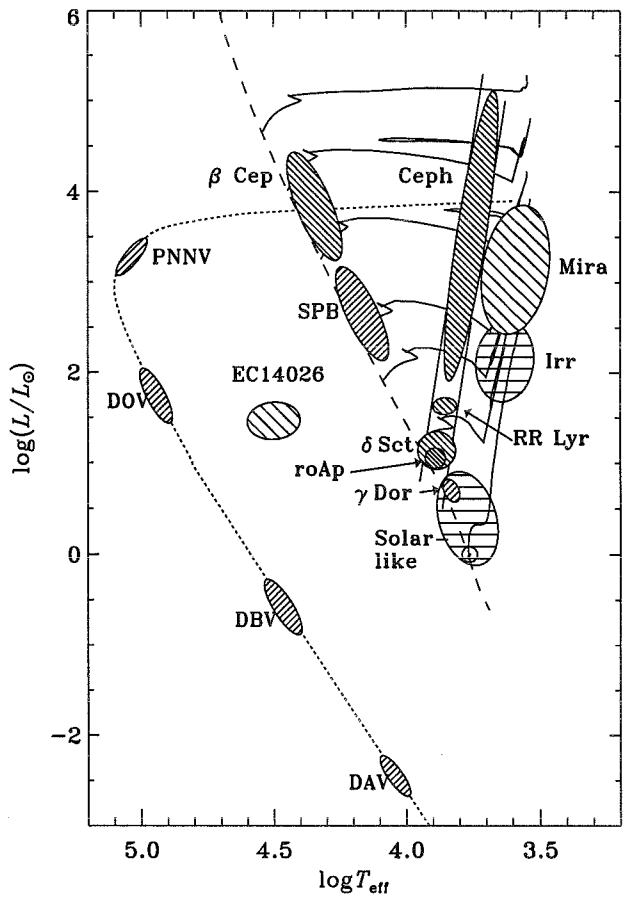

Figure 1.1: A schematic Hertzsprung-Russell diagram, showing the regions occupied by pulsating stars. Also shown are the zero-age main sequence (ZAMS), evolution tracks for 1, 2, 3, 4, 7, 12, and 20 $M_\odot$ stars, the horizontal giant branch and the white-dwarf cooling track. Figure first produced by Jørgen Christensen-Dalsgaard.

to obtain very accurate frequencies because of the high precision data that will shortly be available. For example the quoted accuracy (see Baglin et al., 2001) of the upcoming space mission COROT is given as 0.6μHz for a 9th magnitude star observed for 20 days, a magnitude and observation length picked as typical for the mission.

Rotation affects a star in two main ways: The first is by Coriolis force, which comes in at order Ω; the second is centrifugal effects, for instance by distortion of the background state of the star, which comes in at order Ω^2. Whilst the mean rotation of the Sun is roughly 28 days, which allows effective neglection of centrifugal force, an average γ-Doradus star (γ-Doradus stars are another class of pulsating stars, which will be discussed in detail later) has a mean rotation period of the order of approximately 3 days, causing centrifugal effects to be of the order of a hundred times larger than the Sun, and may hence possibly be non-negligible.

The distortion of the background state away from spherical symmetry also suggests viewing the problem of modes in ellipsoidal co-ordinates; Lignières et al. (2001) looked briefly at acoustic modes in ellipsoidal co-ordinates, taking into account the chaos of ray dynamics and such factors, and found that this distortion from sphericity would lead to alterations above the quoted accuracy of, for example, the upcoming asteroseismological mission COROT mentioned above. Thus this change of basis is a factor to take into consideration.

One important thing to note is that the different methods given always[4] involve truncating expansions in the rotation rate,

[4]This is not the case for extensive numerical modelling of individual pulsations of an individual stellar model, as done by Dintrans and Rieutord (2000); however, this can become extremely computationally intensive (although it holds many possibilities for the future, as mentioned in chapter 9). We shall focus on (at least partially) perturbative theory.

but we can find different expansion parameters which can be more sensible in certain cases.

1.3 OUTLINE

As has been mentioned, pulsating stars are located all over the H-R diagram, with different values of radius, R, mass, M, luminosity, L, effective temperature, $T_{\rm eff}$, composition, $\boldsymbol{X}$, angular velocity, Ω, and pulsational frequency, ω, amongst others. In fact, one could be excused for thinking just about the only consistent feature in the modelling of these stars is the constant of gravitation, G !

If we look at the list above, it is apparent that three dimensionless parameters including rotation are possible[5]:

$$\nu = \frac{2\Omega}{\omega} , \tag{1.31}$$

$$f = \frac{\Omega}{\sqrt{GM/R^3}} , \tag{1.32}$$

$$d = \frac{L}{MR^3\Omega^3} . \tag{1.33}$$

We shall not include d in our analysis, but it is listed here for completeness; the remaining two parameters show us that we can define "large" rotation rates in at least two ways – by large ν or large f. The ν scaling takes account of the direct effect of the Coriolis force on the dynamics of the oscillations, whereas the f scaling takes account of the geometrical distortion of the star. These scalings define a multi-dimensional parameter space within which we *must* work.

[5]The factor of two in (1.31) is not strictly needed, but will prove to be useful later.

1.3 Outline

This thesis will present a method of dealing with these two scalings separately, which does not obviously break down for large ν (unlike the normal perturbative method), via the Traditional Approximation, from geophysics. The approximation will be analysed, tested and generalized in order to model stars previously inaccessible to detailed investigation. The thesis is laid out in the following way:

- Chapter 2 introduces and discusses the approximation to be used, as well as investigating its realm of validity.
- Chapter 3 introduces the equations for a natural basis for a rotating star which retains orthogonality. This is done for barotropic equations of state.
- Chapter 4 looks at the theory concerning the alteration that this basis causes to pulsational eigenfrequencies, eigenfunctions, and mode trapping.
- Chapter 5 presents results from chapters 3 and 4.
- Chapter 6 discusses a rapid way of finding fits to observed pulsational data, via genetic algorithms.
- Chapter 7 generalizes the theories and methods of chapters 3 and 4 to non-barotropic equations of state.
- Chapter 8 presents results of this generalization, with a particular view to γ-Doradus stars.
- Chapter 9 summarises, and discusses future work on this subject.

1.4 γ-DORADUS STARS

One class of star that will be discussed later is that of γ-Doradus stars. Stars of this class have only recently (of the order of ten to fifteen years ago) been classified as a separate type of pulsating star. They are low-frequency (see accompanying table) pulsators (believed to be high-radial-order g-mode pulsators) of moderate (compared with similar stars in the same region of the H-R diagram) raw rotation rate, with masses of the order of $1.5M_{\odot}$. Unsurprisingly, they are found just above the Sun in the H-R diagram on the main sequence. Although they lie in a region overlapping that where δ-Scuti stars are found, only one star (HD 209295) has been found to pulsate with both δ-Scuti (low-radial-order p-mode) and γ-Doradus (as already mentioned, high-radial-order g-mode) pulsations. This star is a member of a close binary system, and is thought to be anomolous, whilst many other candidates (e.g. see Handler and Shobbrook, astro-ph/0202152) have been closely examined without finding any sign of both types of pulsations (indeed, the authors were able to put quite tight upper bounds to the magnitudes of any undetected pulsations). A table of some γ-Doradus stars is displayed below, including the parameter ν which, as we have seen, will become relevant later when considering how to model the pulsations and predict model pulsation frequencies.

1.4 γ-Doradus stars

Star	$v \sin i$ ($/\mathrm{kms}^{-1}$)	$\frac{R_*}{R_\odot}$	$\Omega \sin i$ ($/\mathrm{day}^{-1}$)	$\omega(/\mathrm{day}^{-1})$	$\nu \sin i$
Sun	-	1	$\approx 1/30$	$O(288)$	2e-4
γ Dor	62	1.47	-	1.3210	1.2616
				1.3635	1.2223
9 Aur	20	1.64	-	0.795	0.6062
				0.345	1.3968
HD 277	38	1.44	0.5214	1.111	0.9386
				1.081	0.9465
				1.387	0.7518
HD 62454	11.5	1.64	-	1.6014	0.1730
				1.4368	0.1929
				1.7367	0.1596
				1.8337	0.1511
				1.8075	0.1533
HD 68192	85.5	2.14	-	1.3002	1.2142
				1.202	1.3134
HD 105458	40	1.55	0.5099	1.321	0.7719
				0.946	1.078
				1.251	0.8152
				1.409	0.7238
				1.552	0.6571
				1.091	0.9347
HD 108100	68	1.40	-	1.4045	1.3665
				1.3210	1.4529
HD 155154	180	1.49	2.3868	2.898	1.6472
				3.098	1.5409
				3.200	1.4918
				3.069	1.5554

Star	$v \sin i$	$\frac{R_*}{R_\odot}$	$\Omega \sin i$ (/day^{-1})	ω(/day $^{-1}$)	$\nu \sin i$
HD 160314	59	1.85	0.6301	1.208 1.184	1.0432 1.0644
HD 164615	60	1.66	-	1.2321	1.1592
HD 206043	140	1.57	1.7618	2.432 2.360 2.524 2.599 2.266 2.461	1.4488 1.4931 1.3558 1.3558 1.5550 1.4318
HD 207223	9.1	1.76	-	0.3855	0.5300
HD 218396	37.5	1.74	-	1.9791 1.7268 1.6498	0.4303 0.4931 0.5162
HD 224638	24	1.87	-	0.6848 0.8115	0.7406 0.6249
HD 224945	55	1.82	-	0.6692 0.9330	1.7844 1.2799

Chapter 2

The Traditional Approximation

"Each problem that I solved became a rule which served afterwards to solve other problems." – Descartes, Discours de la Méthode, 1637.

2.1 Introduction

Once we have seen from equations (1.31) and (1.32) that the Coriolis and centrifugal forces are characterized by different dimensionless parameters, which often differ in magnitude, we must think how to deal with them. One option is to proceed with a perturbative method, expanding to higher and higher order, which may, or may not, increase the realm of validity, but must itself break down eventually. Another method is to switch entirely to numerical simulation; this would, if there were adequate resolution, solve the problem completely, but can be prohibitive in terms of computational resources, especially if a many-parameter survey is sought for fitting stellar data.

Another way to proceed is to simplify the mathematical system, by approximating the equations in a manner that casts them into a more tractable form. One such approximation is what is known in geophysics as the "Traditional Approximation", which we shall call the TA. In essence, it neglects the contribution of $\Omega_{\rm h}$, the horizontal component of the angular velocity, to the Coriolis force.

This approximation has been used for some time in geophysics to good effect, and has also been used recently in astronomy: for example, to analyse the angular behaviour of eigenfunctions (Lee and Saio, 1997); to investigate the surface trapping and leakage of g modes (Townsend, 2000); and to expand asymptotically[1] the angular oscillation equations for very large values of the parameter ν (Townsend, 2003b).

As with all approximations, there are circumstances in which the TA is not valid and should not be used. It is therefore important to determine under what conditions the TA can be used. In this chapter, the TA shall be presented, examined, and its realm of validity explored. One method of doing this will be by solving the "exact" problem (by formal expansion) in the range of small ν in which it is valid.

2.2 Formulation of the System

Returning to equations (1.12), (1.14), and (1.16), under the Cowling approximation, and assuming a spherical background state, we have:

$$-\omega^2\xi_r + 2\mathrm{i}\omega\Omega\sin\theta\ \xi_\phi = \frac{-1}{\rho}\frac{\partial p'}{\partial r} - g\frac{\rho'}{\rho}\ , \qquad (2.1)$$

$$-\omega^2\xi_\theta - 2\mathrm{i}\omega\Omega\cos\theta\ \xi_\phi = \frac{-1}{\rho r}\frac{\partial p'}{\partial \theta}\ , \qquad (2.2)$$

$$-\omega^2\xi_\phi + 2\mathrm{i}\omega\Omega\cos\theta\ \xi_\theta - 2\mathrm{i}\omega\Omega\sin\theta\ \xi_r = \frac{-1}{\rho r\sin\theta}\frac{\partial p'}{\partial \phi}\ , \qquad (2.3)$$

$$\rho' + \frac{1}{r^2}\frac{\partial}{\partial r}(r^2\rho\xi_r) + \frac{\rho}{r\sin\theta}\frac{\partial}{\partial\theta}(\sin\theta\xi_\theta) + \frac{\rho}{r\sin\theta}\frac{\partial}{\partial\phi}(\xi_\phi) = 0\ , \qquad (2.4)$$

[1] Due to the parameter ranges focused upon in this thesis, we shall not use these asymptotic expansions.

$$\frac{p'}{p} = \gamma_1 \left(\frac{\rho'}{\rho} + A\xi_r \right) \quad (2.5)$$

2.2.1 THE TRADITIONAL APPROXIMATION

Under this approximation, we neglect terms containing $\Omega \sin\theta$. This removes the direct rotational coupling between the radial and horizontal parts of the momentum equation, leaving the sole coupling via the pressure gradient and buoyancy, as in the corresponding non-rotating system.

Once this is done, it can be seen from the interplay between the altered versions of (2.1), (2.4) and (2.5) that the equations will now admit separable solutions of the form:

$$f(r,\theta,\phi) = f(r)\Theta(\mu,\nu)\, e^{\mathrm{i}m\phi} , \quad (2.6)$$

where we have used the parameter ν given in equation (1.31), and f represents ξ_r, ρ' or p'.

To see and derive this separability, we re-arrange equations (2.2) and (2.3) in terms of p'/ρ and its angular derivatives[2]:

$$\xi_\theta = \frac{-1}{\omega^2 r} \frac{\sqrt{1-\mu^2}}{1-\nu^2\mu^2} \left(\frac{\partial}{\partial\mu} - \frac{\mathrm{i}\nu\mu}{1-\mu^2} \frac{\partial}{\partial\phi} \right) \frac{p'}{\rho} , \quad (2.7)$$

$$\xi_\phi = \frac{1}{\omega^2 r} \frac{\sqrt{1-\mu^2}}{1-\nu^2\mu^2} \left(\mathrm{i}\nu\mu \frac{\partial}{\partial\mu} + \frac{1}{1-\mu^2} \frac{\partial}{\partial\phi} \right) \frac{p'}{\rho} . \quad (2.8)$$

Substituting these expressions for ξ_θ and ξ_ϕ into equation (2.4) gives:

$$\rho'\Theta + \frac{1}{r^2} \frac{\mathrm{d}}{\mathrm{d}r}(r^2\rho\xi_r)\Theta + \frac{p'(r)}{\omega^2 r^2} \mathcal{L}_\nu[\Theta] = 0 , \quad (2.9)$$

[2]Note that this re-arrangement has assumed that ρ has no angular derivatives, a fact that will become important when we seek to generalize the TA.

where

$$\mathcal{L}_\nu[\Theta(\mu;\nu)] \equiv \frac{\mathrm{d}}{\mathrm{d}\mu}\left(\frac{1-\mu^2}{1-\nu^2\mu^2}\frac{\mathrm{d}\Theta}{\mathrm{d}\mu}\right) + \frac{1}{1-\nu^2\mu^2}\left(m\nu\frac{1+\nu^2\mu^2}{1-\nu^2\mu^2} - \frac{m^2}{1-\mu^2}\right)\Theta \ . \tag{2.10}$$

From this equation, it is easy to see that the requirement for separability is that

$$\mathcal{L}_\nu[\Theta(\mu;\nu)] = -L^2\Theta(\mu;\nu) \ , \tag{2.11}$$

where L^2 is a constant (but depends on ν)[3]. Equation (2.11) is Laplace's Tidal Equation (which reduces to the associated Legendre equation when $\nu = 0$); its solutions are Hough functions. The solutions are determined by requiring regularity of the solution at the singular points $\mu = \pm 1$. From the symmetry of the equation, we can see that the solutions are alternately (ordering according to $L^2(\nu)$) even and odd functions of μ.

The solutions to this equation have been extensively discussed (by Lee and Saio, 1997, already mentioned); however, owing to possible concerns about regularity at interior mesh points, it is preferred to use the coupled first-order equations of Townsend (2003b):

$$\frac{d}{d\mu}\Theta = \frac{1}{1-\mu^2}\left[(\nu^2\mu^2-1)\hat{\Theta} + m\nu\mu\Theta\right] \ , \tag{2.12}$$

$$\frac{d}{d\mu}\hat{\Theta} = \frac{1}{1-\mu^2}\left[\left(L^2(1-\mu^2)-m^2\right)\Theta - m\nu\mu\hat{\Theta}\right] \ , \tag{2.13}$$

with

[3]This constant is often denoted by λ_{km}, but we use L^2 here to emphasize that it is the analogue of the constant $L^2 = l(l+1)$ in a non-rotating star.

$$\hat{\Theta} \equiv \frac{1}{1-\mu^2\nu^2}\left(-(1-\mu^2)\frac{d}{d\mu} + m\nu\mu\right)\Theta \ . \tag{2.14}$$

Whilst it is possible to enforce regularity using Lee & Saio's formulation by placing mesh points at $\mu = \nu^{-1}$ (with due care), we wish to search for ν as a coupled eigenvalue, rather than prescribe it, as they did. The formulation given here avoids this problem.

Returning to the equations for the radial part of the eigenfunction, we see that they can be written in one of the two following forms:

$$\frac{1}{r^2}\frac{\mathrm{d}}{\mathrm{d}r}\left(r^2\xi_r\right) - \frac{g}{c^2}\xi_r + \left(1 - \frac{L^2c^2}{\omega^2r^2}\right)\frac{p'}{c^2} = 0 \ , \tag{2.15}$$

$$\frac{\mathrm{d}p'}{\mathrm{d}r} + \frac{g}{c^2}p' + (N^2-\omega^2)\rho\xi_r = 0 \ , \tag{2.16}$$

or[4]:

$$r\frac{dz_1}{dr} = \left(\frac{V_\mathrm{h}}{\gamma_1} - 3\right)z_1 + \left(\frac{L^2}{c_1\bar{\omega}^2} - \frac{V_\mathrm{h}}{\gamma_1}\right)z_2 \ , \tag{2.17}$$

$$r\frac{dz_2}{dr} = (c_1\bar{\omega}^2 - rA)z_1 + (1-U-rA)z_2 \ . \tag{2.18}$$

The first form shows the physics of the pulsations, whereas the second form is easier for numerical evaluation. It should also be noted that these equations are identical to those given by an analysis for a non-rotating star, with the only alteration that L^2 is no longer a constant integer value, by instead is dependent upon the rotation.

The boundary conditions adopted here are those of ensuring

[4] $z_1 = \xi_r(r)/r$, $z_2 = p'(r)/gr\rho$; for the rest of the definitions, the reader is directed to appendix A.

regularity of the displacement as we approach the origin, and of having a vanishing fractional Lagrangian pressure perturbation at the surface.

These equations (equations (2.17) and (2.18)) can then be represented by finite difference equations, which are then solved by relaxation. Second-order accuracy centred differences were used to represent derivatives, and the differential equations were represented midway between the mesh points. The boundary condition of regularity at the centre translates mathematically to:

$$z_1 \ , \ z_2 \ \sim x^{\alpha} \ , \tag{2.19}$$

$$\alpha \ \equiv \frac{\sqrt{1+4L^2}-5}{2} \ . \tag{2.20}$$

It is remarked that the limit of $\nu = 0$ recovers the limit we would expect.

2.2.2 The use of the Cowling Approximation

For the previous analysis, we employed the Cowling Approximation; the question arises whether we can find separable solutions if Φ' is not ignored. Were we not to neglect the perturbation to the gravitational potential, the equations would be:

$$-\omega^2\rho\boldsymbol{\xi} + 2\mathrm{i}\omega\rho[(\boldsymbol{\Omega}\times\mathbf{r})\cdot\nabla]\boldsymbol{\xi} \ = -\nabla p' - \rho'\nabla\Phi - \rho\nabla\Phi' \ , \tag{2.21}$$

$$\rho' + \frac{1}{r^2}\frac{\partial}{\partial r}(r^2\rho\xi_r) + \frac{\rho}{r\sin\theta}\frac{\partial}{\partial\theta}(\sin\theta\xi_\theta) + \frac{\rho}{r\sin\theta}\frac{\partial\xi_\phi}{\partial\phi} \ = 0 \ , \tag{2.22}$$

$$\frac{p'}{p} \ = \gamma_1\left(\frac{\rho'}{\rho} + A\xi_r\right) \ , \tag{2.23}$$

$$\nabla^2\Phi' \ = 4\pi G\rho' \ . \tag{2.24}$$

Now the benefits of the TA under the Cowling approximation hinge upon p', ρ' and ξ_r having the same angular form, that of $\Theta(\mu,\nu)$. With the above equations, especially (2.21), it is apparent that we would need Φ' also to have this angular form – i.e. sharing the angular form of ρ'. The question then arises whether equation (2.24) is consistent with this.

Placing a Hough function into $\nabla^2_{\rm h}$ gives:

$$\nabla^2_{\rm h}\Theta = \frac{1}{r^2}\Bigg(- L^2(1-\nu^2\mu^2) + \frac{1}{1-\nu^2\mu^2}\left(m\nu(1+\nu^2\mu^2) - 2\mu\nu^2(1-\mu^2)\frac{\partial}{\partial\mu}\right)\Bigg)\Theta\ , \quad (2.25)$$

$$\nRightarrow \nabla^2_{\rm h}\Theta \propto \Theta\ . \quad (2.26)$$

These equations make it apparent that the Traditional Approximation cannot be valid if the Cowling Approximation is not adopted. However, we shall be able later to use a variational principle to correct for the Cowling Approximation after calculating the eigenfunctions and eigenfrequencies.

(Were we to return to this argument after reading chapters 3 and 4, thinking about generalizing the Traditional Approximation in a distorted co-ordinate system, expanded in powers of f^2, the above analysis is true to $O(f^0)$. A possible suggestion would be to think about the inclusion of the metric co-efficients h_i in our expression for ∇^2 and wonder if that would make a difference, but the inconsistency here is in terms of ν, whereas the h_i are expanded in f^2; because these are different scalings, this reasoning cannot rectify the problem.)

2.3 Benefits of the Traditional Approximation

The TA has three major benefits:
(i) *Separability*: By rendering the solutions separable, the TA reduces the dimensionality of the system (and possibly simplifies the topology of the solutions). The radial component of any eigenfunction satisfies an ordinary differential eigenvalue equation of only second order (in the Cowling approximation), of which there is much theoretical analysis. Moreover, it is straightforward to determine the angular dependence.
(ii) *Relation to the nonrotating case*: Aside from the values of L^2, equations (2.15) and (2.16) are identical to those for a non-rotating star. Therefore essentially all of the techniques for solving the equations for non-radial oscillations[5], and many of the results obtained from them, can be transferred from the studies of the oscillations of non-rotating stars. In particular, provided that the Hough functions evolve continuously away from the associated Legendre functions without bifurcation as ν increases from zero (which they appear to), it is likely (indeed, definitely under the Cowling approximation) that many of the modes of oscillation can be identified with their nonrotating counterparts.
(ii) *No expansion is required*: As a result of the separation, the governing equations can be solved straightforwardly as a one-dimensional problem, essentially exactly (albeit numerically), for any angular velocity Ω without expansion.

Formally the TA provides frequencies for any rotation rate. In simply solving the equations there is no concern whether the oscillations correspond to large or small values of ν. Note, however, that owing to our assumption in this study that the background state is spherically symmetrical, we must take care that the value

[5]Whilst the TA strictly can be used for radial modes, an examination of equation (2.3) quickly shows that this is not sensible.

of $r\Omega^2/g$ is never so large as to make the effect of the centrifugal force significant. Moreover, we must also be concerned about the validity of the TA. Nevertheless, we bear in mind that the approximation has been used by geophysicists for a long while, and often appears to work well, although perhaps not always. To quote from p96 of Eckart (1960):

> '... the question arises: "What terms of the equations are responsible for the mathematical difficulties?" ... observationally it is true for all large-scale motions on the earth. It cannot be foreseen, without detailed study, whether it will be true under all circumstances.'

In the following sections, the result of such a study is presented. This is essential before transferring the procedure over to astrophysics where the consequences cannot so easily be assessed by observation as they can in geophysics.

Our assessment is possible in a number of ways: for low values of ν we have a traditional perturbation expansion which we can compare with, and for high values of ν we can look at the size of the neglected terms in equations (2.1) and (2.3) compared to the kept ones. These are both numerical exercises, but we shall begin with a local wave analysis to acquire a prior opinion of the conditions under which we might expect the TA to be valid.

2.4 A JUSTIFICATION OF THE TA - LOCAL ANALYSIS

To begin a local wave analysis, we shall consider the magnitude k_h of the horizontal wavenumber to be large compared with r^{-1}. In this case we can consider the background to be approximated by a locally plane-parallel stratification under a constant gravitational acceleration g. We shall set up local Cartesian coordinates

(x, y, z) such that $\mathbf{e}_x$, $\mathbf{e}_y$ and $\mathbf{e}_z$ coincide with $\mathbf{e}_\phi$, $-\mathbf{e}_\mu$ and $\mathbf{e}_r$, respectively. Then the angular velocity $\boldsymbol{\Omega}$ is of the form $(0, \Omega_y, \Omega_z)$ in this coordinate system; and we shall consider all perturbed variables to be proportional to $e^{\mathrm{i}(k_x x + k_y y)}$.

We can, by following a procedure similar to that used by Lamb (1932) and Gough (1993), manipulate equations (2.1)-(2.5) to a single second-order equation for $\nabla \cdot \boldsymbol{\xi}$; upon scaling the new dependent variable ($\Psi = \rho^{\frac{1}{2}} c^2 \nabla \cdot \boldsymbol{\xi}$) to remove the first derivative of the dependent variable, we arrive at

$$\nabla^2 \Psi + \frac{\omega^2 - \omega_{\mathrm{c}}^2}{c^2} \Psi - \frac{N^2}{\omega^2} \nabla_h^2 \Psi \; = -2\mathrm{i}\omega^{-1} \rho^{\frac{1}{2}} F \; , \qquad (2.27)$$

where $\omega_{\mathrm{c}}^2 = (1 - 2\mathrm{d}H/\mathrm{d}r) c^2 / 4H^2$ is the square of the critical cutoff frequency, H is the density scale height, and the function F on the right-hand side contains all the (linear) effects of rotation:

$$F \; = \left(\omega^2 - g \frac{\partial}{\partial r} \right) \nabla \cdot (\boldsymbol{\Omega} \times \boldsymbol{\xi}) + g \nabla^2 (\boldsymbol{\Omega} \times \boldsymbol{\xi})_z \; . \qquad (2.28)$$

To express the function F in terms of Ψ, we eliminate p' and ρ' from equations (2.1) - (2.5) in favour of $\chi = \nabla \cdot \boldsymbol{\xi}$, using equations (2.4) and (2.5), yielding:

$$\omega^2 \boldsymbol{\xi} + 2\mathrm{i}\boldsymbol{\Omega} \times \boldsymbol{\xi} \; = -\nabla (c^2 \chi - g \xi_z) - g^{-1} c^2 N^2 \chi \boldsymbol{n} \; , \qquad (2.29)$$

where $\boldsymbol{n}$ is a unit vector in the z direction. The three components of this equation can then be used to express the three components of $\boldsymbol{\xi}$ in terms of χ.

The advantage of this procedure over some others (such as replacing χ by $\nabla \cdot \boldsymbol{\xi}$ and eliminating two of the components of $\boldsymbol{\xi}$ to obtain a single equation for the third) is that in this case the

determinant, Δ, of the coefficients is a constant.

$$\Delta \ = \omega^4(\omega^4 g^2 k_{\rm h}^2 + 4\omega g k_x \Omega_y - 4\omega^2\Omega^2) \ . \tag{2.30}$$

The components of $\boldsymbol{\xi}$ will be written out later. The formula (2.28) for F can then be written:

$$-2{\rm i}\omega^{-1}\rho^{\frac{1}{2}}F \ = 2\omega^2\Delta^{-1}\sum_{n=0}^{2} a_n \frac{\partial^n \Psi}{\partial z^n} \ , \tag{2.31}$$

in which

$$\begin{aligned}
a_0 \ &= \ -\omega\left[2\omega^2 g\left(k_{\rm h}^2 + \omega_{\rm c}^2/c^2\right) - H^{-1}(\omega^4 + g^2 k_{\rm h}^2)\right] k_x \Omega_y \\
&+ \ 2\omega^4\left(k_x^2\Omega_y^2 + k_{\rm h}^2\Omega_z^2\right) - 2g^2 k_y^2 k_{\rm h}^2 \Omega_y^2 \\
&+ \ 2\left(\omega^4\Omega_y^2 + g^2 k_{\rm h}^2\Omega_z^2\right)\omega_c^2/c^2 - 2\omega^2 g H^{-1} k_{\rm h}^2\Omega^2 \ , \qquad (2.32) \\
a_1 \ &= \ 4{\rm i}(\omega^4 - g^2 k_{\rm h}^2) k_y \Omega_y \Omega_z \ , \qquad (2.33) \\
a_2 \ &= \ 2\omega^3 g k_x \Omega_y + 2\omega^4\Omega_y^2 + 2g^2 k_n^2 \Omega_z^2 \ . \qquad (2.34)
\end{aligned}$$

After substituting these expressions into equation (2.27), the resulting equation can be reduced to standard form, removing the first derivative of the dependent variable, by writing $\Psi = {\rm e}^{{\rm i}(k_x x + k_y y - \alpha z)}\Phi(z)$, where $\alpha = \omega^2\Delta^{-1}a_0(1 + 2\omega^2\Delta^{-1}a_1)$ and Φ is not to be confused with the gravitational potential, yielding

$$\frac{{\rm d}^2\Phi}{{\rm d}z^2} + K^2\Phi \ = 0 \ , \tag{2.35}$$

where

$$\begin{aligned}
K^2 \ &= \ \frac{1}{1 + 2\omega^2\Delta^{-1}a_1}\left[\frac{\omega^2 - \omega_c^2}{c^2} + k_{\rm h}^2\left(\frac{N^2}{\omega^2} - 1\right)\right. \\
&+ \ \left. 2\omega^2\Delta^{-1}a_3 + \frac{\omega^4\Delta^{-2}a_2^2}{1 + 2\omega^2\Delta^{-1}a_1}\right] \ . \qquad (2.36)
\end{aligned}$$

Then, by writing $\mathrm{d}/\mathrm{d}z = \mathrm{i}k_\mathrm{v}$ and $k^2 = k_\mathrm{h}^2 + k_\mathrm{v}^2$, we arrive at the following dispersion relation[6]:

$$\omega^4 - (k^2c^2 + \omega_\mathrm{c}^2 + 4\Omega^2)\omega^2 + 2\omega\Gamma(\boldsymbol{n}\times\boldsymbol{k}).\boldsymbol{\Omega} + c^2[N^2k_\mathrm{h}^2 + 4(\boldsymbol{k}.\boldsymbol{\Omega})^2] + 4\omega_\mathrm{c}^2(\boldsymbol{n}.\boldsymbol{\Omega})^2 \simeq 0 \ . \qquad (2.37)$$

Notice that if the equilibrium state were isothermal and γ_1 were constant, this dispersion relation would reduce almost to equation (33.9) of Unno et al. (1989), save for the sign of ω_c^2, provided that k is identified with the magnitude of the real part of the wavenumber $\tilde{\boldsymbol{k}}$ of Unno *et al.* which itself must necessarily be complex if ω is real; the imaginary part of $\tilde{\boldsymbol{k}}$ accounts for the scaling between χ and Ψ.

Looking at this dispersion relation, we see that for high-order g modes that satisfy $|k_\mathrm{v}| \gg |k_\mathrm{h}|$ and $k^2c^2 \gg \omega_\mathrm{c}^2 + 4\Omega^2$, the frequency ω satisfies $\omega^2 \ll c^2k^2$, and we can therefore approximate equation (2.37) by:

$$\omega^2 \approx \frac{N^2k_\mathrm{h}^2 + (2\boldsymbol{\Omega}.\boldsymbol{k})^2}{k^2} \simeq N^2\frac{k_\mathrm{h}^2}{k^2} + (2\boldsymbol{n}.\boldsymbol{\Omega})^2 \ . \qquad (2.38)$$

The rotational contribution due to the Coriolis force is therefore dominated by the vertical component of $\boldsymbol{\Omega}$, and Ω_h can hence be safely neglected; only very near the equator, where $\boldsymbol{n}.\boldsymbol{\Omega}$ almost vanishes, does the term $2\omega\Gamma(\boldsymbol{n}\times\boldsymbol{k}).\boldsymbol{\Omega}$ in equation (2.37) formally become more important than $4c^2(\boldsymbol{k}.\boldsymbol{\Omega})^2$. However, its influence extends over such a small region – and in any case the term is small compared with $c^2N^2k_\mathrm{h}^2$ – that it is unlikely to have a substantial influence on the global properties of the modes.

This argument leads us to expect the TA to be a good approximation for g modes of high order n satisfying $n \gg l$ (more

[6] $\Gamma = g - c^2N^2/g$, and the other symbols are as already defined.

formally $|k_{\rm v}| \gg |k_{\rm h}|$). It is noteworthy that for such modes the Cowling approximation, which we have adopted here, provides a good representation to the full equations.

In the case of high-order p modes, once again having $|k_{\rm v}| \gg |k_{\rm h}|$, the inequalities $\omega \simeq kc \gg |N|$, $\omega \gg |\omega_{\rm c}|$ are satisfied everywhere in the region of propagation except near the upper turning point, and the dispersion relation (2.38) reduces to

$$\omega^2 \simeq k^2 c^2 + \omega_{\rm c}^2 + 4\Omega_{\rm h}^2 \tag{2.39}$$

In that case the TA is going to be a very poor approximation indeed.

For grave p and g modes, the influence of $\Omega_{\rm h}$ and $\Omega_{\rm v}$ appear to be comparable; the local analysis provides no clear prediction, and it requires a more careful analysis to assess the accuracy of the TA.

2.4.1 EXPLICIT FORMULAE FOR THE COMPONENTS OF $\boldsymbol{\xi}$

Returning to the local analysis, we can write the components of the eigenvector as:

$$\begin{aligned}
\frac{{\rm i}\rho^{\frac{1}{2}}\Delta}{\omega^3\Psi}\xi_x &= \omega^2(\omega k_x + 2{\rm i}k_y\Omega_z - 2gk_y^2\Omega_y) \\
+\Big[\omega(gk_x &- 2\omega\Omega_y) + 2{\rm i}gk_y\Omega_z\Big]\left({\rm i}k_{\rm v} - \frac{1}{2H}\right)\Big) , \qquad (2.40)\\
\frac{{\rm i}\rho^{\frac{1}{2}}\Delta}{\omega^3\Psi}\xi_y &= \omega^3 k_y + 2\left(gk_xk_y\Omega_y - 2\omega k_y\Omega_y^2 - {\rm i}\omega^2 k_x\Omega_z\right) \\
+\Big[g(\omega k_y &- 2{\rm i}k_x\Omega_z) + 4{\rm i}\omega\Omega_y\Omega_z\Big]\left({\rm i}k_{\rm v} - \frac{1}{2H}\right) , \qquad (2.41)\\
\frac{{\rm i}\rho^{\frac{1}{2}}\Delta}{\omega^3\Psi}\xi_z &= -{\rm i}\omega\Big[\left(gk_{\rm h}^2 + 2\omega k_x\Omega_y - 4{\rm i}k_y\Omega_y\Omega_z\right)
\end{aligned}$$

$$+ \quad (\omega^2 - 4\Omega_z^2)\left(\mathrm{i}k_\mathrm{v} - \frac{1}{2H}\right)\Bigg] \,, \tag{2.42}$$

which will prove useful later.

2.4.2 THE LIMIT $\nu \to \infty$

Considering the fact that the Coriolis force acts as an equatorial waveguide of width $|\nu|^{-1}$ for g modes, whilst looking at equations (2.7) and (2.8) we see that in the limit $\nu \to \infty$ we would expect $k_x/k_y \sim 1/\nu$. As k_x can be associated with the m value for a mode, and hence viewed as constant, this may also lead us to question the assumption in this limit that $|k_\mathrm{v}| \gg |k_\mathrm{h}|$.

Indeed, looking at equation (2.37) under the TA, we arrive at the balance:

$$\begin{aligned} k_\mathrm{v}^2(4\Omega_z^2 - \omega^2) &= k_\mathrm{h}^2(\omega^2 - N^2) \\ &+ \frac{4\omega^2\Omega_z^2}{c^2} + \frac{\omega^4 - \omega_\mathrm{c}^2(\omega^2 - 4\Omega_z^2)}{c^2} \,. \end{aligned} \tag{2.43}$$

From this we can see that, taking ν to infinity with modest rotation (i.e. Ω^2 is not dwarfed by N^2), the assumption of $|k_\mathrm{v}| \gg |k_\mathrm{h}|$ breaks down and hence the above analysis to justify the TA becomes invalid. Physically, we can tie this to the fact that the equatorial waveguide focuses the mode to a region for which neglecting the overall effects of $\Omega_y = \Omega\sin\theta$ compared with those of $\Omega_z = \Omega\cos\theta$ is no longer sensible. This leads us to question the TA under very high ν.

2.5 A JUSTIFICATION OF THE TA - NUMERICAL INVESTIGATION

2.5.1 INFLUENCE ON THE FREQUENCIES FOR SMALL ν

For small values of ν, we can see to what extent the predictions for the behaviour of ω as a function of ν agree with those of solving the problem "exactly" with a formal expansion. As we are not considering the alteration of background structure at this point, we shall expand only to first order in the rotation rate in order to provide a "clean" analysis. Due to the reduction of equation (2.11) to the equation for associated Legendre functions at $\nu = 0$, the two methods for determining ω will agree. But do, for instance, the gradients of the functions $\mathrm{d}\omega/\mathrm{d}\nu$ agree?

The effects of rotation can be discussed in the framework of Hilbert space[7]; under the definition for the inner product of two oscillation eigenfunctions $\boldsymbol{\xi}$ and $\tilde{\boldsymbol{\xi}}$:

$$\langle \boldsymbol{\xi}, \rho\tilde{\boldsymbol{\xi}} \rangle \equiv \tfrac{1}{4\pi} \int_{\mathcal{V}} \boldsymbol{\xi}^* . \tilde{\boldsymbol{\xi}} \rho \mathrm{d}V = \int_0^R (\xi^* \tilde{\xi} + \eta^* \tilde{\eta}) \rho r^2 \mathrm{d}r \ , \qquad (2.44)$$

the first integral being over the volume $\mathcal{V}$ of the star[8]. The asterisk denotes complex conjugate. The system, which may be described formally by $\mathcal{H}\boldsymbol{\xi} + \omega^2 \boldsymbol{\xi} = \mathbf{0}$ in which the differential operator $\mathcal{H}$ is independent of ω, is self-adjoint when $\boldsymbol{\Omega} = \mathbf{0}$ (e.g. Lynden-Bell and Ostriker (1967)).

It follows immediately from the solubility condition for the perturbed eigenfunction that the first-order (in rotation rate) modification to the frequency by Ω may be written in terms of

[7]Completeness of the eigenfunctions satisfying the boundary conditions that we use here was established by Dyson and Schutz (1979).

[8]To obtain the second integral we adopt a normalization of the spherical harmonics Y_l^m according to $\int\int |Y_l^m|^2 \sin\theta \mathrm{d}\theta \mathrm{d}\phi = 4\pi$.

the rotationally unperturbed eigenfunction $\boldsymbol{\xi}_0$, thus[9]:

$$\delta\omega = \mathrm{i}\frac{\langle \boldsymbol{\xi}_0, \rho(\boldsymbol{\Omega}\times\boldsymbol{\xi}_0)\rangle}{\langle \boldsymbol{\xi}_0, \rho\boldsymbol{\xi}_0\rangle} = \frac{-\mathrm{i}}{4\pi I}\int_{\mathcal{V}} \boldsymbol{\Omega}.(\boldsymbol{\xi}_0^*\times\boldsymbol{\xi}_0)\rho \mathrm{d}V \equiv -C\Omega\ , \quad (2.45)$$

where we have defined

$$\langle \boldsymbol{\xi}_1, \boldsymbol{\xi}_0\rangle \equiv \int_{\mathcal{V}} \boldsymbol{\xi}_1^*\boldsymbol{\xi}_0 \mathrm{d}V\ , \quad (2.46)$$

$$I \equiv \langle \boldsymbol{\xi}_0, \rho\boldsymbol{\xi}_0\rangle\ . \quad (2.47)$$

To determine the influence of rotation under the TA, one could simply replace $\boldsymbol{\Omega}$ by its vertical component $\boldsymbol{\Omega}_{\mathrm{v}}$ in equations (2.45). Alternatively, one can simply analyse the system (2.11)–(2.16), using already-established results from the theory of nonrotating stars, although if one is content to stop at the first-order correction the former procedure is more straightforward. But also one could, for example, introduce $\Psi = (g\rho r^{-3}\tilde{f})^{-1/2}\delta p$, $\tilde{f}$ now being the f-mode discriminant:

$$\tilde{f} = \frac{\omega^2 r}{g} + 2 + \frac{r}{H_g} - \frac{L^2 g}{\omega^2 r}\ , \quad (2.48)$$

where H_g is the scale height of the gravitational acceleration g.

In the Cowling approximation Ψ satisfies an equation of the form

$$\frac{\mathrm{d}^2\Psi}{\mathrm{d}r^2} + \mathcal{K}^2\Psi = 0\ , \quad (2.49)$$

where $\mathcal{K}(\omega; L(\nu))$ is essentially a local vertical wavenumber (for example, see Gough, 1993):

[9]One could argue this alternatively from the variational properties of $I^{-1}\langle\xi, \mathcal{P}\xi\rangle$, as did Lynden-Bell and Ostriker (1967).

$$\mathcal{K}^2 = \frac{\omega^2 - \omega_c^2}{c^2} - \frac{L^2}{r^2}\left(1 - \frac{N^2}{\omega^2}\right) . \tag{2.50}$$

Equation (2.49) is also self-adjoint, because (it can be shown that) $\Psi \mathrm{d}\Psi/\mathrm{d}r$ vanishes at $r = 0$ and $r = R$. Consequently the first-order rotational perturbation to the frequency may be written:

$$\delta_{\mathrm{TA}}\omega = -\nu \frac{\mathrm{d}L^2}{\mathrm{d}\nu} \frac{\int_0^R (\partial\mathcal{K}^2/\partial L^2)\Psi_0^2 \mathrm{d}r}{2\omega_0 \int_0^R (\partial\mathcal{K}^2/\partial\omega^2)\Psi_0^2 \mathrm{d}r} , \tag{2.51}$$

the value of $\mathrm{d}L^2/\mathrm{d}\nu$ being obtained from equation (2.11); once again the subscript zero denotes the value in the absence of rotation. However, as we have pointed out above, the TA may be valid also when ν is not small, so it is better to solve equation (2.49), or equivalently equations (2.15)–(2.16), exactly.

The terms omitted by the TA from the expressions for $\delta\omega$ in equations (2.45) may be written

$$\Delta\delta\omega = -2mI^{-1}L^{-1}\Omega \int_0^R \xi_0\eta_0\rho r^2 \mathrm{d}r . \tag{2.52}$$

This should not surprise: in the TA the terms in equations (2.1)–(2.3) that have been removed are those that mix ξ_r with ξ_θ and ξ_ϕ, so one should expect that that should be manifest as the removal of the cross term in the integral in equation (2.45). The question now is: how important is that term?

To answer that question we consider the ratio ζ of the neglected term $\Delta\delta\omega$ and the term retained:

$$\zeta := \left|\frac{\Delta\delta\omega}{\delta\omega - \Delta\delta\omega}\right| = \left|\frac{2\int_0^R \xi_0\eta_0\rho r^2 \mathrm{d}r}{\int_0^R \eta_0^2\rho r^2 \mathrm{d}r}\right| , \tag{2.53}$$

for several stellar models. In the following we restrict ourselves

to displaying the case of a polytrope of index n,[10] satisfying[11]:

$$p = K\rho^{1+1/n}; \tag{2.54}$$

we shall present results for other models in later chapters.

One expects ζ to be small particularly for high-order g modes, partly because for such modes $|\xi_0| \ll |\eta_0|$ and partly because the spatial oscillations of ξ_0 and η_0 are asymptotically out of phase. Indeed, since $\xi_0/\eta_0 = \mathrm{O}(n^{-1})$ for large radial order n, application of Riemann's lemma suggests that $|\zeta| = \mathrm{O}(n^{-2})$, and hence, since $\omega_0 \propto n^{-1}$, that $|\zeta| = \mathrm{O}(\omega_0^2)$. For high-order p modes, $|\xi_0| \gg |\eta_0|$, and one might expect, according to Riemann's lemma, that ζ tends to a constant as the order n increases; but to determine whether or not that constant is small requires either more careful analysis or numerical computation.

Values of ζ are plotted in Figures 1, 2 and 3 for modes of degrees l=1, 2 and 3, and for differing polytropic indices. In all cases the ω_0^2 dependence is evident in the envelope at low ω_0. The approach to a (degree-dependent) constant that we expected at large ω_0 is also evident. That constant, for low degree, is not small. Moreover, for grave modes, $|\zeta|$ is typically larger still. Therefore the approximation is not good for p modes and grave g modes; it is only for the high-order g modes that the Traditional Approximation works well. Note that if the neglected and kept terms nearly cancel for large ω, as they seem to in the Sun, the TA is very bad indeed, because the resulting traditionally approximated value for C (defined in equation (2.45)) is almost

[10]Not to be confused with the order of the mode.

[11]For this, and later polytrope calculations, 4000 mesh points were used, and the code was tested for zero rotation against the high-precision (of the time) tabulated g mode periods in Mullan (1989), and found to agree with this work to at least 5 significant figures. As we have not employed Richardson extrapolation or such like, this causes us to trust our results to a high level of precision.

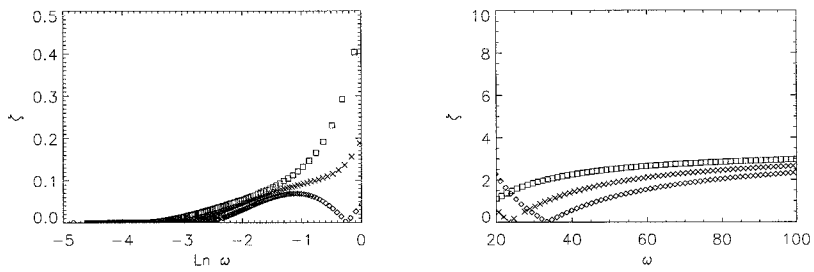

Figure 2.1: Values of ζ for an $n = 3$ polytrope, plotted verses $\ln \omega$ on the left to emphasise g modes, and against ω on the right for p modes. $l = 1,\ 2,\ 3$ are denoted squares, crosses and diamonds respectively. The "bouncing" effect is from taking the modulus in equation (2.53).

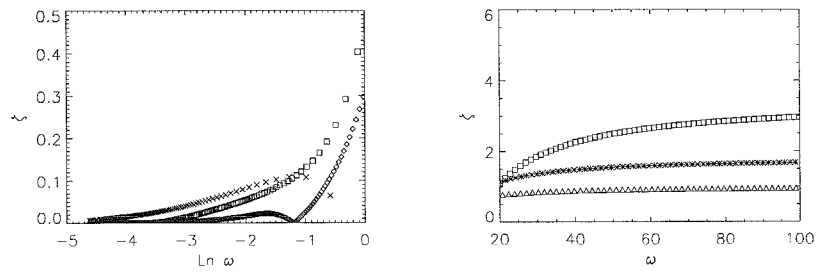

Figure 2.2: As in 2.1, but for $l = 1$ modes in polytropes of index $n = 2,\ 3,\ 4$ denoted by crosses, squares and diamonds respectively.

entirely error.

For g modes whose order is not very high the TA can be used, but its validity must be considered for each case; it is not always true that the neglected term is small enough to be neglected. For example, the effect of ignoring the cross term for an $l = 1$ mode with radial order of $k = 9$ is not very small ($\zeta = 0.132$ for a polytrope of index 3), and such a mode is not atypical of those observed[12].

For p modes, ζ is almost always too large to ignore (apart from a few modes for which $\langle \xi_0,\ \eta_0 \rangle$ is accidentally small). This is true for all the stellar models we have considered. Our tests suggest that it would be dangerous to adopt the TA for such modes, because the accidental cancellation is no doubt model dependent. However, for these modes the Coriolis parameter C is very small, and second-order effects may dominate.

2.5.2 COMPARISON OF TERMS FOR LARGE ν

When ν is large, a formal expansion in ν is no longer valid. However, it is still possible to provide a diagnostic by first computing a solution in the TA and then comparing the neglected terms in equations (2.1) to (2.3) with those that were retained. Accordingly, we define the following ratios:

$$\chi_1(\boldsymbol{r}) = \frac{2\mathrm{i}\rho\omega\Omega \sin\theta \xi_\phi}{-\rho\omega^2\xi_r + \frac{\partial \rho'}{\partial r}}, \tag{2.55}$$

$$\chi_2(\boldsymbol{r}) = \frac{2\mathrm{i}\rho\omega\Omega \sin\theta \xi_r}{-\rho\omega^2\xi_\phi + 2\mathrm{i}\rho\omega\Omega\cos\theta\xi_\theta}, \tag{2.56}$$

$$\chi_3(\boldsymbol{r}) = \frac{2\mathrm{i}\rho\omega\Omega \sin\theta \xi_r}{2\mathrm{i}\rho\omega\Omega\cos\theta\xi_\theta}, \tag{2.57}$$

[12]The gravest g mode detected in GD358, for example, has $k = 9$ (see Kepler et al., 2003).

which one must require to be generally small almost everywhere if one is to expect the TA to provide a reliable outcome.

The ratio χ_3 is included to investigate the approximation when $m = 0$; in this case the rhs of equation (2.3) vanishes, and χ_2 is undefined under the TA. Of course, because the numerators and denominators of these diagnostics are oscillatory functions with zero means, the point values of these diagnostics are unreliable: they are deceptively small near the zeros of the numerators, and they diverge at the zeros of the denominators. We therefore express each of these functions, which we denote here by K, in terms of an amplitude $[K_{\rm A}]$ and a phase ϕ_K, according to

$$K = [K]_{\rm A} \sin \phi_K \ , \tag{2.58}$$

and replace each function K in χ_i by its amplitude. As do Gough et al. (1998), we can use the Hilbert transform, defined as

$$\hat{K}(x) \equiv \mathcal{H}(K(x)) \equiv \pi^{-1}\mathcal{P}\int_{-\infty}^{\infty} \frac{K(\eta)}{\eta - x} d\eta \ , \tag{2.59}$$

where $\mathcal{P}$ denotes the principal part. It is the case that for any constants A, $\kappa > 0$ and phase shift α, the following identities hold:

$$\mathcal{H}\left[A\cos(\kappa x + \alpha)\right] = -A\sin(\kappa x + \alpha) \ , \tag{2.60}$$

$$\mathcal{H}\left[A\sin(\kappa x + \alpha)\right] = A\cos(\kappa x + \alpha) \ . \tag{2.61}$$

Therefore, the amplitude of our function K can be estimated in terms of K and its Hilbert transform $\hat{K}$ as:

$$[K]_{\rm A} = \sqrt{K^2 + \hat{K}^2} \ . \tag{2.62}$$

Incidentally, this also shows the way to calculate the Hilbert transform easily: as it is far more straight forward to express the

2.5 A Justification of the TA - Numerical Investigation

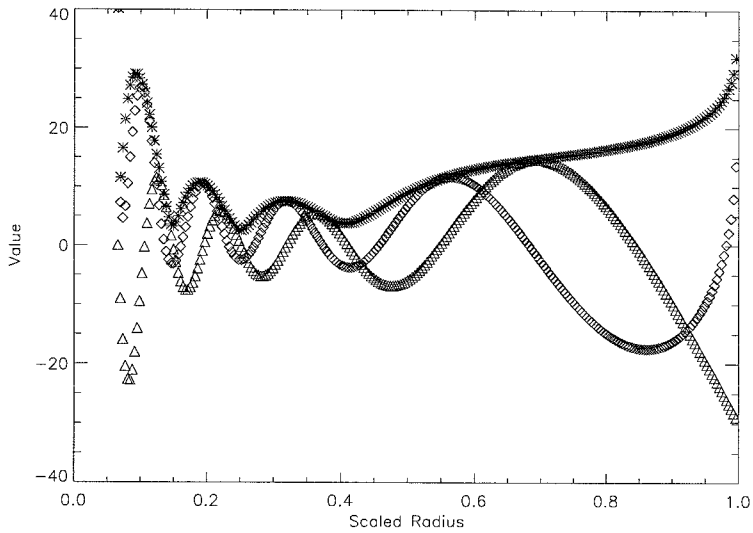

Figure 2.3: The value of $\xi_r(r)$ (triangles), its Hilbert transform (diamonds), and hence the amplitude function (asterixes). The mode displayed is the radial part of what would be an $(n, l, m) = (9, 2, 2)$ g mode, under the TA with a rotation $f = 3 \times 10^{-3}$

function as a Fourier series, carry out the Hilbert transform on this, and then convert back, rather than calculate residues of the function $K(\eta)/(\eta - x)$ and so forth. However, using this method *does* introduce the problem of the Gibb's phenomenon, and also the complication that we need $[K]_{\mathrm{A}}$ and κ to vary on a scale much greater than κ^{-1}, which can break down towards the centre of the star. For this second reason, we shall consider only the functions after the first zero in the eigenfunction $\xi(r)$, and plot from this point. An example of this is shown in figure 2.3.

As can be seen, even with this truncation before the centre, because $[K]_{\mathrm{A}}$ does not vary on a large enough length scale, it

still contains some oscillatory structure. We shall hence use the mean value of $K_{\rm A}$, over the range going from the first zero to the surface, for our graphs.

Using the separable-solution expansions for the components of $\boldsymbol{\xi}$, we can replace the ratios by:

$$\chi_1(\boldsymbol{r}) = \frac{-\nu p'(r)}{\frac{\partial p'(r)}{\partial r} - \rho\omega^2\xi_r(r)} \times \frac{\left(m - \nu\mu(1-\mu^2)\frac{\partial}{\partial\mu}\right)\Theta}{(1-\mu^2\nu^2)\Theta} , \tag{2.63}$$

$$\chi_2(\boldsymbol{r}) = \left(\frac{-\nu\omega^2}{m}\frac{r\rho\xi_r(r)}{p'(r)}\right) \times (1-\mu^2) , \tag{2.64}$$

$$\chi_3(\boldsymbol{r}) = \frac{\rho r\omega^2\xi_r(r)}{p'(r)} \times \frac{(1-\mu^2)(1-\mu^2\nu^2)\Theta}{\mu\left(m\nu\mu - (1-\mu^2)\frac{\partial}{\partial\mu}\right)\Theta} . \tag{2.65}$$

To look at the variance of these diagnostics with ν, figures 2.4 and 2.5 show the average values of the radial parts of these χ_i. It is interesting to note that, despite having $\nu\omega^2$ (i.e. ω) in the numerator of its definition, χ_2 climbs as $\omega \to 0$.

Returning to the asymptotic theory from earlier, we can place the expansions for ξ_x to ξ_z (equations (2.40) to (2.42)) into the definitions of the χ_i. Upon doing this, we see that the limits of $\chi_{1,2}/\Omega$ do **not** tend to zero as $\omega \to 0$, whereas the expansion for χ_3 does.

This implies that the TA is not valid as $\nu \to \infty$, which the confirms our analytic predictions for this limit by performing a short-wavelength dispersion relation and expansion.

2.5 A Justification of the TA - Numerical Investigation

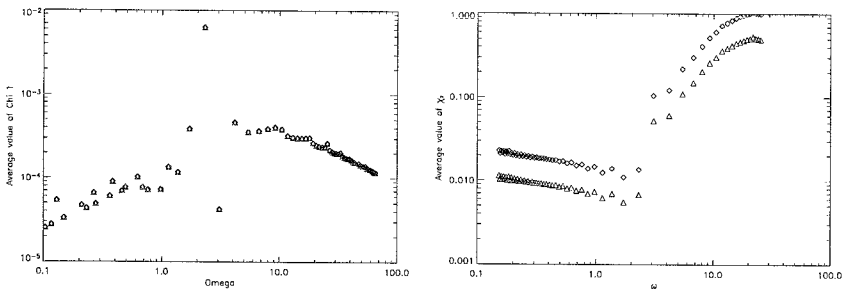

Figure 2.4: Average values of χ_1 and χ_2 for $m = 2$ modes around $l = 2$, with $f = 3 \times 10^{-3}$ (squares) and $f = 6 \times 10^{-3}$ (triangles).

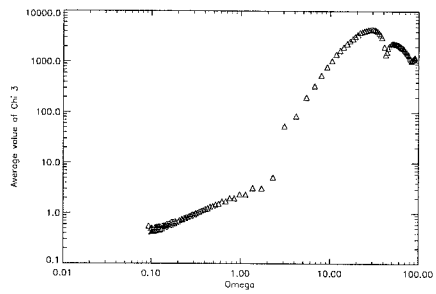

Figure 2.5: Average values of χ_3 for $m = 0$ modes around $l = 2$, $f = 3 \times 10^{-2}$.

2.5.3 CONCLUSIONS

We have discussed the Traditional Approximation, why it works, and its benefits. Also, we have developed a diagnostic structure and asymptotic formalism under which to quantify its validity.

These three methods (asymptotic theory, and numerics for small and large ν) encourage us to retain the TA only for mid-degree g-modes for modest rotation. For high-order p-modes, equation (2.39) shows that the TA is a poor approximation for all non-zero rotation rates, whereas for low-order p-modes the diagnostic ζ shows that it gives bad predictions for low ν, with no sign of it improving for larger ν.

Also, the TA is questionable in the limit $\nu \to \infty$. This leaves modest-ν g modes as the regime in which we can use the TA, but we must always quantify our use of it, which shall be done with the χ_i diagnostics.

Whilst this might seem like a disappointment, we are saved by the fact that mid-range-ν g modes are *exactly* the modes seen in many stars; thus the realm of (quantifiable) validity is the one of interest! It is also the case that the Traditional Approximation can be generalized, which we now proceed to do.

Chapter 3

Alteration to structure for a barotropic equation of state

"Ubi materia, ibi geometria." (Where there is matter, there is geometry.) – Johannes Kepler

3.1 Motivation

The alteration due to rotation of the structure and shape of a star with a barotropic equation of state is a long-studied subject. For instance, James (1964) computed the surface displacement at the equator and the poles for uniform rotation in polytropes by expanding the full equations in Legendre polynomials for given rotation rates, and Chandrasekhar and Lebovitz (1962) calculated the first order (in f^2) distortion to the surface, with terms of second order being added by Anand (1968).

Whilst these explorations are useful for observational selection, as they detail the surface, it is desired to know the full structure of the inside of the star to investigate its pulsations.

In this chapter, only barotropic equations of state are dealt with; these equations of state admit a simple hydrostatic rotating structure, avoiding Von Ziepel's paradox and the necessity of an Eddington-Sweet flow. This is done for mathematical ease, and will be generalized in chapter 7.

Thinking physically, a given perturbed fluid element is not going to know about the global properties of the star, but will just

feel it's local equipotentials and flow. Thus, whilst not mathematically pleasant, the equipotental surfaces (as used by Papaloizou and Pringle, 1978) naturally form the most physically sensible basis to work in. Gough and Thompson (1990) looked at rescaling the r co-ordinate to coincide with these surfaces, and the extra terms that this rescaling introduced, for instance, into ∇.

This work proved to be incredibly useful, but it will be necessary, in addition to being physically sensible, to retain the orthogonality of the distorted coordinate basis. It will be convenient to work with the analogue of $\mu \equiv \cos\theta$. The distorted (r, μ) will be labelled as (x, η). It should be noted that some of the equations in this chapter are somewhat complicated, but necessary. Some results from the theory presented in this chapter are displayed in chapter 5.

3.2 MATHEMATICAL FRAMEWORK

To define a transformation between the two co-ordinate systems just mentioned, it is possible to use either of them ((r, θ) or (x, η)) as the independent variables. Whilst these give the same answer, physically the perturbation equations that will be considered will be in the distorted star, so it will work out as more convenient in the long run to work in that basis. Therefore, the following transformations are defined[1]:

$$r = x\left(1 + \sum_{l\geq 0, a>1} f^{2a} P_{2l}(\eta)\lambda_{l,a}(x)\right) , \qquad (3.1)$$

$$\mu = \eta\left(1 + \sum_{l\geq 0, a>1} f^{2a} P_{2l}(\eta)t_{l,a}(x)\right) . \qquad (3.2)$$

[1]The ϕ co-ordinate is left unaltered.

(The choice of orthogonal functions in which to expand the angular dependence is natural, owing to the angular dependence of centrifugal force in spherical polar co-ordinates being $\sin^2\theta = 1-\mu^2 = \frac{2}{3}[1-P_2(\mu)]$.)

To define ∇, ∇^2 and other operators in the new co-ordinate basis, it is convenient to obtain the metric coefficients h_i in the following expression:

$$\begin{aligned}\delta\mathbf{r} &= \delta r\mathbf{e}_r + r\delta\theta\mathbf{e}_\theta + \delta\phi\, r\sin\theta\mathbf{e}_\phi \\ &= h_1\delta x\mathbf{e}_x + h_2\delta\eta\mathbf{e}_\eta + h_3\delta\phi\mathbf{e}_\phi\ . \end{aligned} \tag{3.3}$$

Once these are obtained, then formulae for, for example, ∇,$\nabla\cdot$ and $\nabla\times$ exist (see appendix C).

3.3 CALCULATION OF THE h_i IN TERMS OF $\lambda_{l,a}$

There are two effects that govern the distortion of the h_i from those of spherical polars: the first is that the r and $\sqrt{1-\mu^2}$ factors appearing in the $h_{i,\text{spherical}}$ will be expanded according to equations (3.1) and (3.2); these are straightforward to calculate.

The second effect is more subtle, in that the fractional changes δ of one coordinate in equation (3.3) must be made at *fixed values of the remaining coordinates in the coordinate system in which the first coordinate is contained.* Thus δx really means $(\delta x)_{\eta,\phi}$. This shows itself, for example in the fact that, in spherical polar coordinates:

$$\mathbf{e}_r.\mathbf{e}_x \equiv \mathbf{e}_r.\widehat{\nabla x} \propto \left(\frac{\partial x}{\partial r}\right)_{\mu,\phi}\ , \tag{3.4}$$

The derivative on the right-hand side is evaluated at fixed μ ($\leftrightarrow$ fixed θ), whereas the transformation between the co-ordinate systems is defined in terms of (x,η). It is thus necessary to use:

3.3 Calculation of the h_i in terms of $\lambda_{l,a}$

$$\delta r = \left(\frac{\partial r}{\partial x}\right)_{\eta,\phi} \delta x + \left(\frac{\partial r}{\partial \eta}\right)_{x,\phi} \delta\eta \ , \tag{3.5}$$

$$\delta \mu = \left(\frac{\partial \mu}{\partial x}\right)_{\eta,\phi} \delta x + \left(\frac{\partial \mu}{\partial \eta}\right)_{x,\phi} \delta\eta \ , \tag{3.6}$$

to obtain:

$$\left(\frac{\partial x}{\partial r}\right)_{\mu} = \left[\left(\frac{\partial r}{\partial x}\right)_{\eta} - \left(\frac{\partial r}{\partial \eta}\right)_{x}\left(\frac{\partial \mu}{\partial x}\right)_{\eta}\left(\frac{\partial \eta}{\partial \mu}\right)_{x}\right]^{-1} \ , \tag{3.7}$$

which can then be calculated using equations (3.1) and (3.2). Similar equations exist for the other derivatives, but they are straightforward to calculate and are not displayed here.

When we place both of these effects into equation (3.6), and calculate the expansions, to order (f^4), the following equations are obtained:[2]

$$\begin{aligned} h_1 = 1 + f^2 \sum_{l\geq 0} P_{2l}\left(x\lambda_{l,1}\right)' + f^4 \Bigg[& \sum_{l\geq 0} P_{2l}\left(x\lambda_{l,2}\right)' \\ & + \sum_{l,m\geq 0} \left(3P_{2l}P_{2m}\left(x\lambda_{l,1}\right)'\left(x\lambda_{m,1}\right)' \right. \\ & \left. -(1-\eta^2)P'_{2l}P'_{2m}\lambda_{l,1}\lambda_{m,1}\right) \Bigg] \ , \end{aligned} \tag{3.8}$$

[2]The listing of the independent variables has been dropped to save room – all are functions of x, apart from Legendre polynomials, which are functions of η. To save on space, derivatives with respect to the argument are denoted by primes, and will be either $\frac{\partial}{\partial x}$ or $\frac{\partial}{\partial \nu}$ as appropriate.

$$
\begin{aligned}
h_2 \;&= \frac{x}{\sqrt{1-\eta^2}}\Bigg\| 1 \\
&+f^2 \sum_{l\geq 0}\left[(P_1P_{2l})'t_{l,1} + P_{2l}\left(\lambda_{l,1} + \frac{\eta^2 t_{l,1}}{1-\eta^2}\right)\right] \\
&+f^4\Bigg\{\sum_{l\geq 0}\left[(P_1P_{2l})'t_{l,2} + P_{2l}\left(\lambda_{l,2} + \frac{\eta^2 t_{l,2}}{1-\eta^2}\right)\right] \\
&+\sum_{l,m\geq 0}\Big[P_{2l}(P_1P_{2m})'\lambda_{l,1}t_{m,1} - 3(1-\eta^2)P'_{2l}P'_{2m}\lambda_{l,1}\lambda_{m,1} \\
&\qquad +2P_{2l}P_{2m}\left(x\lambda_{l,1}\right)'\left(x\lambda_{m,1}\right)' \\
&\qquad +\frac{\eta^2 t_{l,1}t_{m,1}}{1-\eta^2}\left(P_{2l}(P_1P_{2m})' + P_{2l}P_{2m}\right)\Big]\Bigg\}\Bigg\|\,, \qquad (3.9)
\end{aligned}
$$

$$
\begin{aligned}
h_3 \;&= x\sqrt{1-\eta^2}\Bigg[1 + f^2\sum_{l\geq 0}P_{2l}\left(\lambda_{l,1} - \frac{\eta^2 t_{l,1}}{1-\eta^2}\right) \\
&\qquad +f^4\sum_{l\geq 0}P_{2l}\left(\lambda_{l,2} - \frac{\eta^2 t_{l,2}}{1-\eta^2}\right) \\
&+f^4\sum_{l,m\geq 0}\frac{\eta^2 t_{l,1}}{1-\eta^2}P_{2l}P_{2m}\left(\lambda_{m,1} - \frac{t_{m,1}}{1-\eta^2}\right)\Bigg]\,. \qquad (3.10)
\end{aligned}
$$

It should also be noted that we have conserved the handedness of the system, allowing us to preserve vector identities (such as summation convention for $\mathbf{A}\times\mathbf{B}$). It is straightforward to see that the limit of $f = 0$ recovers a spherical co-ordinate system.

3.4 CALCULATION OF THE $\lambda_{l,a}$

Consider a general barotropic equation of state $p = p(\rho)$ and uniform rotation[3] at a rate Ω; hydrostatics gives (in spherical polar co-ordinates):

$$\nabla p = -\rho\nabla\Phi + \rho\nabla\left\{\frac{1}{3}\Omega^2 r^2[1 - P_2(\mu)]\right\} , \quad (3.11)$$

$$\nabla^2\Phi = 4\pi G\rho . \quad (3.12)$$

Thus it is convenient to define a modified potential $V = \Phi - \frac{1}{3}\Omega^2 r^2[1 - P_2(\mu)]$, which gives the analogous equations to these two above as:

$$\frac{1}{\rho}\nabla p = -\nabla V , \quad (3.13)$$

$$\nabla^2 V = 4\pi G\rho - 2\Omega^2 , \quad (3.14)$$

which equations have no reference to basis choice beyond what is contained implicitly in the ∇ and ∇^2.

The definition of x is such that it is constant on surfaces of constant modified equipotential, V. This means that only the x component of ∇V is non-zero, and thus, by taking the curl of equation (3.13), $p = p(x)$ and $\rho = \rho(x)$ also, so our surfaces of constant p, ρ and V coincide: there is no baroclinicity. This fact that p, ρ and V have the same asphericity is what we expect for a barotropic equation of state. However, it is worth noting that because of this, V and ρ contain no Ω^2 terms. Thus

[3]We have picked uniform rotation for simplicity; the analysis given proceeds almost identically for conservative rotation laws, giving very similar equations.

$$\frac{1}{\rho}\frac{\partial p}{\partial x} = -\frac{\partial V}{\partial x} , \tag{3.15}$$

$$\frac{\partial^2 V}{\partial x^2} + \frac{2}{x}\frac{\partial V}{\partial x} = 4\pi G\rho , \tag{3.16}$$

which is the same form of equations as for a non-rotating star, but now viewed in the distorted co-ordinate frame. Although this result has to be the case (consider the case of zero rotation, $f = 0$, with x and r being the same), it is still very significant, as it means that the results from zero rotation are still consistent to zeroth order for a rotating star.

To higher orders, equation (3.13) does not yield any more equations, as it only differs from the zero-rotation case by a multiplicative factor of h_1^{-1} identically on both sides. However, our modified Poisson equation, having subtracted equation (3.16) yields:

$$\left(\frac{1}{h_1^2} - 1\right)\frac{\partial^2 V}{\partial x^2} + \left(\frac{1}{h_1 h_2 h_3}\frac{\partial}{\partial x}\left(\frac{h_2 h_3}{h_1}\right) - \frac{2}{x}\right)\frac{\partial V}{\partial x} = -2\Omega^2 , \tag{3.17}$$

which gives, at orders f^2 and f^4 respectively[4]

$$\lambda''_{l,1}(x\tilde{V}') + \lambda'_{l,1}(2x\tilde{V}'' + 4\tilde{V}') + \lambda_{l,1}\left(\frac{\tilde{V}'}{x}(4 - 2l(2l+1)) + 2\tilde{V}''\right) = \delta_{l,0}\left(2\frac{\tilde{V}}{V}\frac{\Omega^2}{f^2}\right) , \tag{3.18}$$

[4] $\tilde{V}$ is a suitably scaled V. As before, the listing of the independent variables has been dropped to save room – all are functions of x, apart from Legendre polynomials, which are functions of η. To save on space, derivatives are denoted by primes, and will be either $\frac{\partial}{\partial x}$ or $\frac{\partial}{\partial \nu}$ as appropriate.

3.4 Calculation of the $\lambda_{l,a}$

$$\lambda''_{l,2}(x\tilde{V}') + \lambda'_{l,2}(2x\tilde{V}'' + 4\tilde{V}') + \lambda_{l,2}\left(\frac{\tilde{V}'}{x}(4 - 2l(2l+1)) + 2\tilde{V}''\right) = -B_l \ . \quad (3.19)$$

We can calculate the B_l as being the coefficient of P_{2l} in

$$\begin{aligned}
&\sum_{l,m} \Big\| \tilde{V}'' \Big[3P_{2l}P_{2m}(x\lambda_{l,1})'(x\lambda_{m,1})' \\
&-2(1-\eta^2)P'_{2l}P'_{2m}\lambda_{l,1}\lambda_{m,1} \Big] + \tilde{V}' \Big\{ \frac{6}{x}P_{2l}P_{2m}(x\lambda_{l,1})'(x\lambda_{m,1})' \\
&-\frac{4}{x}(1-\eta^2)P'_{2l}P'_{2m}\lambda_{l,1}\lambda_{m,1} - 2P_{2l}(\eta P_{2m})'(\lambda_{l,1}t_{m,1})' \\
&+[(\eta P_{2l})'t'_{l,1} + 2P_{2l}\lambda'_{m,1}][(\eta P_{2m})'t_{m,1} + 2P_{2m}\lambda_{m,1}] \\
&+2P_{2l}(x\lambda_{l,1})'[(\eta P_{2m})'t'_{m,1} + 2P_{2m}\lambda'_{m,1}] \\
&-2\lambda_{l,1}\lambda'_{m,1}[P_{2l}P_{2m} - 2(1-\eta^2)P'_{2l}P'_{2m}] \\
&+\frac{\lambda_{l,1}}{x}(x\lambda_{m,1})'\left[(1-\eta^2)P'_{2l}P'_{2m} - 2l(2l+1)P_{2l}P_{2m}\right] \\
&+\frac{3\lambda_{l,1}}{x}t_{m,1}\left[(1-\eta^2)P'_{2l}(\eta P_{2m})'' - 2l(2l+1)P_{2l}(\eta P_{2m})'\right] \\
&-P_{2l}P_{2m}(x\lambda_{l,1})'(x\lambda_{m,1})'' \Big\} \Big\| \ , \quad (3.20)
\end{aligned}$$

which will later give non-zero B_l for l in $\{0,\ 1,\ 2\}$, and $B_l = 0$ otherwise.

Once the non-rotating structure is calculated, it is a conceptually simple matter to solve the equations (3.18) and (3.19), once we have boundary conditions, to give the $\lambda_{l,a}$.

Alteration to structure for a barotropic equation of state

3.4.1 Boundary conditions for $\lambda_{l,a}$

We have arrived at second-order equations ((3.18) and (3.19)) for the distortion of the star, but must consider the boundary conditions that complete the statement of the problem and allow a unique solution to be found.

Imposing regularity at $x = 0$ of the solution to these equations gives one of the boundary conditions for this system; it is[5]

$$\lim_{x \to 0} \lambda_{l,1} = A_1 \delta_{l,0} \ , \tag{3.21}$$

$$\lim_{x \to 0} \lambda_{l,2} = A_2 \delta_{l,0} \ . \tag{3.22}$$

At the surface, $x = x_0$, we match Φ onto a vacuum solution

$$\Phi_{\text{vac}} = \sum_{l \geq 0} \frac{a_l}{r^{l+1}} P_l(\mu) \tag{3.23}$$

expressed in terms of x and η, to obtain the second boundary condition. To order f^0 this gives:

$$a_l \propto \delta_{l,0} \tilde{V}'(x_0) \ . \tag{3.24}$$

Which will result for solid body rotation, to order f^2, (as will be seen in chapter 5) in non-zero outer boundary conditions only for $l = 0$ and $l = 1$. From this fact and equation (3.18) it can be seen that the only non-zero $\lambda_{l,1}$ are for l equal to 0 and 1, greatly simplifying some of the summations throughout this chapter.

The f^4 outer boundary conditions contain $t_{l,1}$, and thus it is apparent that, before proceeding, consideration must now be turned to these $t_{l,a}$.

[5]The fact that $\lim_{x \to 0} \lambda_{1,1} = 0$ requires some algebra, owing to the cancellation that will occur inside the bracket multiplying $\lambda_{1,1}$ in equation (3.18). However, it is easy to appreciate physically that our equipotential surfaces tend towards spheres as we approach the centre of the star.

3.4 Calculation of the $\lambda_{l,a}$

3.4.2 Defining the $t_{l,a}$ by orthogonality

One of the central points of this basis choice is that it retains the orthogonality of the basis vectors by the rescaling effect of the $t_{l,a}$ in equation (3.2). This defines the $t_{l,a}$, and is implicit in the equations for the metric coefficients h_i. However, an explicit derivation will be presented here.

It is possible to define $\mathbf{e}_x \equiv \widehat{\nabla x}$ and $\mathbf{e}_\eta \equiv \widehat{\nabla \eta}$ in spherical polar co-ordinates, as in equation (3.4). Taking the scalar product of these two vectors shows that the conditions for orthogonality are, to order f^2 and f^4 respectively:

$$\sum_{l \geq 0} \eta P_{2l} t'_{l,1} = -\sum_{l \geq 0} (1-\eta^2) P'_{2l} \frac{\lambda_{l,1}}{x} , \quad (3.25)$$

$$\sum_{l \geq 0} \eta P_{2l} t'_{l,2} = -\sum_{l \geq 0} (1-\eta^2) P'_{2l} \frac{\lambda_{l,2}}{x} + \sum_{l,m \geq 0} (1-\eta^2) P'_{2l} \frac{\lambda_{l,1}}{x} \left[(x\lambda_{m,1})' P_{2m} + 3(\eta P_{2m})' t_{m,1} \right] . \quad (3.26)$$

Now equation (3.25), using the fact that $\lambda_{l,1} = 0$ for all x if l is not 0 or 1, gives:

$$t'_{l,1} = 2\frac{\lambda_{1,1}}{x} \times (-\delta_{l,0} + \delta_{l,1}) . \quad (3.27)$$

Thus the $t_{l,1}$ are determined to within a constant. For $l > 1$ it is obviously sensible to pick this to be 0, so that these $t_{l,1}$ vanish. For $l \in \{0, 1\}$ we realise that it is desired to map both $\eta = 0$ onto $\mu = 0$, which is automatically satisfied, and $\eta = 1$ onto $\mu = 1$. To order f^2, this needs $t_{1,1} = -t_{1,0}$ for all x. The derivatives obviously allow this with the choice $t_{1,1}(0) = -t_{1,0}(0)$.

To select our remaining constant, there remains an arbitrary choice, but choosing $t_{1,0}(0) = 0$ is sensible owing to the fact

that very close to the centre the equipotentials are approximately spherical.

The choice of $t_{l,a}$ and the fact that $\lambda_{l,1} \equiv 0 \; \forall \, i > 1$ tightens the outer boundary conditions for $\lambda_{l,2}$ to be non-zero only for l equal to 0, 1, or 2. Thus, similarly to the f^2 correction terms, the only non-zero $\lambda_{l,2}$ are for these l. This, likewise, tightens the equations in (3.26) to:

$$\begin{aligned} t'_{0,2} &= -2\frac{\lambda_{1,2}}{x} + \frac{44}{9}\frac{\lambda_{2,2}}{x} \\ &- \frac{2\lambda_{1,1}}{x}\left[\frac{9}{5}t_{1,1} + \frac{1}{5}(x\lambda_{1,1})' - (x\lambda_{0,1})'\right] , \end{aligned} \tag{3.28}$$

$$\begin{aligned} t'_{1,2} &= 2\frac{\lambda_{1,2}}{x} - \frac{80}{9}\frac{\lambda_{2,2}}{x} \\ &- \frac{2\lambda_{1,1}}{x}\left[\frac{-5}{7}(9t_{1,1} + (x\lambda_{1,1})') + (x\lambda_{0,1})'\right] , \end{aligned} \tag{3.29}$$

$$t'_{2,2} = 4\frac{\lambda_{2,2}}{x} - \frac{36}{35}\frac{\lambda_{1,1}}{x}\left[9t_{1,1} + (x\lambda_{1,1})'\right] , \tag{3.30}$$

and $t'_{l,2} = 0$ otherwise. As for f^2, the mapping needs to take $\eta = 0$ and $\eta = 1$ to $\mu = 0$ and $\mu = 1$ respectively. The first is automatically satisfied, and the second reduces to the constraint $t_{0,2}(x) + t_{1,2}(x) + t_{2,2}(x) = 0$. Now, adding the equations for $t'_{l,2}$ obtains:

$$t'_{0,2} + t'_{1,2} + t'_{2,2} = 0 \, . \tag{3.31}$$

So again the equations allow $\eta = 1$ to map to $\mu = 1$, as long as the constants of integration are chosen suitably. Again the physics of the problem encourages us to pick the surfaces near $x = 0$ to be spherical ($t_{l,2}(\epsilon) \approx 0$).

3.5 Mass "Alteration" resulting from the change of Basis

When scaling the frequencies of a star, especially polytropes, the natural scaling often used is to divide by $\sqrt{GM/R^3}$. Obviously, when then scaling up the frequencies thus calculated, changes in the mass will lead to different predicted frequencies.

Were we hypothetically to spin up a star, centrifugal force would cause the star to become oblate and occupy a larger volume. This would occur without changing the mass, meaning a change in pressure and density at points in the star, specifically a reduction in central pressure and density. However, mathematically the structure equations are often solved by integrating from a given central pressure and density.

Many authors (for example Saio, 1981) keep the central density and pressure (hence polytropic constant) fixed. This causes the mass they give to vary, as given in, with some values tabulated, James (1964). For a barotropic equation of state this "alteration" to the mass can be removed by re-scaling of the central density, but we must be careful to act in a consistent manner, or confusion can arise, as has been noted by Christensen-Dalsgaard and Thompson (1999).

This re-scaling of central pressure and density cannot be done for a non-barotropic equation of state, and is not sensible even for barotropic equations of state. The reason for this is that for a lone star, we cannot measure the mass, but only the effective temperature and luminosity of the object, from which the mass is deduced. Thus if we are seeking to model stars, we should leave the mass as a variable to be resultant from, rather than driving, our analysis.

We therefore need to quantify how much taking a given density profile for a rotating star changes the mass from the result that would be given by taking the same density profile in a rotating star.

Alteration to structure for a barotropic equation of state

It has been seen from equations (3.15) and (3.16) that the structure of $\rho(x)$ for the centrifugally distorted star is the same as $\rho(r)$ for the equivalent non-rotating star. However, the mass of the star is defined as:

$$M = \int_0^{2\pi} \int_{-1}^{1} \int_0^{R_*(\mu,\phi)} \rho(r,\mu) r^2 \mathrm{d}r\mathrm{d}\mu\mathrm{d}\phi \ , \tag{3.32}$$

which in the new co-ordinates is:

$$\begin{aligned} M &= \int_0^{2\pi} \int_{-1}^{1} \int_0^{x_0} \rho(x) r^2(x,\eta) \frac{\partial(r,\mu)}{\partial(x,\eta)} \mathrm{d}x\mathrm{d}\eta\mathrm{d}\phi \\ &= 2\pi \int_{-1}^{1} \int_0^{x_0} \rho(x) r^2(x,\eta) \frac{\partial(r,\mu)}{\partial(x,\eta)} \mathrm{d}x\mathrm{d}\eta \ , \end{aligned} \tag{3.33}$$

with both r^2 and the Jacobian being able to be calculated as before. This again has a natural decomposition into coefficients of f^{2a}, $M = M_0 + f^2 M_1 + f^4 M_2$, with

$$M_0 = 4\pi \int_0^{x_0} \mathrm{d}x \rho(x) x^2 \ , \tag{3.34}$$

$$M_1 = 4\pi \int_0^{x_0} \mathrm{d}x \rho(x) x^2 \left((x\lambda_{0,1})' + 2\lambda_{0,1} \right) \ , \tag{3.35}$$

$$\begin{aligned} M_2 &= 4\pi \int_0^{x_0} \mathrm{d}x \rho(x) x^2 \\ &\times \left[(x\lambda_{0,2})' + 2\lambda_{0,2} + \frac{3}{5}(x\lambda_{1,1})' t_{1,1} + \lambda_{1,1}^2 \right] \ . \end{aligned} \tag{3.36}$$

This allows us to quantify the "alteration" to the mass by carrying across a given density profile from spherical polar co-ordinates into our new co-ordinates mapping out the surfaces of constant modified equipotential V in the rotating star. However, as dis-

cussed in chapter 6, a thoughtful consideration of M_0 is important before the analysis begins.

Chapter 4

Adiabatic pulsations in the new basis

'*We used to think that if we knew one, we knew two, because one and one are two. We are finding that we must learn a great deal more about "and"*' – Sir Arthur Eddington

4.1 Motivation

In the last chapter, a generalized orthogonal co-ordinate system mapping out the modified equipotentials was described, and a way of finding the mapping between these surfaces and standard spherical polars was shown. In this basis, it is desired to calculate the pulsations. The method for doing this is given in this chapter, with results displayed in chapter 5.

4.2 Pulsation equations in the new basis

As with standard pulsational theory, it is possible to perturb the equations of hydrostatic support (equations (3.13) and (3.14)) in the new basis[1], doing this under uniform rotation and the Cowling Approximation. It gives, along with the equations governing adiabatic pulsations and the continuity equation (assuming $e^{-i\omega t}$

[1]Note that the mapping is not perturbed.

dependence; p', ρ' and V' are the Eulerian perturbations to p, ρ and V respectively):

$$-\rho\omega^2\boldsymbol{\xi} + 2\mathrm{i}\rho\omega\Omega \times \boldsymbol{\xi} = -\nabla p' - \rho'\nabla V - \rho\nabla V' \,, \tag{4.1}$$

$$\nabla^2 V' = 4\pi G\rho' + 2\Omega^2 \,, \tag{4.2}$$

$$\frac{p'}{p} = \gamma_1 \left(\frac{\rho'}{\rho} + (\boldsymbol{\xi}.\nabla)\left(\ln\rho - \frac{1}{\gamma_1}\ln p \right) \right) \,, \tag{4.3}$$

$$\rho' + \nabla.(\rho\boldsymbol{\xi}) = 0 \,. \tag{4.4}$$

These are almost the same equations as for a spherically symmetric configuration, the only changes being replacing Φ with V, and the extra $2\Omega^2$ term in equation (4.2). Thus, under the Cowling Approximation, setting ϵ to be $\Omega.\mathbf{e}_\eta$ and ν to be $2\boldsymbol{\Omega}.\boldsymbol{e}_x/\omega$:

$$-\rho\omega^2\xi_x + \frac{1}{h_1}\frac{\partial p'}{\partial x} + \rho'\frac{1}{h_1}\frac{\partial V}{\partial x} = -2\mathrm{i}\rho\omega\epsilon\xi_\phi \,, \tag{4.5}$$

$$-\rho\omega^2\xi_\eta - \mathrm{i}\rho\omega^2\nu\xi_\phi + \frac{1}{h_2}\frac{\partial p'}{\partial \eta} = 0 \,, \tag{4.6}$$

$$-\rho\omega^2\xi_\phi + \mathrm{i}\rho\omega^2\nu\xi_\eta + \frac{1}{h_3}\frac{\partial p'}{\partial \phi} = 2\mathrm{i}\rho\omega\epsilon\xi_x \,. \tag{4.7}$$

Thus an obvious outworking of the generalization of the Traditional Approximation would be to ignore the terms that couple the x component of equation (4.1) to the other equations for components of $\boldsymbol{\xi}$ (i.e assuming ϵ to be a factor whose effects are considered small). The form of the terms neglected is geometrically the same, as the choice of equator is such that $\boldsymbol{\Omega}$ is orthogonal to $\boldsymbol{e}_\phi$, apart from the coefficient of ϵ changing between ξ_x and ξ_ϕ.

With this approximation, it is possible to write ξ_η and ξ_ϕ in terms of p'/ρ (note that we *can* place $1/\rho$ inside the angular derivatives owing to the choice of co-ordinate system); placing

these in the continuity equation gives (with $e^{im\phi}$ dependence):

$$\begin{aligned}
&(h_1h_2h_3)\rho' + \frac{\partial}{\partial x}(h_2h_3\rho\xi_x) \\
&+\frac{\rho}{\omega^2}\left[\frac{\partial}{\partial\eta}\left(\frac{h_1}{1-\nu^2}\left(\frac{h_3}{h_2}\frac{\partial}{\partial\eta}+\nu m\right)\right)\right. \\
&\left.-\frac{mh_1}{1-\nu^2}\left(\nu\frac{\partial}{\partial\eta}+\frac{mh_2}{h_3}\right)\right]\left(\frac{p'}{\rho}\right) = 0\ . \qquad (4.8)
\end{aligned}$$

This equation, the equation governing ξ_x, (equation (4.5)), and the adiabatic equation, (equation (4.3)), describe the pulsations. From here the analysis proceeds as in the introduction. It is worth noting that these equations ((4.1), (4.3) and (4.8)) give the right limit when $f = 0$ and we recover spherical polar co-ordinates.

For a non-rotating basis, the square bracket in equation (4.8) is the only thing explicitly involving angular dependence, so we assume a separable solution, the angular part of which is an eigenfunction of the square bracket with eigenvalue $-L^2$. However, with our new basis, the h_i contain sums of angular functions, so it is apparent that it is necessary to think of another way or be a little more clever about it.

4.3 RE-CASTING THE PULSATION EQUATIONS IN SELF-ADJOINT FORM

Lynden-Bell and Ostriker (1967)[2] re-cast the pulsational equations in a self-adjoint form, which thus had an associated variational principle with it. The equation they obtained was:

$$-\omega^2\mathbf{A}.(\boldsymbol{\xi}) + \omega\mathbf{B}.(\boldsymbol{\xi}) + \mathbf{C}.(\boldsymbol{\xi}) = 0\ , \qquad (4.9)$$

[2]To save on space, their analysis is not reproduced here.

with, for no background flow[3],

$$\begin{aligned}
\mathbf{A} &= \rho_0 \mathbf{I} \ , && (4.10)\\
\mathbf{B}.(\boldsymbol{\xi}) &= 2\mathrm{i}\rho_0 \boldsymbol{\Omega} \times \boldsymbol{\xi} \ , && (4.11)\\
\mathbf{C}.(\boldsymbol{\xi}) &= \mathbf{T}.(\boldsymbol{\xi}) + \mathbf{P}.(\boldsymbol{\xi}) + \mathbf{V}.(\boldsymbol{\xi}) \ , && (4.12)\\
\mathbf{T}.(\boldsymbol{\xi}) &= \rho_0 \boldsymbol{\Omega} \times (\boldsymbol{\Omega} \times \boldsymbol{\xi}) \ , && (4.13)\\
\mathbf{P}.(\boldsymbol{\xi}) &= \nabla \left[(1-\gamma_1) p_0 \nabla . \boldsymbol{\xi} \right] - p_0 \nabla (\nabla . \boldsymbol{\xi}) \\
&- \nabla \left[(\boldsymbol{\xi} . \nabla) p_0 \right] + (\boldsymbol{\xi} . \nabla) \nabla p_0 \ , && (4.14)\\
\mathbf{V}.(\boldsymbol{\xi}) &= \rho_0 (\boldsymbol{\xi} . \nabla) \nabla \Phi_0 \ . && (4.15)
\end{aligned}$$

It should be noted that, written in the form of equations (4.10)-(4.15), these equations make no reference to basis choice, and are self-adjoint over the inner product[4]:

$$\langle \tilde{\boldsymbol{\xi}}, \boldsymbol{\xi} \rangle = \int \tilde{\boldsymbol{\xi}}^* . \boldsymbol{\xi} d^3\mathbf{x} \ . \qquad (4.16)$$

4.3.1 Generalizing the Traditional Approximation

There are two obvious possible definitions of the generalized Traditional Approximation; one is only to replace $\mathbf{B}$ with $\mathbf{B}_{\mathrm{TA}}$, given by:

$$\mathbf{B}_{\mathrm{TA}} \equiv 2\mathrm{i}\Omega\rho_0\eta \begin{pmatrix} 0 & 0 & 0 \\ 0 & 0 & -1 \\ 0 & 1 & 0 \end{pmatrix} \ . \qquad (4.17)$$

The other is to neglect consistently all terms in $\Omega.\mathbf{e}_\eta$, including the terms in $\mathbf{T}.(\boldsymbol{\xi})$. This second definition includes the steps

[3]To obtain equation (4.15), the Cowling approximation has been implicitly assumed.

[4]Note this is the same definition as given by equation (2.44), but has been reproduced here.

taken for the first, but goes further in a search for consistency. However, it also neglects terms in the centrifugal force, making it unclear which is the better assumption.

To arrive at our background state, we have absorbed the centrifugal effects of rotation into the definition of V (see, for example, equations (3.13) and (3.14)) before perturbing. This means that the operator $\mathbf{T}.(\boldsymbol{\xi})$ will be "absorbed" into $\mathbf{V}.(\boldsymbol{\xi})$, replacing equation (4.15) with

$$\tilde{\mathbf{V}}.(\boldsymbol{\xi}) = \rho_0(\boldsymbol{\xi}.\nabla)\nabla V_0 \,, \tag{4.18}$$

and altering the definition of $\mathbf{C}.(\boldsymbol{\xi})$ to:

$$\mathbf{C}.(\boldsymbol{\xi}) = \mathbf{P}.(\boldsymbol{\xi}) + \tilde{\mathbf{V}}.(\boldsymbol{\xi}) \,. \tag{4.19}$$

If one looks at the definition of $\mathbf{B}_{\mathrm{TA}}$, given by equation (4.17), the matrix is obviously Hermitian, and therefore $\mathbf{B}_{\mathrm{TA}}$ is self-adjoint over the inner product in equation (4.16). Thus the new system, given by:

$$-\omega^2\mathbf{A}.(\boldsymbol{\xi}) + \omega\mathbf{B}_{\mathrm{TA}}.(\boldsymbol{\xi}) + \mathbf{C}.(\boldsymbol{\xi}) = 0 \tag{4.20}$$

is still self adjoint, and has an associated variational principle, which will now be exploited.

4.4 EQUATIONS FOR THE FREQUENCY SHIFTS AND THE ALTERATION TO EIGENFUNCTIONS

4.4.1 FREQUENCY SHIFTS

The distorted orthogonal co-ordinates calculated in the previous chapter retain the structure of the pulsational equations. However, ∇ and associated operators have f^2 and f^4 corrections to them[5], which can be viewed as perturbations about the f^0 state

[5]We shall be neglecting higher orders than these.

for small values of f.

We define δ as the alteration to order f^2 of the object (eigenvalue, eigenvector or operator) upon which it acts, and δ_2 as the alteration to order f^4. Thus, expanding $\mathbf{C} \to \mathbf{C} + f^2\delta\mathbf{C} + f^4\delta_2\mathbf{C}$, and the other terms similarly[6] in equation (4.20), and taking the inner product given by equation (4.16) (which it should be noted also needs to be expanded in powers of f, owing to the presence of the Jacobian $\partial(x, y, z)/\partial(x, \eta, \phi)$), the following formulae are obtained:

$$\delta\omega = \frac{\langle \boldsymbol{\xi}, \delta\mathbf{C}.(\boldsymbol{\xi})\rangle_0}{-2\omega\langle \boldsymbol{\xi}, \rho_0\boldsymbol{\xi}\rangle_0}, \quad (4.21)$$

$$\delta_2\omega = -\frac{(\delta\omega)^2}{2\omega} + \frac{\omega\langle \boldsymbol{\xi}, \delta\mathbf{B}_{\mathrm{TA}}.(\delta\boldsymbol{\xi})\rangle_0 + \langle \boldsymbol{\xi}, \delta_2\mathbf{C}.(\boldsymbol{\xi})\rangle_0 + \langle \boldsymbol{\xi}, \delta\mathbf{C}.(\delta\boldsymbol{\xi})\rangle_0}{-2\omega\langle \boldsymbol{\xi}, \boldsymbol{\xi}\rangle_0}. \quad (4.22)$$

It should be noted to re-derive these equations that much cancellation occurs both from the constraint that we take $\delta\boldsymbol{\xi}$ and $\delta_2\boldsymbol{\xi}$ orthogonal to $\boldsymbol{\xi}$, and from the use of previous orders of governing equations to cancel terms inside, for example, $\langle\ ,\ \rangle_2$ terms in the equation for $\delta_2\omega$. This will be done in appendix B. However, the exact equations for, for example, $\delta_2\mathbf{C}$ in terms of the $\lambda_{l,a}$ are extremely long and involved, and will not be reproduced here; the derivation of these equations is outlined in appendix D.

The completeness of the $\delta\boldsymbol{\xi}$ has also been assumed; this will be touched upon later.

[6] It will prove mathematically useful to take the perturbations to the eigenfunction (i.e. $\delta\boldsymbol{\xi}$ and $\delta_2\boldsymbol{\xi}$) orthogonal, under the inner product given, to the original eigenfunction; this is allowed, as components in the direction of the original eigenfunction can be absorbed into the normalization of $\boldsymbol{\xi}$.

4.4.2 ALTERATION TO EIGENFUNCTIONS

To calculate the alteration to the eigenfunctions, it is necessary to return to the continuity equation, and also the equation governing ξ_x, after the elimination of ρ':

$$-\rho\omega^2\xi_x + \frac{1}{\rho h_1}\frac{\partial p'}{\partial x} + \frac{1}{h_1}\frac{\partial V}{\partial x}\left(\frac{p'}{\gamma_1 p} - \frac{\xi_x A}{h_1}\right) = 0 \ , \tag{4.23}$$

$$(h_1h_2h_3)\left(\frac{p'}{\gamma_1 p} - \frac{\xi_x A}{h_1}\right) + \frac{1}{\rho}\frac{\partial}{\partial x}(h_2h_3\rho\xi_x) + \frac{1}{\omega^2}\mathcal{L}_{\rm tot}\left(\frac{p'}{\rho}\right) = 0 \ , \tag{4.24}$$

with

$$A \equiv \frac{\partial}{\partial x}\left(\ln\rho - \frac{1}{\gamma_1}\ln p\right) \ , \tag{4.25}$$

$$\mathcal{L}_{\rm tot} \equiv \frac{\partial}{\partial\eta}\left(\frac{h_1}{1-\nu^2}\left(\frac{h_3}{h_2}\frac{\partial}{\partial\eta} + \nu m\right)\right) - \frac{mh_1}{1-\nu^2}\left(\nu\frac{\partial}{\partial\eta} + \frac{mh_2}{h_3}\right) \ . \tag{4.26}$$

Equations (4.23) and (4.24) can then be themselves expanded in terms of f^2, as above, and then re-arranged to provide the governing equations for the perturbation to the eigenfunction in terms of $\delta\omega$ and the zeroth-order solution. The equations thus derived are of the same form as those for the zeroth-order solution, with an extra forcing function being linear in the zeroth-order solution. For numerical ease, the scalings used are those used in equations (2.17) and (2.18), and the resulting equations are

4.4 Equations for the frequency shifts and the alteration to eigenfunctions

$$x\frac{\partial(\delta z)_1}{\partial x} = \left(\frac{V_\mathrm{h}}{\gamma_1} - 3\right)(\delta z)_1 + \left(\frac{L_1^2}{c_1\omega_0^2} - \frac{V_\mathrm{h}}{\gamma_1}\right)(\delta z)_2 + H(\mathbf{x}) \,, \tag{4.27}$$

$$x\frac{\partial(\delta z)_2}{\partial x} = (c_1\omega_0^2 + xA)(\delta z)_1 + (1 - U - xA)(\delta z)_2 + K(\mathbf{x}) \,, \tag{4.28}$$

with

$$H(\mathbf{x}) \equiv -xz_1 \sum_l (2\lambda'_{l,1}P_{2l} + t'_{l,1}(\eta P_{2l})') - z_2\frac{V_\mathrm{h}}{\gamma_1}\sum_l (x\lambda_{l,1})'P_{2l} + \left[\mathcal{L}_1 + \left(\frac{-2\omega_1}{\omega_0} + \sum_l (2\lambda_{l,1}P_{2l} + t_{l,1}(\eta P_{2l})')\right)\mathcal{L}_0\right]\frac{z_2}{c_1\omega_0^2} \,, \tag{4.29}$$

$$K(\mathbf{x}) \equiv z_1\left[2c_1\omega_0\omega_1 + (c_1\omega_0^2 + xA)\sum_l (x\lambda_{l,1})'P_{2l}\right] \,. \tag{4.30}$$

It is important to note both that the completeness of the normal modes of oscillation in a general co-ordinate system was shown by Dyson and Schutz (1979), and also that the Traditional Approximation provides a description of p and g modes, *and* r modes simultaneously. These facts allow and encourage the use of the zeroth-order solutions as an expansion basis.

4.4.2.1 Angular dependence

It should be noted that the solutions of equations thus derived from equations (4.23) and (4.24) (i.e. equations (4.27) and (4.28))

are obviously not themselves separable, but, just as the forcing, can be defined as the sum of separable functions. The most natural decomposition is into Hough functions for the particular value of $\nu = 2\Omega/\omega_0$, which, as was remarked in chapter 2, form a complete set. Thus we pick:

$$\delta\boldsymbol{\xi} = \sum_l \delta\boldsymbol{\xi}_l(x)\Theta_{l,m}(\eta)e^{\mathrm{i}m\phi} \ . \tag{4.31}$$

However, computationally we need to truncate the expansion in Hough functions.

To calculate a good way to do this truncation, note that the metric coefficients h_i contain only $P_2(\eta)$ and terms which are constant in η. Were the eigenfunction expansion to have been in Legendre polynomials, this expansion would have contained only three terms (remember $P_2(\mu)P_{2l}(\mu) = N_1P_{2l-2}(\mu) + N_2P_{2l}(\mu) + N_3P_{2l+2}(\mu)$ for some coefficients N_i). Motivated by this, it would be expected that the magnitude of the integral:

$$N_{l,k} = \int_{-1}^{1} P_2(\eta)\Theta_{l,m}(\eta)\Theta_{k,m}(\eta)\mathrm{d}\eta$$

and similar integrals would drop-off rapidly as l counts away from k. This is indeed the case, as can be seen in figure 4.1.

This trend of very fast drop off for increasing $|l-k|$ continues for higher ν, and thus it is required to consider at most three or four $\Theta_{l,m}$ to either side of the $\Theta_{k,m}$ for approximating the perturbation to the eigenfunction. For more on this, the reader is directed to Chapman and Lindzen (1970).

4.4.2.2 BOUNDARY CONDITIONS

For the equations for the calculation of the alteration to the eigenfunction, the outer boundary condition remains that the derivative of the relative Lagrangian pressure perturbation vanishes.

4.4 Equations for the frequency shifts and the alteration to eigenfunctions

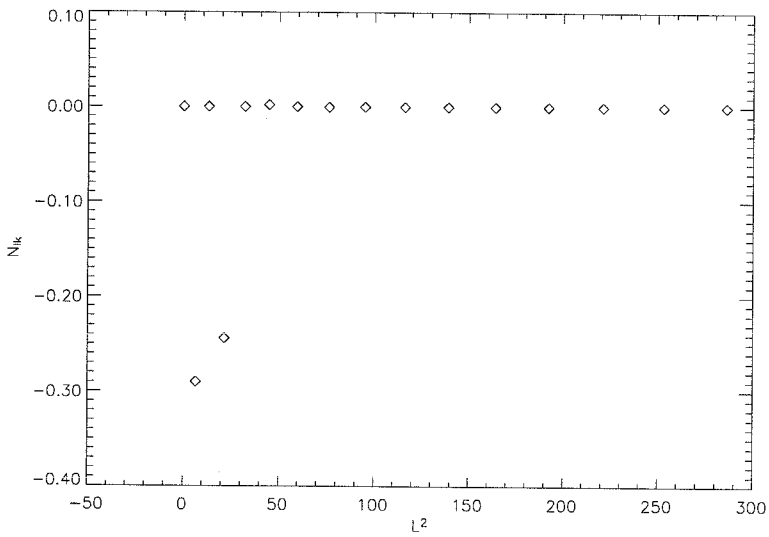

Figure 4.1: A graph of the value of $N_{l,k}$. The x-axis is the value of L^2 for l, with $\Theta^{k,m}$ being of even parity and $\lambda_0 = 6.7570$, $\nu = 0.3$ and $m = 2$.

For the inner boundary condition, note that the value of L^2 for the individual $\delta\boldsymbol{\xi}_l(x)$ is not necessarily the L_0^2 of the original mode; thus, as in chapter 2, the homogeneous system would desire $\delta\boldsymbol{\xi}_l(x) \sim x^\alpha$ with $\alpha = (-5 + \sqrt{1 + 4L^2})/2$, whereas the forcing behaves like x^β with $\beta = (-5 + \sqrt{1 + 4L_0^2})/2$. This gives rise to three possibilities:

- $\alpha < \beta$: behaviour of solution as $x \to 0$ becomes explicitly independent of the forcing of the original mode.
- $\alpha = \beta$: inner boundary condition fully contains the forcing.
- $\alpha > \beta$: assumption that the form of the solution as $x \to 0$ is governed by the homogenous equation breaks down; physically this is due to the fact that the interference pattern of all the modes of a given type does not cancel perfectly at the centre of the star.

4.5 MODE TRAPPING

It is also possible to explore the consequences of the distorted co-ordintate system for mode trapping; returning to equations (4.23) and (4.24), changing variables to $\delta p = p' - \rho g h_1^{-1} \xi_x$ and eliminating ξ_x between the two resultant equations gives a second-order equation for δp. As per standard mode trapping (Gough, 1993), we then introduce a new variable Ψ defined by

$$\Psi \equiv \left(\frac{g\rho\tilde{f}}{x h_2 h_3} \right) \delta p \,, \qquad (4.32)$$

$$\tilde{f} \equiv \frac{\omega^2 x}{g} h_1 + \frac{x g \Lambda_{\text{tot}}}{\omega^2 h_1^2 h_2 h_3} + \frac{x}{h_1} \frac{\partial}{\partial x} \left(\ln \left(\frac{h_1 h_2 h_3}{g} \right) \right) \,, \qquad (4.33)$$

to eliminate the single derivatives of δp. Doing this yields

$$\frac{\partial^2\Psi}{\partial r^2} + K^2\Psi = 0 \,, \tag{4.34}$$

with the following definitions:

$$\frac{\omega^2 c^2 K^2}{h_1^2} = (\omega^2 - \omega_+^2)(\omega^2 - \omega_-^2) \,, \tag{4.35}$$

$$\omega_\pm^2 \equiv \frac{1}{2}(S_l^2 + \omega_c^2) \pm \sqrt{\frac{1}{4}(S_l^2 + \omega_c^2)^2 - S_l^2\tilde{\mathcal{N}}^2} \,, \tag{4.36}$$

$$S_l^2 \equiv \frac{-c^2\Lambda_{\rm tot}}{h_1 h_2 h_3} \,, \tag{4.37}$$

$$\tilde{\mathcal{N}}^2 \equiv \frac{1}{h_1^2}\left(g\left(\tilde{\mathcal{H}}^{-1} - \frac{g}{c^2} - 2\tilde{h}^{-1}\right) + \frac{\partial}{\partial x}(\ln\Lambda_{\rm tot})\right) \,, \tag{4.38}$$

$$\omega_c^2 \equiv \frac{1}{h_1^2}\left(\frac{c^2}{4\tilde{\mathcal{H}}^2}\left(1 - 2\tilde{\mathcal{H}}'\right) - g\tilde{h}^{-1}\right) \,, \tag{4.39}$$

$$\tilde{h}^{-1} \equiv \frac{\partial}{\partial x}(\ln(h_2 h_3)) + H_g^{-1} - H_{h_1}^{-1} \,, \tag{4.40}$$

$$\tilde{\mathcal{H}}^{-1} \equiv \frac{\partial}{\partial x}(\ln(h_2 h_3)) + H_g^{-1} + H_{\tilde{f}}^{-1} + H^{-1} + \frac{1}{x} \,, \tag{4.41}$$

and $\Lambda_{\rm tot}$ is the outcome of the operator $\mathcal{L}_{\rm tot}$ having acted upon the angular part of Ψ:

$$\mathcal{L}_{\rm tot}\Psi = \Lambda_{\rm tot}\Psi \,. \tag{4.42}$$

Once again, note that these equations reduce to what is expected for zero rotation.

Equation (4.34) provides an immediate way to tell, by looking at the sign of K^2 if a mode is propagative ($K^2 > 0$, so solutions are of the form $\Psi = A\sin(Kx + B)$) or evanescent ($K^2 < 0$, so solutions are of the form $\Psi = A\exp(\pm Kx)$). Equation (4.35) reveals the fact that this requirement for the modes to be prop-

agative is either

$$\omega \; > \; \omega_+ \, , \, \omega_- \tag{4.43}$$

or

$$\omega \; < \; \omega_+ \, , \, \omega_- \, . \tag{4.44}$$

With a natural definition of p modes (ω satisfies the inequalities (4.43)) and g modes (ω satisfies the inequalities (4.44)) arising from this, as for non-rotation[7]. It is then possible to plot both ω_- and ω_+ *as functions of both* x *and* η for a given frequency (note that this must be included for $\tilde{f}$ and its derivatives) to explore mode trapping as a function of latitude. Again, results for this are shown in the next chapter.

[7]It is worth noting that these equations ((4.32)-(4.41)) reduce to the known forms in the cases both of a plane parallel atmosphere and spherical geometry.

Chapter 5

Results for barotropic equations of state

"...mathematical proofs, like diamonds, are hard and clear, and will be touched with nothing but strict reasoning." – John Locke

Now that we have constructed the mathematical framework in which we can study the effects of rotation upon the pulsations, we can begin to quantify these effects, in the test case of barotropic equations of state. This will be broken down into viewing the immediate effects of the Coriolis force under the TA, then looking at how the star will distort due to centrifugal effects, and then the changes that these effects produce upon both the frequencies and the eigenfunctions. Mode trapping will also be explored.

5.1 Effects of the TA upon frequencies

The pulsational system has been reduced to the following form[1]

$$\begin{aligned} \mathcal{L}_\nu[\Theta(\mu;\nu)] &\equiv \frac{\mathrm{d}}{\mathrm{d}\mu}\left(\frac{1-\mu^2}{1-\nu^2\mu^2}\frac{\mathrm{d}\Theta}{\mathrm{d}\mu}\right) \\ &+ \frac{1}{1-\nu^2\mu^2}\left(m\nu\frac{1+\nu^2\mu^2}{1-\nu^2\mu^2} - \frac{m^2}{1-\mu^2}\right)\Theta \\ &= -L^2\Theta(\mu;\nu)\ , \end{aligned} \tag{5.1}$$

[1]Reproduced from equations (2.11), (2.15) and (2.16).

5.1 Effects of the TA upon frequencies

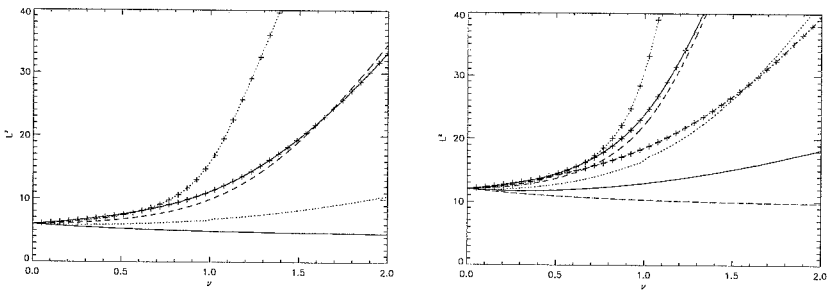

Figure 5.1: Left panel: L^2 dependence with ν for angular functions that start as $l = 2$. $m = 2, 1, 0, -1, -2$ are displayed as the solid curve, the dotted curve, the dashed curve, the dotted curve with crosses and the solid curve with crosses respectively. Right panel: as for left panel, but for functions that start as $l = 3$, $m = 3, -3$ are displayed in addition, by dot-dash lines and dot-dash lines with crosses respectively.

$$\frac{1}{r^2}\frac{\mathrm{d}}{\mathrm{d}r}\left(r^2\xi_r\right) - \frac{g}{c^2}\xi_r + \left(1 - \frac{L^2c^2}{\omega^2 r^2}\right)\frac{p'}{c^2} = 0\,, \tag{5.2}$$

$$\frac{\mathrm{d}p'}{\mathrm{d}r} + \frac{g}{c^2}p' + (N^2 - \omega^2)\rho\xi_r = 0\,; \tag{5.3}$$

we can see that the angular and radial parts of the system are only weakly coupled via the eigenvalues L^2 and ν.

Taking equation (5.1) alone for different given values of ν, the ν dependence of L^2 for an angular function that starts as $l = 2$ is displayed in figure 5.1 for various m values.

It can be seen that, as we would expect from equation (5.1), the shape of the ν dependence varies strongly with the m value. In fact, the L^2 values cross at various values of ν (the most obvious in figure 5.1 being the crossing of $m = 0$ and $m = -2$ curves at $\nu \approx 1.65$)[2]. Thus for large values of ν, we are going to deviate

[2]Figure 5.1 is similar to figure 2 in the paper by Bildsten et al. (1996),

by a very large extent from even splitting in m – in fact, we shall end up with the $m = 0$ and $m = -2$ modes being very finely split.

It is also worth noting that the L^2 value grows quickly with increasing ν for non-positive m values; thus were we to naïvely attempt a mode identification for large ν, we would mis-identify the l-value of the mode, possibly with non-negligable consequences. Also, rotation will produce selection effects upon the detection of modes, as the mode will be concentrated toward the equator, meaning that we might be unable to detect it if we see the star pole-on.

One of the most remarkable things about the left-hand panel of figure 5.1 is that it is the $m = -1$ mode that grows the fastest, not either the $m = 0$ nor the $m = -2$ mode. If we then look at the right-hand side of figure 5.1, it is apparent that this large growth is for the negative m values which begin neither having their dependence entirely in the μ nor in the ϕ direction.

The fact that it is negative values of m (i.e. retrograde) that will feel the effect of increasing ν most can be seen in the fact that for ν around unity there is no cancellation between the terms in the second bracket of equation (5.1). The fact that it is the modes that begin by not having their variation solely in the μ nor ϕ direction that are most effected by increasing rotation should not surprise us either, as these modes are the ones that will be distorted most by Coriolis terms under the TA.[3]

Figure 5.2 shows the evolution of the g_{13}, "$l = 2$" mode frequencies in an $n = 3$ polytrope with increasing f, in the co-rotating frame.

---

but these crossings appear to have gone unremarked.

[3]Mathematically, it is evident that the second bracket in equation (5.1) will vanish for $m = 0$. For an example of how the $L^2 \approx m^2$ can result in different mathematical structure (in the regime of $\nu \gg 1$), the reader is directed to the paper by Townsend (2003b).

5.1 Effects of the TA upon frequencies

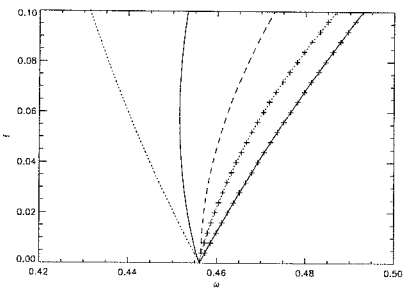

Figure 5.2: Evolution of the g_{13}, "$l = 2$" mode frequencies with increasing f, in the co-rotating frame. Key is as for figure 5.1.

We can see, as would be expected due to the fact that the only coupling of the angular behaviour into the radial behaviour is via the eigenvalue $L^2(\nu)$, that the evolution of the frequencies (in the co-rotating frame) follows a very similar pattern to the L^2 values. Looking at the asymptotic regime, Lee and Saio (1987) found that low-frequency g modes trapped between the boundary of the convective core ($r = r_c$) and the surface of a rotating early-type star have eigenfrequencies of[4]

$$\omega = \frac{2\sqrt{L^2}}{(k + n_e/2 - 1/6)} \int_{r_c}^{R} \frac{|N|}{r} \mathrm{d}r \qquad (5.4)$$

From equation (5.4) the broad qualitative similarity of the behaviour of L^2 (or rather $\sqrt{L^2}$) and ω as ν departs from zero for various m values can be seen. This similarity in pattern is going to cause, for mid- to high-ν, the frequencies to differ drastically from the even rotational splitting in m that is given by a perturbative

[4]This is derived by approximating the eigenfunction near the surface by the Bessel function of order n_e, where n_e is the effective polytropic index at the surface. k is the radial order of the mode.

analysis of the first order effects of rotation.

5.2 ROTATIONAL DISTORTION FOR POLYTROPES

For a polytropic equation of state with polytropic index n

$$p = K\rho^{1+1/n} , \tag{5.5}$$

we can make the following definitions

$$\rho = \rho_c\theta^n , \tag{5.6}$$

$$\tilde{V} = \frac{V}{K\rho_c(n+1)} , \tag{5.7}$$

which gives

$$\nabla\theta = -\nabla\tilde{V} ; \tag{5.8}$$

and the Lane-Emden equation for the zeroth-order solution:

$$\theta'' + \frac{2}{x}\theta' = -\theta^n . \tag{5.9}$$

Placing this in equations (3.18) and (3.19), after substituting for θ'', gives[5]

$$\lambda''_{l,1} = \frac{(2x\theta^n)\lambda'_{l,1} + \lambda_{l,1}\left(2\theta^n + 2l(2l+1)\frac{\theta'}{x}\right) - 2\xi_0^2\delta_{l,0}}{x\theta'} , \tag{5.10}$$

$$\lambda''_{l,2} = \frac{(2x\theta^n)\lambda'_{l,2} + \lambda_{l,2}\left(2\theta^n + 2l(2l+1)\frac{\theta'}{x}\right) + B_l}{x\theta'} . \tag{5.11}$$

[5]Units have been removed entirely, and the radial mesh rescaled to [0,1] by multiplying the equation by the square of the radius ξ_0. Note $\Omega = f\sqrt{4\pi G\rho_c}$ for polytropes.

5.2 Rotational Distortion for Polytropes

Returning to the boundary conditions for $\lambda_{l,a}$, equation (5.10) shows that imposing regularity at $x = 0$ gives:

$$\lim_{x \to 0} \lambda_{l,1} = \xi_0^2 \delta_{l,0} \ , \tag{5.12}$$

$$\Rightarrow \lim_{x \to 0} B_l = -9\,\tilde{\theta}'' \xi_0^4 \delta_{l,0} \ , \tag{5.13}$$

$$\lim_{x \to 0} \lambda_{l,2} = -\frac{1}{2} \lim_{x \to 0} B_l \ . \tag{5.14}$$

The outer boundary conditions (from matching Φ onto a vacuum solution) are[6]

$$a_l = \delta_{l,0} \frac{\theta'(x_0)}{\xi_0^2} \ , \tag{5.15}$$

$$\lambda'_{0,1} = \frac{-1}{a_0} \ , \tag{5.16}$$

$$2\lambda_{1,1} + \lambda'_{1,1} = \frac{5}{3a_0} \ , \tag{5.17}$$

$$\lambda_{l,1} = 0 \ , \ l > 1 \ , \tag{5.18}$$

to order f^0 and f^2. To order f^4,

$$\begin{aligned} 2\lambda_{0,2} - \lambda'_{0,2} &= \frac{-1}{a_0} \left((\lambda_{0,1} + \lambda'_{0,1}) + \frac{1}{3}(\lambda_{1,1} + \lambda'_{1,1}) \right) \\ &+ \frac{1}{5} \left(2\lambda_{1,1}^2 + 4\lambda_{1,1}\lambda'_{1,1} + 3t_{1,1}\lambda'_{1,1} - 6t_{1,1}\lambda_{1,1} \right) \ , \end{aligned} \tag{5.19}$$

$$\begin{aligned} 4\lambda_{1,2} - \lambda'_{1,2} &= \frac{1}{a_0} \left(\frac{5}{3}(\lambda_{0,1} - \lambda'_{0,1}) + \frac{17}{21}(\lambda_{1,1} - \lambda'_{1,1}) \right) \\ &+ \Big(-8\lambda_{0,1}\lambda_{1,1} + \lambda_{0,1}\lambda'_{1,1} + \lambda_{1,1}\lambda'_{0,1} + \frac{8}{7}\lambda_{1,1}\lambda'_{1,1} \end{aligned}$$

[6]Note that x_0 is 1.

$$+ \quad \frac{3}{7}t_{1,1}\lambda'_{1,1} - \frac{12}{7}t_{1,1}\lambda_{1,1} - \frac{10}{7}\lambda_{1,1}^2\Big) \ , \tag{5.20}$$

$$6\lambda_{2,2} - \lambda'_{2,2} = \frac{6}{7a_0}(3\lambda_{1,1} + \lambda'_{1,1})$$

$$+ \quad \frac{36}{35}\left(2\lambda_{1,1}\lambda'_{1,1} + 6\lambda_{1,1}t_{1,1} - \lambda'_{1,1}t_{1,1} - 7\lambda_{1,1}^2\right) \ , \tag{5.21}$$

$$\lambda_{l,2} = 0 \ , \ l > 2 \ . \tag{5.22}$$

5.2.1 RESULTS

As has been mentioned already, the alteration of the surface of the star is a long-studied subject, so as such, there are results (for instance, as published by James (1964) for polytropes) that we can compare the end values of our function to. Such a comparison is shown in figure 5.3.

For rotation rates up to roughly 25% of breakup, the agreement with the alternative method of calculating the equatorial and polar radii is very good indeed (the difference being of the order of the last decimal place given by James (1964)). The agreement remains good except for predicting polar radii for a rotation rate above 35–40% of the breakup value, when the f^4 correction proves too large. It is the case that the polar radius remains robust to increases in rotation rate until near breakup, when it shrinks dramatically with increasing rotation; thus a perturbation model has difficulty modelling high, but non-huge, rotation rates.

Whilst this fact requires us to check that we are not modelling a regime where the adoption of this perturbative method might cause problems, the method works very well for all rotation rates that we can foresee modelling.

The rescaling functions $\lambda_{l,a}(x)$ and $t_{l,a}(x)$ for this $n = 3$ polytrope are shown in figure 5.4. These are smooth, and the size of $\lambda_{i,2}$ is comparable with $\lambda_{j,1}^2$, as we would expect because of the form of B_l in equation (3.19). These facts are in accordance with

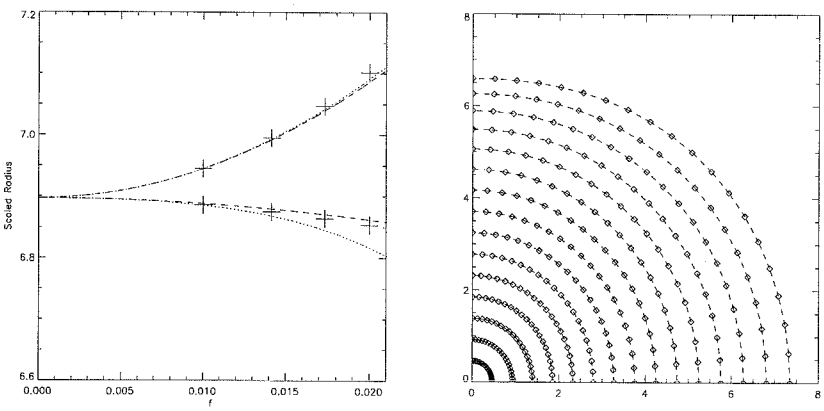

Figure 5.3: Left panel: Predictions to f^2 (dashed lines) and f^4 (dotted lines) for the equatorial (upper branch) and polar (lower branch) radii for a rotating polytrope of index $n = 3$; crosses are values from James (1964) using a numerical expansion in legendre polynomials for a given rotation rate; breakup is approximately at $f = 0.044$. Right panel: predictions of the surfaces of constant modified equipotential for this polytrope with a rotation rate of $f = 0.03$; diamonds map out curves of constant η. The oblate structure is clearly visible.

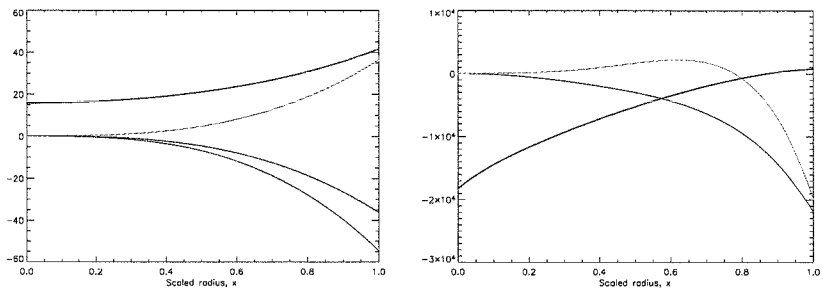

Figure 5.4: Graphs of rescaling functions for an $n = 3$ polytrope. Left panel: $\lambda_{0,1}$ (black), $\lambda_{1,1}$ (red), $t_{0,1}$ (green) and $t_{1,1}$ (blue). Right panel: $\lambda_{0,2}$ (black), $\lambda_{1,2}$ (red), and $\lambda_{2,2}$ (green).

what we would expect and desire.

5.3 EIGENFREQUENCY SHIFTS DUE TO CENTRIFUGAL FORCE

Graphs of the eigenfrequency for an $L^2 \approx 6$, g_{81} mode in a $n = 3$ polytrope (again used as an example), for various m values, rotation rates and order of corrections, are displayed in figure 5.5.

Several things are immediately noticeable from figure 5.5:

The first is that for this mode, and moderate rotation rates ($\approx$15% of breakup), the geometrical corrections[7] can dominate the non-geometrical Coriolis corrections, and are very large (depending upon the mode, the assumption of the centrifugal force as a perturbation breaks down; for example, for the worst case ($m = 1$) from about 18% of breakup; this should not surprise us,

[7]Note that these are not simply the corrections of centrifugal force upon the mode, but also the combination of Coriolis force and the basis distortion. Despite this, for brevity these will be referred to as "Centrifugal corrections".

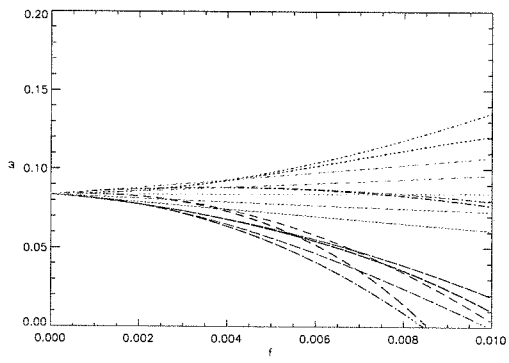

Figure 5.5: Graphs of the eigenfrequencies of a $L^2 \approx 6$, g_{81} mode (again for the $n = 3$ polytrope, viewed in an inertial frame) for different m values plotted and orders of corrections against rotation rate. Green is taking just into account the effects of the Traditional Approximation, red is with $O(f^2)$ corrections, black is with $O(f^4)$ corrections; $m = \{2, 1, 0, -1, -2\}$ are denoted by long dashed, dash dot dot dot, dotted, dashed and dash dot lines respectively.

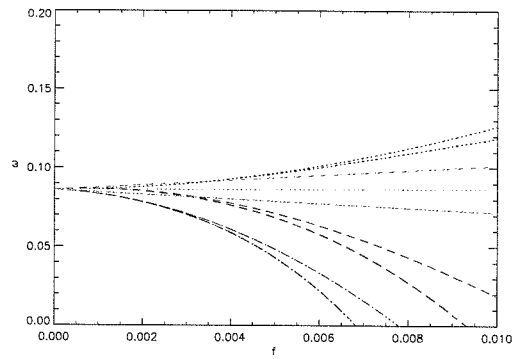

Figure 5.6: As for figure 5.5, but this time for g_{45}, $L^2 \approx 2$, hence only $m = \{1, 0, -1\}$ are shown with same key as for figure 5.5.

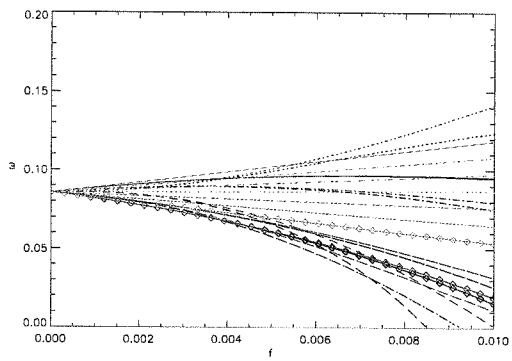

Figure 5.7: As for figure 5.5, but this time for g_{113}, $L^2 \approx 12$, hence in addition $m = \{-3, 3\}$ are also displayed by solid lines and solid lines with diamonds respectively.

given figure 5.3).

The second is that certain modes are far more resistant to large alteration by the effects of rotation than others. This is the result of a large number of effects cancelling each other out and may mean physically that the mode is more probable to occur, should the forcing be suitable[8].

The third is that the $|m| = 2$ modes have a smaller centrifugal correction to their frequency than the $|m| = 1$ modes in figure 5.5. If we then look at figure 5.7, we see that this is a general trend, that the higher the value of $|m|$, the smaller the centrifugal correction. This again makes physical sense, as the mode becomes more and more azimuthally dependent, the distortion of the equipotentials becomes less and less important, as this distortion is not in the ϕ-coordinate, only the (x, η) coordinates.

To investigate when the assumption of the Centrifugal force acting as a perturbation breaks down for a given mode, figure 5.8 shows the f^2 correction to the eigenfrequency against eigenfrequency (under the Traditional Approximation) for several rotation rates.

It is immediately noticeable that the form of the graphs for various rotation rates are very similar until ν becomes significantly different from zero. This is obviously what would be expected, but confirms the observation from figure 5.5 that for modes with small Coriolis parameter ν, the centrifugal corrections dominate.

The form of the graph is that the f^2 correction term grows quickly with decreasing ω_0 (roughly as ω_0^{-2}, half of which can be easily explained by the ω_0^{-1} factor in equation (4.21)) then turning over as the eigenfunction becomes increasingly oscilatory, so

[8]It is the case that observationally, we see more prograde γ-Doradus pulsations than other types, but this statement is an interesting observation of theoretical predictions only.

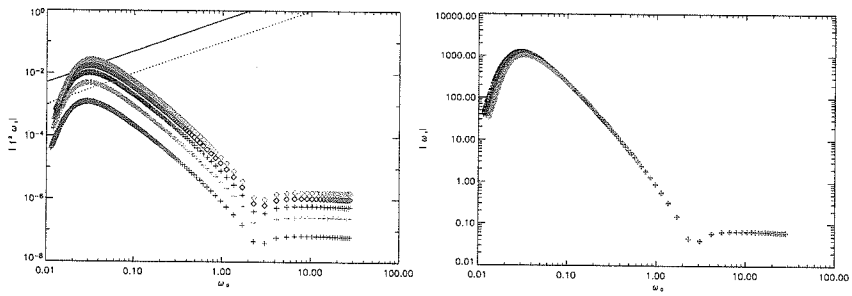

Figure 5.8: Left panel: Absolute values of the f^2 corrections to the eigenfrequency plotted versus eigenfrequency; $f = \{1, 2, 3, 4, 5\} \times 10^{-3}$, are denoted by green diamonds, red, green and blue crosses and red diamonds respectively. The lines at which $f^2\omega_1 = 0.5\omega_0$ and $f^2\omega_1 = 0.1\omega_0$ are also given (solid and dashed respectively). Right panel: same as for the left panel, but scaled by the respective f^{-2}. Modes have $m = -2$.

any radial variations in $\delta\mathbf{C}$ quickly become over so comparatively large a length-scale (compared to the oscillations) that the integral shrinks rapidly with decreasing ω_0.

This means that, for a given f, the Coriolis force will establish itself as the main perturbation to the eigenfrequency much faster than a possibly expected ω_0^{-1} rate once this point is reached. However, the initial growth means that we must always examine the size of the centrifugal corrections, even if we then go on to neglect them.

5.4 ALTERATION TO THE EIGENFUNCTIONS

To look at the shape of the perturbation to the eigenfunction, figure 5.9 shows some of the η and x dependence of one part of the $\delta\xi_x$ and $\delta\xi_\mathrm{h}$ for the following mode:

m	-2
f	0.008
k	14
ω	0.4299
L^2	6.08

Both because of the forcing, and because of the fact that the eigenfunction is not determined by the system, in both of equations (4.27) and (4.28), the perturbation to the eigenfunction is not nearly as strongly peaked as the original eigenfunction, instead sampling the whole star, albeit to a much smaller level (the original eigenfunction has been scaled down by a factor of 200 in figure 5.9). Also the perturbations become reasonably large as $x \longrightarrow 1$.

If we view the pulsation physically, the sampling of the star by a global oscillation mode is governed by the paths a ray is encouraged to take; as we are perturbing the geometry of the star, the interference pattern built up by many rays will no longer cancel

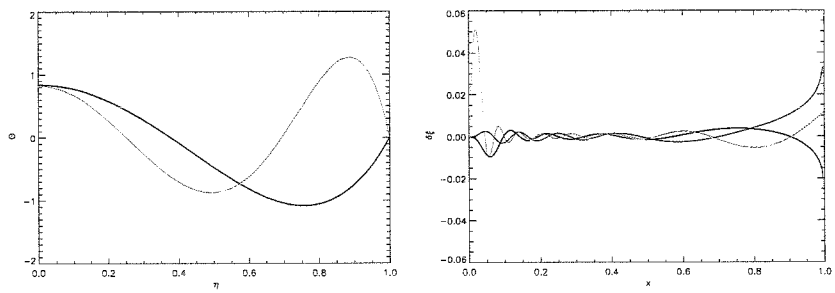

Figure 5.9: Left panel: Hough functions with $(L^2, \nu) = (20.12, 0.035)$ and $(L^2, \nu) = (42.21, 0.035)$ (black and red respectively). Compare $P_4^2(\eta) \propto \left(7\eta^4 - 8\eta^2 + 1\right)$. Right panel: Radial-like dependence of the parts of $\delta\xi_x$ and $\delta\xi_h$ with angular dependence of the black Hough function on the left (black and red respectively). The green curve is ξ_x scaled down by a factor of 200 for comparison.

as completely as they would have, meaning that the perturbation samples almost the whole star to a small level. Also, the regions sampled towards the surface are going to be the ones with the most change to them, meaning the perturbation will be peaked there. It is worth noting that the fact that the peak is very confined to the surface, where ρ (and such-like) is very small, means that the f^4 correction will not be dominated hugely by this peak.

5.5 MODE TRAPPING

To explore mode trapping, one of these modes was taken ($m = -2$, $L^2 \approx 6$) for an arbitrary choice[9] of $\bar{\omega} = 0.2$, and the behaviour of $\omega_\pm$ looked at for various rotation rates, f.

[9] $\bar{\omega} \equiv \omega/\sqrt{GM/R^3}$ is required for $\tilde{f}$, and to calculate the value of $L^2(\nu)$ and the behaviour of Λ_{tot} in $\tilde{f}$ and S_l^2 (equations (4.33) and (4.37) repectively).

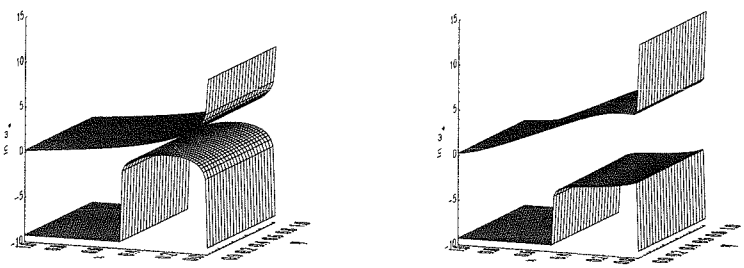

Figure 5.10: Graphs of $\omega_{\pm}$ against x and η for a $n = 3$ polytrope and $\bar{\omega} = 0.2$, $m = -2$, $L^2 \approx 6$. Left panel is for ($f = 0$, $L^2 = 6$), the right for ($f = 0.005$, $L^2 = 6.10$).

The functions $\omega_{\pm}(x, \eta)$ to order f^2 are shown in figures 5.10 and 5.11. It is important to note that we have considered the angular behaviour of Ψ to be governed by the single Hough function, $\Theta_{k,m}$, for the particular (m, ν, L^2), in our calculation of Λ_{tot}; and because of this have artificially removed terms involving Θ'/Θ in producing these graphs. This is because there are, in both of $\omega_{\pm}$, values of η when the denominator of these terms goes through zero and the numerator (Θ' multiplied by various coefficients arising from the h_i) does not. This is found not to change the shape of the $\omega_{\pm}$ beyond removing these numerical "spikes".

For these graphs, the Hough-function like P_2^2 is peaked towards the equator. The shape of these types of graphs is surprisingly robust to changes in the value of $L^2(\nu)$ – the left panel of figure 5.11 is almost identical to the left panel of figure 5.10, meaning that the main effects are geometrical.

The primary effect of rotation is to begin to exclude low-radial-order modes (ω_- is lowered, whilst ω_+ is raised) from near the centre of the star. These modes with fewer nodes (and therefore larger length scales) find it hardest to remain propagative in the distorted state, which has increasingly different length scales

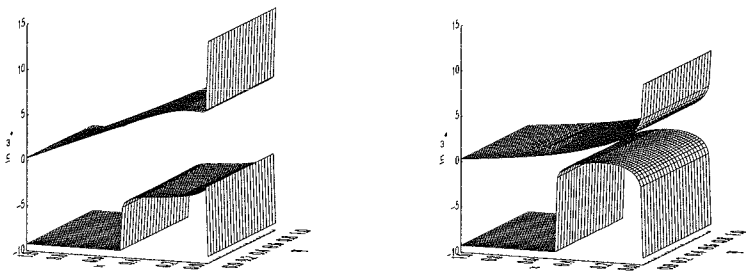

Figure 5.11: As for figure 5.10, but with ($f = 0.01$, $L^2 = 6.21$) (left) and ($f = 0.12$, $L^2 = 13.82$) with no f^2 corrections, just the altered Hough functions (right).

at different latitudes with increasing rotation rate. Thus finding a neatly separable propagative solution becomes impossible.

Of important note is the fact that these results describe the "radial" effects trapping of the mode. As already mentioned, the Coriolis force will act as an equatorial waveguide, causing the amplitude of the mode to be strongly peaked towards the equator, a well-studied subject.

5.6 WHITE-DWARF ROTATIONAL DISTORTION

As another test case, we can investigate the distortion of a zero-temperature-white-dwarf model having an equation of state given implicitly by

$$p = af(z) \ , \ \rho = bz^3 \ , \tag{5.23}$$

$$f(z) = z(2z^2 - 3)\sqrt{z^2 + 1} + 3\sinh^{-1} z \ , \tag{5.24}$$

with $a = \pi m_e^4 c^5 / 3h^3$, $b = 8\pi \mu_e m_e^3 c^3 / 3N_0 h^3$ and $z = p_0/mc$, where p_0 is the electron Fermi momentum (m_e is the electron mass, c

is the speed of light, h is Planck's constant, N_0 is Avogadro's number and μ_e is the mean mass of the fluid per free electron).

Thus[10]

$$\nabla p = -\rho \nabla V \ , \tag{5.25}$$

$$\Rightarrow V = -\frac{8a}{b}\sqrt{1+z^2} \ ; \tag{5.26}$$

$$\therefore \ -\frac{8a}{b}\nabla^2\sqrt{1+z^2} = 4\pi G b z^3 + 2\Omega^2 \ . \tag{5.27}$$

Then the rescalings

$$y^2 = z^2 + 1 \ , \tag{5.28}$$

$$y = y_c\theta \ , \ D = y_c^{-2} \ , \tag{5.29}$$

$$x = \sqrt{\frac{2a}{\pi G b^2 y_c}}\tilde{x} \ , \tag{5.30}$$

$$\Omega^2 = \frac{2\pi G b}{D} f^2 \tag{5.31}$$

give[11]

$$\tilde{\nabla}^2\theta = -(\theta^2 - D)^{3/2} + f^2 \ . \tag{5.32}$$

This equation, after the correct non-dimensionalization, differs from that for the polytrope only in its zeroth order solution, although we cannot eliminate θ'' in the same way as we did for equation (5.10). Thus, to successive orders in f^2, starting from f^0:

[10] The definition of V is once again given by $V = \Phi - \frac{1}{3}\Omega^2 r^2(1 - P_2(\mu))$.

[11] $\tilde{\nabla}$ denotes ∇ after the non-dimensionalization of length.

$$\theta'' = -\frac{2\theta'}{x} - (\theta^2 - D)^{3/2} , \tag{5.33}$$

$$\begin{aligned} x\theta'\lambda''_{l,1} &= 2x(\theta^2 - D)^{3/2}\lambda'_{l,1} \\ &+ \lambda_{l,1}\left(2(\theta^2 - D)^{3/2} + 2l(2l+1)\frac{\theta'}{x}\right) \\ &- \xi_0^2\delta_{l,0} , \end{aligned} \tag{5.34}$$

$$\begin{aligned} x\theta'\lambda''_{l,2} &= 2x(\theta^2 - D)^{3/2}\lambda'_{l,2} \\ &+ \lambda_{l,2}\left(2(\theta^2 - D)^{3/2} + 2l(2l+1)\frac{\theta'}{x}\right) \\ &+ B_l . \end{aligned} \tag{5.35}$$

The only difference to the boundary conditions is now that

$$\lim_{x\to 0}\lambda_{l,1} = \frac{\xi_0^2}{2(1-D)^{3/2}}\delta_{l,0} , \tag{5.36}$$

$$\Rightarrow \lim_{x\to 0} B_l = \frac{-3\xi_0^4}{4(1-D)^{3/2}}\delta_{l,0} , \tag{5.37}$$

$$\& \lim_{x\to 0}\lambda_{l,2} = \frac{-1}{2(1-D)^{3/2}}\lim_{x\to 0} B_l ; \tag{5.38}$$

equations (5.15)–(5.22) and the definitions of the $t_{l,a}$ (such as given by equation (3.27)) are unchanged.

Figure 5.12 shows an example of the $\lambda_{l,1}$ and $t_{l,1}$, and ratios of the equatorial over polar radii against rotation rate for various values of D.

The overall form of the distortion functions $\lambda_{l,1}$ and $t_{l,1}$ are very similar to those for the polytrope, although the scale makes it very obvious that the white dwarf considered ($D = 0.2$) is much less compressible and thus more resistant to rotational distortion than the $n = 3$ polytrope. This also shows from the range of f

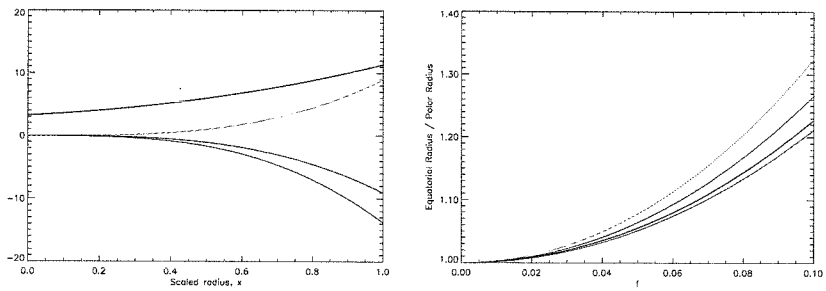

Figure 5.12: Left panel: $\lambda_{l,1}$ and $t_{l,1}$ for a zero-temperature white-dwarf with $D = 0.2$; key as for figure 5.4. Right panel: Equatorial radius divided by polar radius for various zero-temperature white dwarf models plotted against rotation rate; $D = 0.025, 0.5, 1, 2$ are denoted by green, red, black and blue lines respectively.

values shown in the right-hand panel of figure 5.12. However, not too much should be made of this as the f values are difficult to compare directly, owing to the different scalings used.

The non-rotating radii are again in excellent agreement with James (1964); a direct comparison with his rotating radii is not made owing to concerns over scaling; however, the result that the equatorial radius is far more affected by the rotation than the polar radius is well reproduced. Pulsations will not be considered in these models, as the Brunt-Väisäla frequency is zero throughout the star.

5.7 CONCLUSIONS

We can see that the method presented in chapters 3 and 4 gives sensible, and quantifiable, answers for these test barotropic equations of state (polytropes and zero-temperature white dwarfs), and are able to exhibit the results of both Coriolis (under the

TA) and centrifugal forces.

For more compressible equations of state, it has been seen that the centrifugal distortion can cause the assumption that the centrifugal terms cause a perturbation to the eigenfrequency to break down at a rotation rate lower than the accuracy of predicting the oblate structure would imply (although still at a significant fraction of the breakup rotation rate).

The results produced by this method are in accordance with what we expect from a physical understanding, and thus give us confidence in generalizing the theory to real equations of state, as will be done in chapter 7, with results presented in chapter 8.

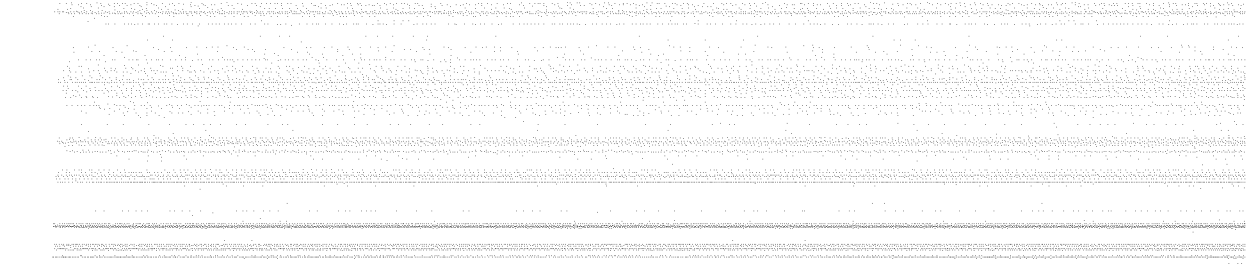

Chapter 6

Genetic algorithms

"We will now discuss in a little more detail the struggle for existence" – The Origin of Species, chapter 3.

6.1 Background

6.1.1 A problem in forward modelling

The problem of asteroseismology is, at its heart, a simple one; we have an equation like the following, governing stellar pulsations:

$$\omega^2 \boldsymbol{\xi} = \mathcal{F}\boldsymbol{\xi} \,, \tag{6.1}$$

where $\mathcal{F}$ depends on our background state - i.e. our model of the star. This equation predicts eigenfunctions and observable pulsational frequencies; if our stellar model predicts the observed frequencies well, it is kept and/or refined whereas if it fails to predict what we observe, then we must adopt a new model. Thus the frequencies are not an input parameter into our models, but a judge of the output.

The aim is thus to make models, and compare them, and then refine our models until we fit the data. Once again, the issue of time arises; how do we do this without being prohibitive in terms of computer time? An answer comes in the form of genetic algorithms.

6.1.2 Genetic algorithms: an introduction

We are seeking to optimize the fit of predicted pulsational frequencies to the observed pulsational frequencies. There are a large number of ways to do this, but we shall focus on one which has become more widely used in recent years: the genetic algorithm.

Genetic algorithms are a powerful way of fitting data; they do suffer from the drawback that they do not prove that the optimal fit found is global, but they have the great advantage of efficiently sampling large parameter spaces.

Before we proceed, it is useful to define many of the terms that will be used from this point on:

- *Phenotype* - the list of parameters that makes up an *individual* in its particular *generation*;
- *Genotype* - the attributes that come out of the individual's phenotype: in our case, these are the pulsational frequencies.

Any genetic algorithm[1] follows the following steps:

1. Calculates random models to form the first generation of the population.
2. Calculates the *suitability* of each member of the population.
3. Calculates breeding partners using an evaluation of their suitability.
4. Breeds these pairings, replacing the previous generation.
5. Mutates some parameters.

[1] As has been pointed out in, for example, Charbonneau (1995), the formal name should probably be "genetic algorithm-based optimizer" – we shall stick to the use of "genetic algorithm"

6. Returns to (2), repeating this until either a pre-determined number of generations is reached, or a tolerance criterion is met.

For a good introduction to genetic algorithms, and their use in Astronomy, the reader is directed to the paper by Charbonneau (1995) already mentioned. This paper also gives a now widely-used genetic algorithm, called PIKAIA; this code is a generally optimized one, and has often already made a decision on a number of issues that will be investigated, so has not been used.

Like most complex search routines, genetic algorithms need to be specialized to the problem. Owing to this fact, there are a number of arenas in which it would be good to investigate the behaviour and results of the algorithm. These will now be listed.

6.1.2.1 BREEDING AND PHENOTYPE CONSTRAINTS

The sampling of parameter space performed by the genetic algorithm is for a large part tied up with how the new generation is obtained from the last. This is known as *breeding.* In humans, we have paired chromosomes, one obtained from each parent, and these are combined to form our phenotypes, with complications like recessive and co-dominant alleles.

The commonly formed breeding method in widely-used genetic algorithms is that of a one-point crossover, where the first m of the n points on the phenotype are from the first parent, and the remaining $n - m$ are from the second parent. The number m is often selected randomly, and there is often a reasonable chance of some asexual reproduction of the first parent, where $m = n$, so, barring mutation, one parent is then automatically reproduced into the next generation. The probability of non-asexual reproduction is know as the *crossover probability.* What is the best value of this, and what is the relation of this value to the population size?

In humans, both parents will flavour their offspring, which can result in the offspring having better inherent characteristics than either parent. Would such an "averaging", probably weighted by the suitability of each parent, for some of the n points on the phenotype, help in finding an optimal solution?

Also, to what extent should we reduce a search range with pre-dispositions about the data? Firstly, is the assumption that "any reduction in search range is beneficial" true? What if the reduction causes the optimal fit to lie on the edge of the range, will this cause the optimal fit to be much harder to find? Will this change the results to our previous questions? As a less-clear-cut issue, what are sensible ranges to put on the "l" values for observed pulsational modes? It is the case that the observable effects of high-l modes will most likely cancel themselves out when integrated over the whole disc, but how much should this flavour our modelling searches?

6.1.2.2 Elitism, Diversity and Mutation probability

Returning to the case of possible asexual reproduction, genetic algorithms often employ *Elitism*, where in any generation the most fit individual in the population is perfectly reproduced into the next generation without mutation. Whilst this ensures that the degree to which the best individual fits the model is a monotonically increasing function of generation number, is this harmful through being too artificial, and would an archiving routine work better?

Another issue is how to ensure that the degree to which the best individual fits increases after many generations (i.e. that the goodness-of-fit does not plateau), and how to prevent the algorithm from getting stuck in a local minimum. Should we enforce a certain diversity of the gene pool, or is this again harmful? What is the best mutation rate for a given population size, and

should we vary the mutation rate to encourage this diversity?

6.1.2.3 SUITABILITY

This is one of the most arbitrary inputs to a genetic algorithm, but also one of the most critical, as it can change many of the results. An often used suitability formula is that of a χ^2 estimator:

$$\chi^2 = \sum \left(\frac{a_{\text{model}} - a_{\text{observed}}}{a_{\text{observed}}} \right)^2 , \tag{6.2}$$

where a are the observables; they can be the frequencies (scaled or unscaled), the periods of oscillation, splitting coefficients, or other things. Which of these is the best to use?

Is it better to use the raw suitability score of an individual for selection (and possible weighted breeding), or should the suitability score be scaled, or simply turned into a linear ranking?

Would it be advantageous to use the quality of the detection signal to weight this fitting? This would mean that the clear detections are fitted preferentially; but would the price paid elsewhere be too great?

These factors will be looked at using the following classes of models:

1. The generalization of the class of toy models considered by Charbonneau (1995) where the phenotype is the x and y values[2], in the range [0,1], and the fitness of the genotype is given by[3]:

$$f_2(x, y) = (16x(1-x)y(1-y)\sin(n\pi x)\sin(n\pi y))^2 , \tag{6.3}$$

[2]Or w, x, y and z for the four-dimensional case

[3]in the two-dimensional case, with the four dimensional case being $f_4(w, x, y, z) = f_2(x, y)f_2(w, z)$

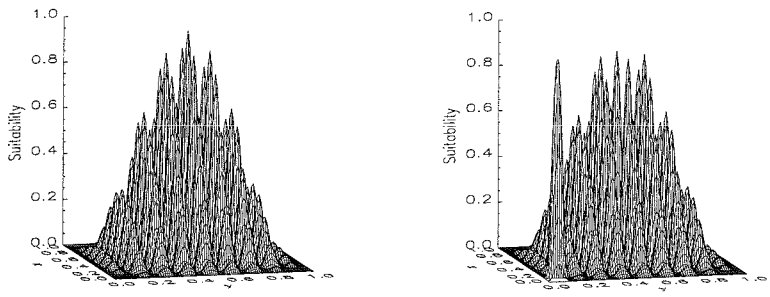

Figure 6.1: Two fitness functions, the left being the function f_2 given by equation 6.3, and the right being the same, but with the central peak shifted to $x,\ y\ \epsilon\ (0, \frac{1}{9})$.

where n will be given, often taking the value 9. The generalization will be constructed by both adding extra peaks in f_2, and by increasing to a four-dimensional parameter space.

2. The same equation as above, but with the middle peak shifted to the edge (so what would have been the f_2 above at $x,\ y\ \epsilon\ (\frac{4}{9}, \frac{5}{9})$ is shifted to $x,\ y\ \epsilon\ (0, \frac{1}{9})$. These two fitness functions are displayed in figure 6.1.

   The reason for this shift is to remove any fortuitous fits that may occur by the optimal peak being surrounded by the next optimal ones.

3. A non-rotating polytrope, with the phenotype being the polytropic index, the scaling of the system, and the l values for the individual modes. The fitness criterion will vary between

   a) using the scaled frequencies,

   b) using the observed frequencies,

   c) using the periods.

4. The rotating polytropes described in chapters 3 to 5, considering only the f^2 change. The reason for stopping at this order is that the time taken for a run is greatly reduced, without losing any of the basic effects. The fitness criterion for this class of models will be given later.

6.2 TOY MODEL

Returning to the toy model, we shall focus on the following points to begin with:

- Elitism: is allowing the fittest individual to replicate into the next generation wise?
- Should we rely upon a ranking system for our data, or retain the raw suitability?
- Is it better to use a one-point crossover, or in our breeding to allow a weighted average?
- Will enforcing diversity help, and what is the best way to accomplish this?

6.2.1 POPULATION SIZE, MUTATION AND CROSSOVER PROBABILITIES

Although the points listed above are the focus of our search, there are a number of input parameters to our model that must be addressed, even though they are not the focus. These include population size, mutation probability and crossover probability, which need to be assigned values.

It has been suggested by a number of authors that good performance requires the choice of a high crossover probability and a low mutation probability (inversely proportional to population size). The following values were chosen as fiducial examples after a brief investigation:

Parameter	Description	Value
p_{cross}	Crossover Probability	0.7
p_{mut}	Mutation Probability	0.1
pop	Population Size	80
cont	Number of individuals selected to contest parent selection	4

,

although variable mutation rates will be used in diversity investigations.

6.2.2 Elitism

Graphs of the fitness of successive generations of the toy model, with the unaltered fitness formula, are shown in figure 6.2. In this, and the following graphs, we have plotted both the fitness of the most fit individual (with diamonds) and the fitness of the individual ranked halfway in a given generation (by the dotted line). Also, owing to the fact that we are using numerical random-number generators which may introduce some additional effects, we have plotted the average fitness of the most fit individuals found from one hundred different initial seed fields.

The first thing to note is that convergence is very rapid indeed: in most cases the optimal peak is found, and centred on, in a few generations. The second point to note is that although in some cases we may get away without Elitism, there can be cases in which it is very advantageous. Elitism also has the great advantage of making the closeness of our optimal fit a monotonic function, a vital thing when computational limitations may cause pre-optimal termination of the algorithm. It can be argued that an archiving procedure might also provide adequate protection, but it is the case, for large enough population sizes, that a benefit is gained by keeping the best fit to flavour future generations, without any real drawbacks. Hence Elitism will be employed for the Toy Model calculations from this point on.

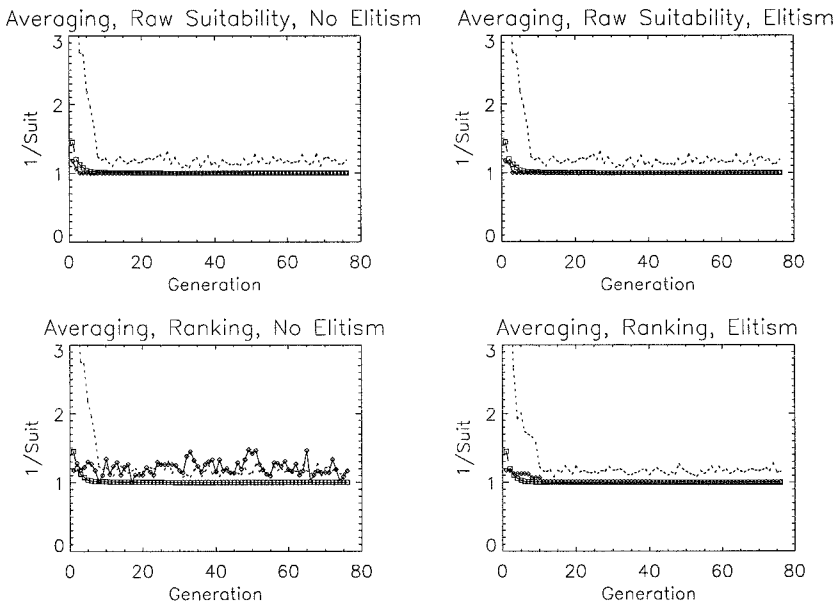

Figure 6.2: Convergence graphs for the unaltered toy model. A weighted average has been used. The fitness of the most fit individual, fitness of the individual ranked halfway in a given generation and average fitness of the most fit individuals found from one hundred different initial seed fields are denoted by diamonds, the dotted line and squares respectively.

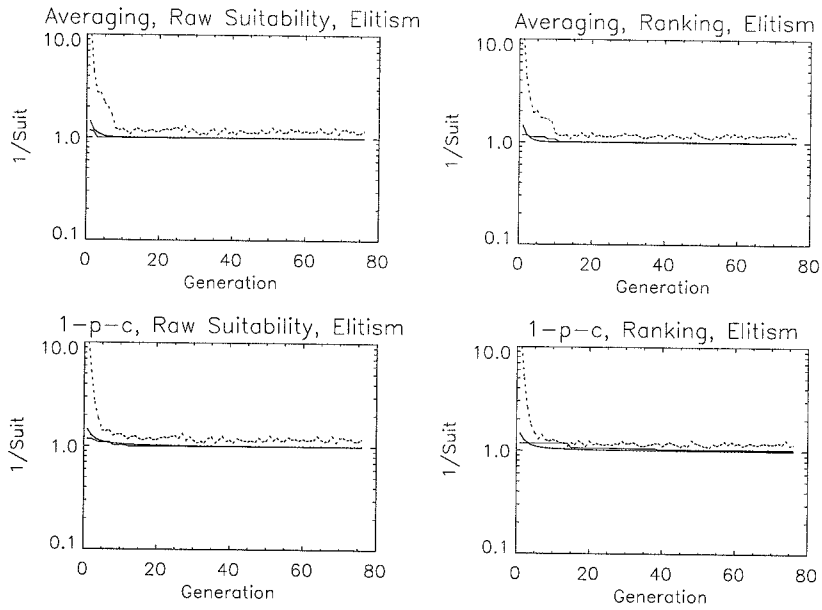

Figure 6.3: Convergence graphs for the unaltered toy model. The fitness of the most fit individual, fitness of the individual ranked halfway in a given generation and average fitness of the most fit individuals found from one hundred different initial seed fields are denoted by the solid line, the dotted line and the solid line with periods respectively.

6.2.3 Ranking and Averaging

Figure 6.3 shows four more convergence graphs; in this case, the variation in choice of method is between a weighted average and an one-point crossover, and between raw suitability and ranking.

The results of this are inconclusive: owing to the very fast convergence, all procedures perform well. However, we are left with a slight preference towards averaging and raw suitability. This is both from our graphs and also from reasoning: for example, although ranking does provide a consistent scaling of the fitness,

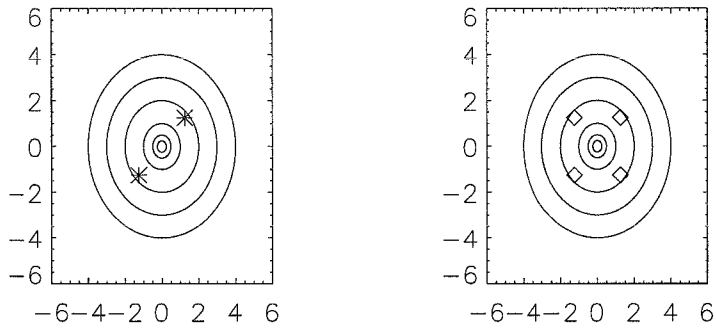

Figure 6.4: Example fitness "potential well". Two parents are shown on the left. The possible offspring under a one-point crossover are shown on the right.

it essentially disassociates the fitness function for the underlying objective function.

We have another reason to favour using weighted averaging in our breeding routine, if we think about late-time development. Consider two breeding individuals equidistant from a two-dimensional optimal fit, as shown on the left of figure 6.4. On the right, all four possible offspring, before mutation, are shown; as can be seen, these are no closer to the extrememum. However, were averaging to be employed, the optimum could be reached in just one more generation. This saves us from having to pursue a fit with a genetic algorithm to a certain point, and then switch to a steepest descent method to further refine the fit, which is often employed – it has advantages, but it requires a perhaps arbitrary decision as to when to switch method.

Should we reduce the search range to having x and y values in the range [0,0.5], in order that the optimal fit now lies on the boundary of our search range, the results are very similar. How-

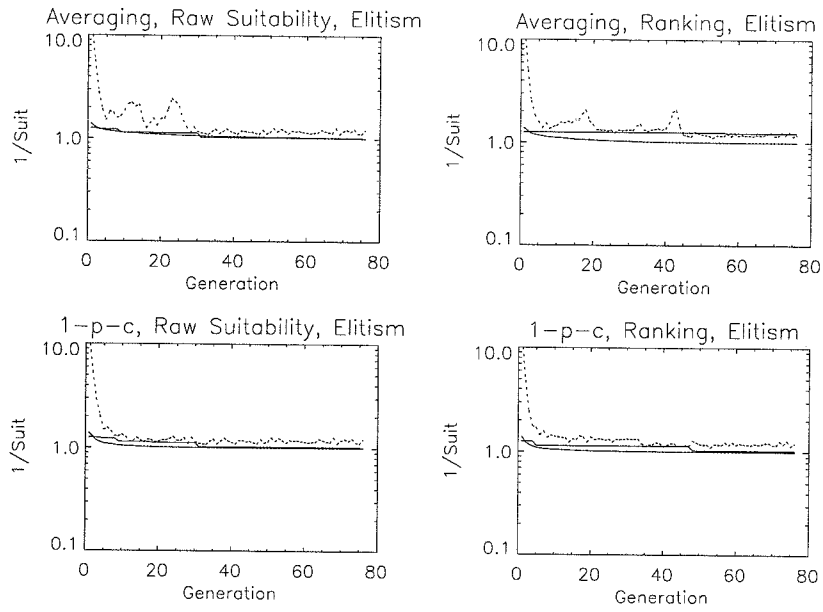

Figure 6.5: Same graphs as for figure 6.3, but with the search range reduced to x and y values in the range [0,0.5]

ever, employing a one-point crossover and taking straight ranking values runs into problems, not converging as quickly as the other methods. The reason for this is fairly obvious, in that a more optimal fit under ranking has very little ability to "pull" the phenotype of its offspring towards its own value. Hence, because the optimal fit is on a mathematically closed boundary, the phenotypes can only approach this fit in an asymptotic-like manner.

6.2.4 DIVERSITY

In looking at the issue of how to optimize the late-term convergence of the genetic algorithm, we are faced with two immediate possibilities should the diversity (which we shall calculate as a straight standard deviation of the phenotype values from the

mean) falls below a cutoff. These are:

- We can enforce the diversity by re-mutating the population at a fixed p_{mut} until a diversity threshold is passed, or
- we can re-mutate the population as above, and then increase p_{mut} towards a maximum, which we shall define as $p_{\text{m,max}}$; the starting value of p_{mut} we shall define as $p_{\text{m,min}}$.

6.2.4.1 FIXED MUTATION RATE

We performed runs with Elitism, using the raw suitability score and the following parameters

Parameter	Value
p_{cross}	0.7
p_{mut}	0.1
pop	80
cont	4

,

and recorded (both for one seed field, and for the average of 100 seed fields) the number of generations needed to get within the maximum fitness.

Figure 6.6 shows the number of generations needed for a given diversity cutoff; it is immediately apparent that enforcing diversity can reduce the number of generations needed by up to a factor of four or more, if the right cutoff is chosen. This reduction continues until a certain point, then the number of generations needed increases. The reason for this increase is that we are trying to enforce too great a diversity for the problem – genetic algorithms work by concentrating the gene pool around a good fit, and enforcing too much diversity causes the algorithm to essentially become closer to repeated sampling.

Other obvious things to notice from figure 6.6 is that, although the trend for the number of generations needed versus diversity

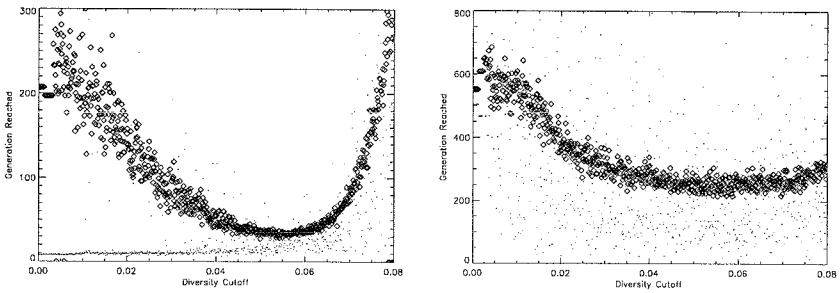

Figure 6.6: Number of generations needed to reach within 5×10^{-5} of the maximum fitness for a given diversity cutoff. Dots are for an individual seed field, diamonds are for the average of 100 seed fields. The left graph is for averaging, the right for one-point crossover. Values of 0 indicate that a maximum of 800 generations was reached without managing to reach the desired level of fitness.

cutoff is the same, one-point crossover is hugely out-performed by averaging, and that an individual run has a much larger scatter in convergence speed. The reason for this was discussed earlier, and lies in the fact that one-point crossover has real problems in converging on a extremum, as is shown in figure 6.4. However, this second fact – that an individual run has a large scatter – is extremely serious when we come to use the genetic algorithm to fit data; so we shall employ averaging from now on.

These results still stand in the 4-d analogue of the toy model (figure 6.7), if we change the value of n in equation (6.3) (figure 6.8), although for the latter figure the fitness threshold was lowered to be that of a level that merely ensured that the fit reached a level better than all the other non-global maxima (i.e. $f > 0.9036$ for $n = 9$ and $f > 0.99348$ for $n = 35$), so the problem with high diversity cutoffs does not appear for the values shown.

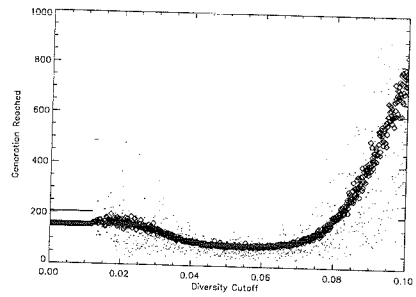

Figure 6.7: As for figure 6.6, but for the 4d analogue of the toy model. Maximum number of generations is now 900.

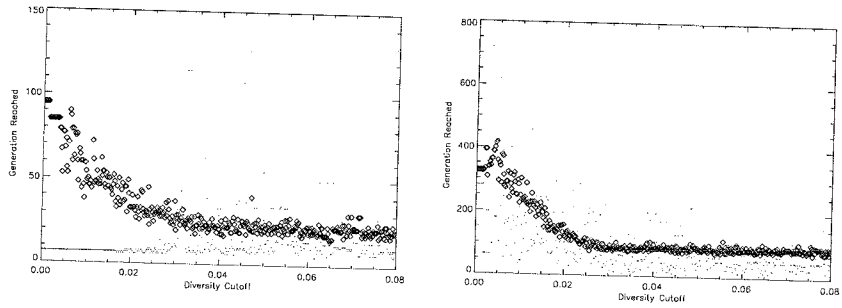

Figure 6.8: As for figure 6.6, for $n = 9$ on the left and $n = 35$ on the right; searching for a fit better than all the other non-global maxima (i.e. $f > 0.9036$ for $n = 9$ and $f > 0.99348$ for $n = 35$)

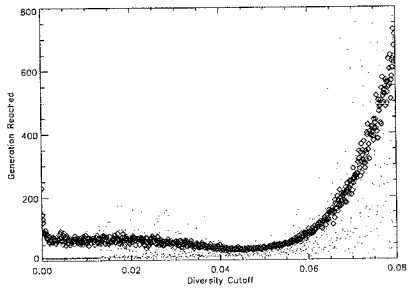

Figure 6.9: As for the left hand slide of figure 6.6, but with a variable mutation rate.

6.2.4.2 VARIABLE MUTATION RATE

To look at the effect of using the variable mutation rate whilst enforcing diversity, the following parameters were used:

Parameter	Description	Value
p_{cross}	Crossover Probability	0.7
$p_{\text{m,min}}$	Minimum Mutation Probability	0.1
$p_{\text{m,max}}$	Maximum Mutation Probability	0.25
pop	Population Size	80
cont	Number of individuals selected to contest parent selection	4

For each run at a given diversity cutoff, p_{mut} was reset to $p_{\text{m,min}}$, and then increased by a five-hundredth of the value of $p_{\text{m,max}} - p_{\text{m,min}}$ when the diversity fell below the cutoff. The analogues of figures 6.6 and 6.8 are shown in figures 6.9 and 6.10 respectively.

Figure 6.9 shows that the main advantage of the variable mutation rates is for a low diversity cutoff, when the variable-mutation-rate method significantly outperforms (by a factor of approximately two in the number of generations needed to obtain the accuracy of fit required) the fixed-mutation-rate method.

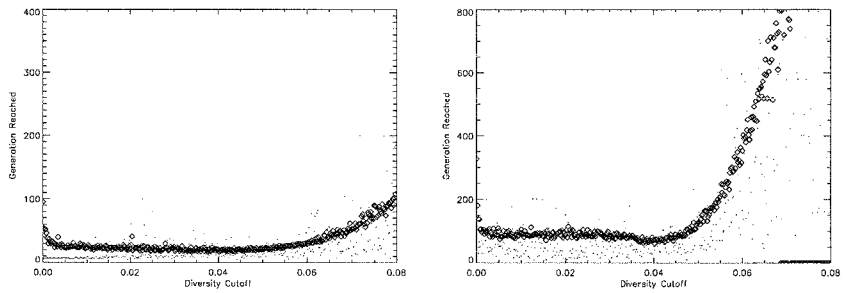

Figure 6.10: As for figure 6.8, but with a variable mutation rate also.

However, for mid-range values of the mutation rate (i.e. a cutoff between 0.03 and 0.065) there is little difference between the two methods; and then for high range, the variable-mutation-rate method is strongly outperformed by the fixed-mutation-rate method. The reason for these two properties is that if the cutoff is too large, the mutation rate quickly spirals to a level at which the algorithm can no longer hone in on an optimum effectively.

Figure 6.10 shows that these same properties (a very rapid improvement in the number of generations required as the diversity cutoff leaves zero, and a falling away of the effectiveness of the algorithm for a too-high diversity cutoff) are robust for changing both the cutoff required and the number of local optima of the fitness function.

However, as we are seeking to pick a diversity cutoff that is low, to avoid the upturn in the number of generations needed, a variable-mutation-rate is recommended, although we have to be aware of its dangers.

6.2.5 ALTERED FITNESS FUNCTION

Again to test the robustness of these results, we have recalculated figures 6.2, 6.3 and 6.6 for the altered fitness function shown in

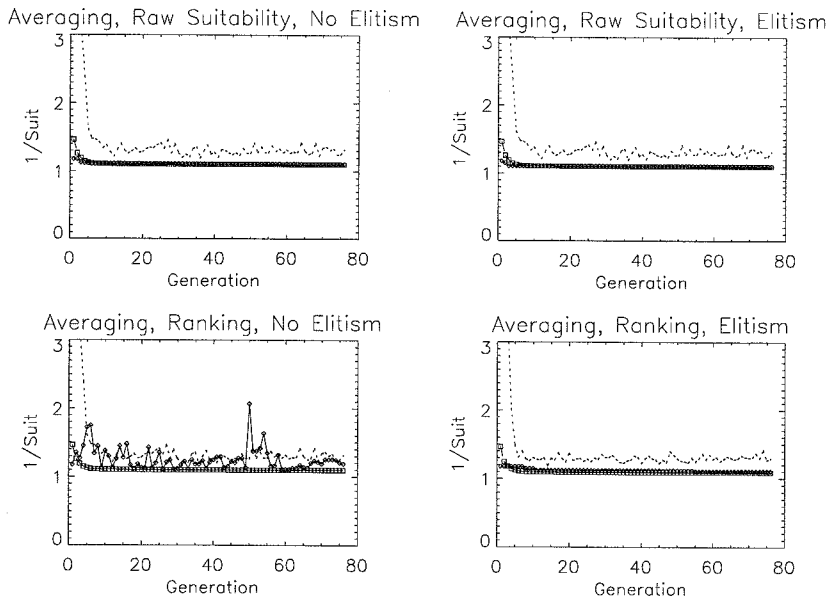

Figure 6.11: As for figure 6.2, but for the altered fitness function.

the right-hand panel of figure 6.1 and described in subsection 6.1.2.3. These graphs are shown in figures 6.11 to 6.13 (note that the required fit for figure 6.13 is slightly lower than for figure 6.6) respectively. Figures 6.11 and 6.12 show that although convergence is slower in these cases (as is understandable), the results and arguments presented for the unaltered fitness function still hold.

However, it is figure 6.13 that is truly significant. Without maintaining the diversity of the gene pool, the time taken to find a fit very close to the optimal solution is prohibitive, whereas enforcing a certain amount of diversity allows close fit to the optimal solution to be found in a reasonable time. It is noteworthy that there is no significant difference between the averaging and

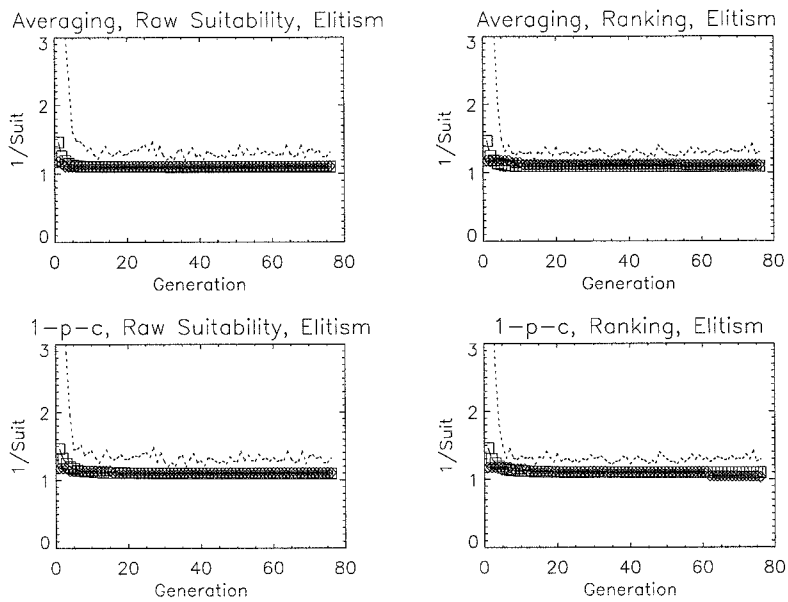

Figure 6.12: As for figure 6.3, but for the altered fitness function.

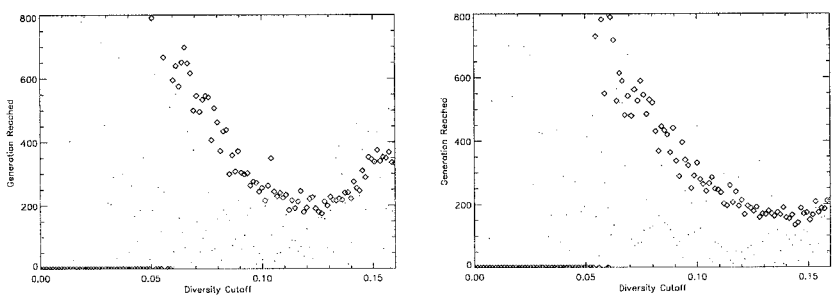

Figure 6.13: As for figure 6.6, but with the altered fitness function and aiming to reach within 5×10^{-3} of the maximum fitness for a given diversity cutoff.

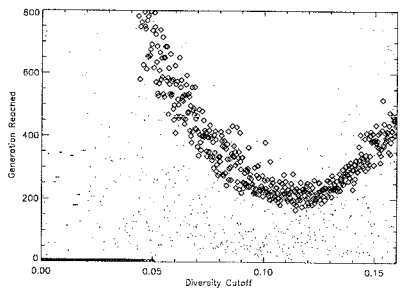

Figure 6.14: As for the left hand slide of figure 6.9, but for the altered fitness function and seeking within 5×10^{-3} of the maximum fitness for a given diversity cutoff.

the one-point crossover methods in this case, although due to averaging outperforming one-point crossover for a more regular fitness function, the former should still be kept.

Figure 6.14 investigates the use of a variable mutation rate for the altered fitness function, with the lower value of required fit but with all the other parameters the same as were used for figure 6.9. This again shows the superiority of enforcing diversity.

6.3 POLYTROPES

6.3.1 NON-ROTATING POLYTROPES

It is the case that genetic algorithms are very problem dependent. Therefore, to be assured that these results are true for fitting pulsational data, whilst still having the construction of models being computationally cheap enough, we look at fitting the following data from an $n = 3$ polytrope[4]:

[4]Frequencies are displayed here only to six decimal places, but were entered to fourteen in the code. To prevent a perfect fit resulting in dividing by zero in the fitness formula (equation (6.4)), the difference between observed

l	ω
1	0.090058
1	0.376890
1	0.726539
2	0.402005

Scaled up (by $\sqrt{GM/R^3}$) as in a star of $M_* = 1.2\ M_\odot$ and $R_* = 2\ R_\odot$ (giving $\sqrt{GM/R^3} = 0.3873\ \sqrt{GM_\odot/R_\odot^3}$).

We shall consider the same questions (of Elitism, Ranking vs. Raw suitability, One-point crossover vs. a weighted average and enforcing diversity) as for the polytrope, and also look at whether using periods or frequencies gives a better result. We shall begin by using frequencies, with a suitability formula of

$$F = \left(\sum \frac{\left(\omega_{\text{model, scaled}} - \omega_{\text{observed, scaled}}\right)^2}{\omega_{\text{observed, scaled}}} \right)^{-1} . \qquad (6.4)$$

The other parameters are given by

Parameter	Description	Value
p_{cross}	Crossover Probability	0.7
p_{mut}	Mutation Probability	0.1
pop	Population Size	100
gens	Maximum number of generations	80
cont	Number of individuals selected to contest parent selection	4

and the parameters to be fitted were[5]

and predicted periods was atificially limited to exceed 1×10^{-20}.

[5]Even though l takes integer values for a non-rotating star, l was considered a real number, the integer part of which was taken in order to calculate the frequencies.

6.3 Polytropes

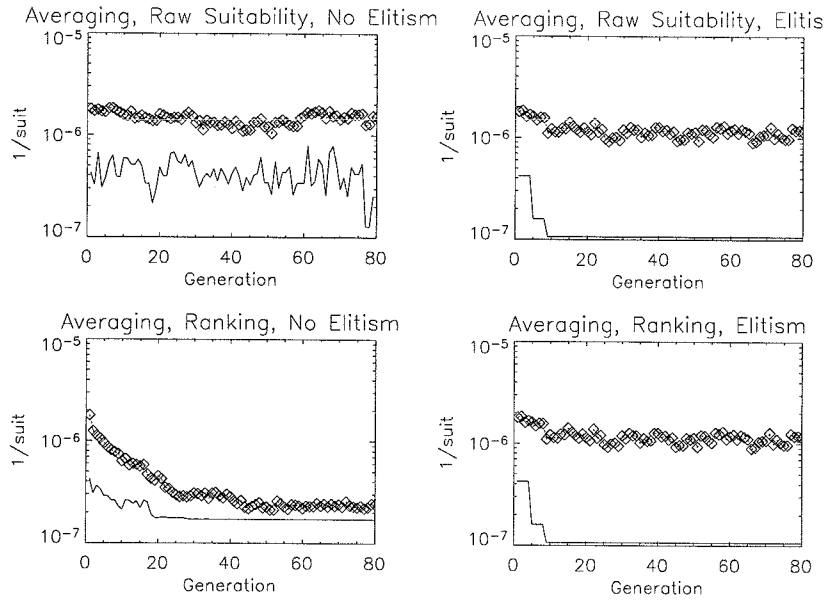

Figure 6.15: The equivalent of figure 6.2, but for the non-rotating polytrope described in this section.

Parameter	Description	Range
l_i	l-value of the ith mode	$1-3$
n	Polytropic index	$2-4$
$\sqrt{\frac{R_\odot^3 M_*}{M_\odot R_*^3}}$	Frequency Scaling	$0.1-1.1$

Results are displayed in figures 6.15 to 6.16. Note that diversity has not been enforced here, as suitable diversity cutoffs will be investigated later.

It can immediately be seen from these figures that the toy model results (strongly encouraging using Elitism and suggestive of using Averaging and the Raw Suitability score) carry over into this problem. Therefore they are now adopted.

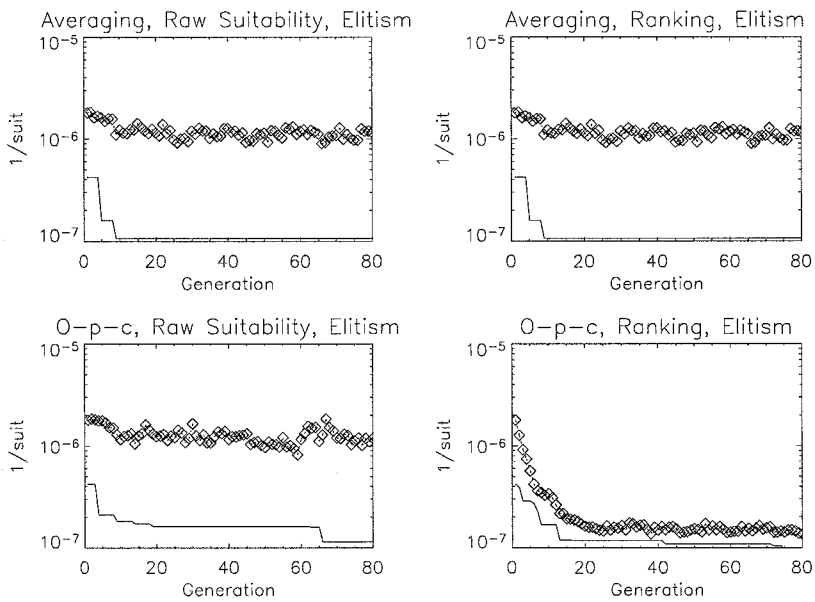

Figure 6.16: The equivalent of figure 6.3, but for the non-rotating polytrope.

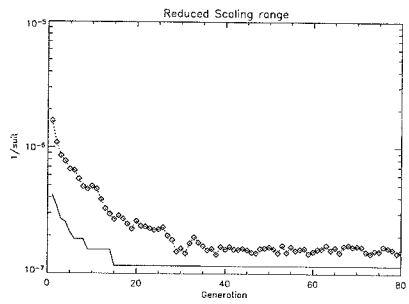

Figure 6.17: Convergence graph for the non-rotating polytrope described in 6.3.2.

6.3.2 RESTRICTING THE SEARCH RANGE

It is not the case that we shall have no information on the location of a given star to be modelled in the H-R diagram: we shall have fairly accurate values both of its luminosity and of its effective temperature. These can be related to a star's age, mass and radius.[6] This information thus puts a fairly tight constraint on the frequency scaling. To model this, we can restrict the search range of the frequency to $\sqrt{(R_\odot^3 M_*)/(R_*^3 M_\odot)} \in (0.3509, 0.4286)$ (equivalent to assuming the values of $(M_*, R_*) = (1.2, 2)$ are in error by 5%). The result of such a search is shown in figure 6.17.

Figure 6.18 shows the results of a further search with this reduced search range in the frequency scaling, but investigating the effects instead searching for l_i in the range $(1, 10)$. The contrast in rate of convergence and closeness of fit between figures 6.17 and 6.18 is considerable: both results are drastically improved by having a reduced search range, strongly suggesting that any reduction we can safely achieve in the search range would prove favourable.

[6] Albeit loosely, and often the effects of rotation, which we see are reasonably important, are often neglected.

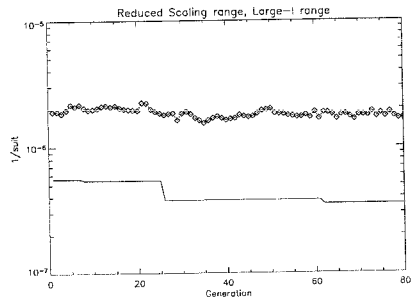

Figure 6.18: As for figure 6.17, but with the large-l range.

6.3.3 FITNESS CRITERION FOR POLYTROPES

The figures analogous to the top left panel of figure 6.16 and figure 6.17, but from using a fitness function of the form[7]

$$\begin{aligned} F &= \left(\sum \frac{\left(\omega^{-1}_{\text{model, scaled}} - \omega^{-1}_{\text{observed, scaled}}\right)^2}{\omega^{-1}_{\text{observed, scaled}}} \right)^{-1} \\ &\equiv \left(\sum \frac{\left(\omega_{\text{model, scaled}} - \omega_{\text{observed, scaled}}\right)^2}{\omega^2_{\text{model, scaled}}\omega_{\text{observed, scaled}}} \right)^{-1} , \end{aligned} \quad (6.5)$$

are figures 6.19 and 6.20. The form of these graphs is very similar to those of their analogues under the original suitability formula; thus, choice of suitability formula has no great influence on the convergence speed. However, making the suitability formula dependent on periods rather than on frequencies can hugely help for trying to match low-frequency modes, especially if one is not searching in a narrow range of parameters, in particular a narrow range of acceptable $\sqrt{GM/R^3}$. This can be seen easily if we consider the fact that the period spacing of g modes tends to an

[7]I.e. using periods instead of frequencies.

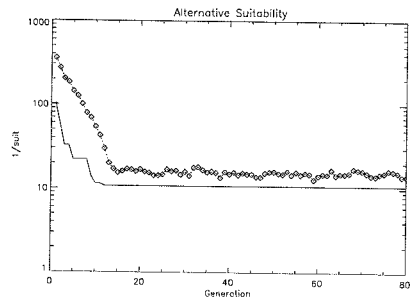

Figure 6.19: The equivalent of the top left panel of figure 6.16, but using the alternative suitability formula of 6.3.3.

asymptotic limit $P_0/\sqrt{l(l+1)}$ with increasing radial order k, for a mode with spherical harmonic degree l and, for example, P_0 to be found in Mullan (1989) for polytropes, including[8]:

Polytropic Index	P_0 (/s)
2.0	11652.8
2.5	6112.6
3.0	3496.5
3.5	1926.9
4.0	915.0

The asymptotic formula shows clearly that the g-mode spectrum becomes more dense as k increases. Thus, local minima are much more easily found for high scalings $\sqrt{GM/R^3}$, as, for high values, the raw frequencies are converted into lower scaled frequencies that are easier to find good matches for. It is thus important, when fitting such low-frequency data, to use a period-based search, and to consider carefully the observational constraints upon M and R before beginning such a search.

[8]Periods have been scaled by a standard frequency of 99.778μHz

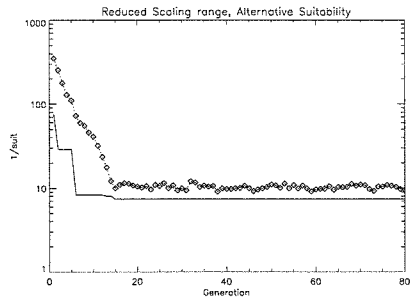

Figure 6.20: The equivalent of figure 6.17, but using the alternative suitability formula of 6.3.3.

6.3.4 DIVERSITY CUTOFFS

Now that we have seen the advantages of Elitism, Averaging and Raw Suitability, we shall investigate the effects of enforcing diversity in obtaining a fitness value (using equation (6.5) to define fitness) above 0.13527 (compare figure 6.20), 0.15, and 0.2. We defined the diversity of the population by a standard-deviation-type measure, but with the difference of each given parameter from the mean weighted by a suitable linear factor that "standardizes" the width of each parameter range to one. The graph of the number of generations needed is displayed in figure 6.21.

We see that the results – an improvement for low diversity thresholds, and then an upturn in the number of generations needed – similar to that found from the toy model.

6.3.5 ROTATING POLYTROPES

Having established good parameters to use for non-rotating polytropes, we shall now look at the fitting of an artificial data set in a "hare-and-hounds" exercise for the rotating polytropes described in chapters 3 to 5, considering only the $O(f^2)$ change. The following parameters were used:

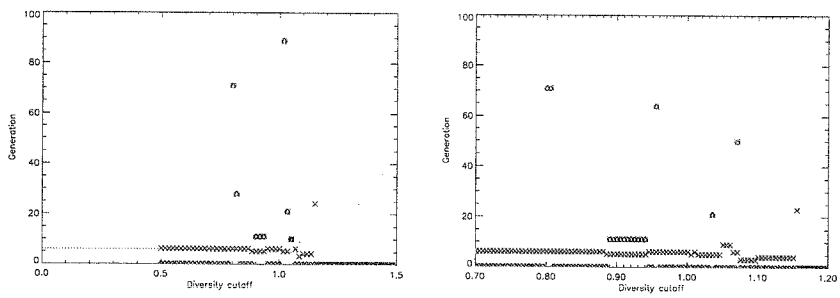

Figure 6.21: Left: The equivalent of figure 6.17, but using the alternative suitability formula of 6.3.3; the number of generations required to reach diversity cutoffs of 0.13, 0.137, 0.139, 0.141, 0.143, 0.145 are denoted by black dots, red asterisks, green pluses, blue diamonds, red triangles and green squares respectively. As having a diversity cutoff of between 0.7 and 1.2 seems to be the area of interest, the right-hand panel shows a blow-up of this region with more points (same key).

Parameter	Value
p_{cross}	0.7
p_{mut}	0.1
pop	100
gens	300
cont	4
n	3
$\sqrt{GM/R^3}$	$0.3873\ \sqrt{GM_\odot/R_\odot^3}$
f	0.005

,

with a fitness function:

$$F = \left(\sum \frac{\left(\omega_{\text{model, scaled}} - \omega_{\text{observed, scaled}}\right)^2}{\omega^2_{\text{model, scaled}} \omega_{\text{observed, scaled}}} \right)^{-1} . \qquad (6.6)$$

We sought to fit the following $L^2 \approx 6$, $m = 2$ data:[9]

ω_{unscaled}	Radial Order
0.34445	18
0.36232	17
0.40431	15
0.45744	13

by varying the following parameters:

[9]As notes to the reader, the f value given is equivalent to the Sun being a solid body rotator with a period of ≈ 3.6 days, and the frequencies to fit are calculated also to an accuracy of $O(f^2)$. However, the given frequencies were calculated with 4000 mesh points, whereas the genetic algorithm evaluations are using only 400 to reduce computational demands. Richardson extrapolation was not employed to refine the search, as we are aiming to establish a fully automated search, as mentioned previously.

Parameter	Range
n	$2.5 - 3.5$
$\sqrt{\frac{R_\odot^3 M_*}{M_\odot R_*^3}}$	$0.351 - 0.429$
f	$0.0025 - 0.01$

Some initial runs suggested that a diversity cutoff[10] value of 0.35 was suitable.

The convergence of the fitness function, the value of n, the value of $\sqrt{(R_\odot^3 M_*)/(R_*^3 M_\odot)}$ and the value of f for the best fit individual and the average over the population, are shown in figure 6.22. As can be seen, the convergence is extremely rapid to begin with; most of the parameters are fitted very accurately by both the average and most-well-fit individual. For the rotation rate, the average fits the data well, but a spurious local minimum is found after 23 generations for the most-well-fit individual. This is an example of an important fact when employing elitism: that we should be aware that the most elite individual is not, by right, indicative of the global minimum, and hence we should be aware of all the information contained in the population reached at the last generation. This may be a contributing factor in the amount of discussion over the exact fraction of crystallisation in the white-dwarf star BPM 37093. This (whether the crystallisation fraction of BPM 37093 is large or small) is an area disagreed over in recent months, due to confusion between calling something a most-well-fit individual found in a run, and calling the fit found a conclusive model of the star in question.

[10]Defining the diversity of the population as a standard-deviation-type measure, but again with the difference of given parameters from the mean weighted by a linear factor to "standardise" the width of each parameter range to 1.

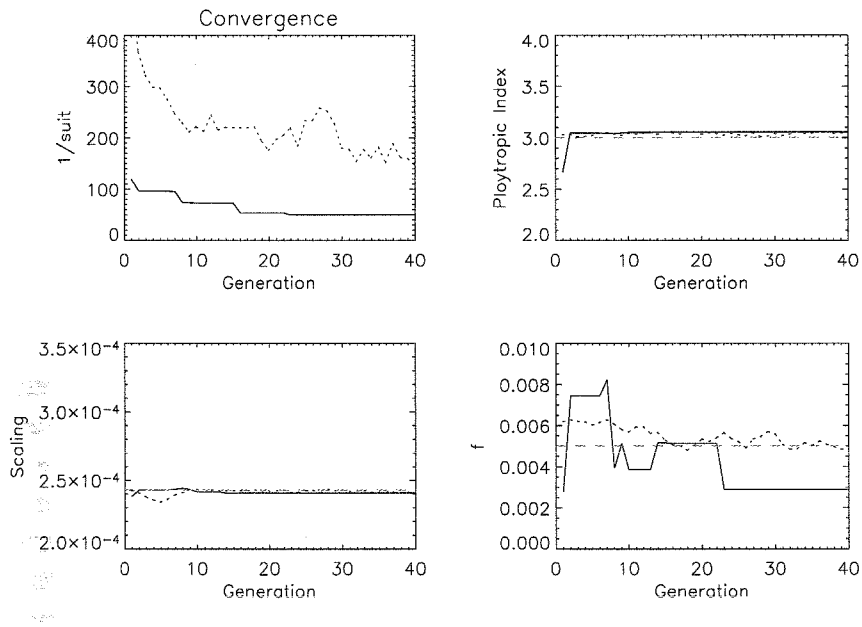

Figure 6.22: The convergence of: (a) the fitness function, (b) the polytropic index, n, (c) the scaling $\sqrt{(R_\odot^3 M_*)/(R_*^3 M_\odot)}$, and (d) the scaled rotation rate, f. The green denotes the "unknown" values of the original parameters, the most-well-fit individual is shown in black, and the average of the gene pool in red. Only the first 40 generations are shown, to concentrate on the early behaviour – the values shown are retained for many further generations.

6.4 Conclusions

We have seen that genetic algorithms provide a rapid fit to data in multi-dimensional parameter spaces. They are also well suited to the problem of forward modelling, which is the form the problem takes when fitting asteroseismic data, as was shown at the beginning of this chapter. This strongly encourages the use of genetic algorithms in fitting asteroseismic data, seeking to fit, amongst other parameters, the rotation rate. As a given shift in frequency can often have a number of causes, this result becomes more pertinent here.

Once we have decided to adopt the genetic-algorithmic approach to fitting our data, it is necessary to investigate how to improve our convergence speed. By fitting data from a known model whilst altering some of the parameters and the functioning of several internal subroutines of the code, we are able to increase our convergence speed greatly, which was the purpose of employing the genetic algorithm in the first case. This is very important when we move to the non-barotropic models of chapters 7 and 8 when model evaluations are far more computationally expensive.

We have seen the superiority of Elitism, Averaging and a use of the raw suitability score, as well as the quantitative effects of enforcing the diversity of the gene-pool, especially for the problem of fitting pulsational data.

This chapter provides quantifiable evidence of the superiority of these factors, giving confidence in the use of these methods and the choice of parameter values.

Chapter 7

THEORY OF NON-BAROTROPIC EQUATIONS OF STATE

"If we knew all the laws of Nature, we should need only one fact, or the description of one actual phenomenon, to infer all the particular results at that point." – Henry David Thoreau

We developed the methods of chapters 3 and 4 for barotropic equations of state. Even though the adoption of this equation of state simplifies the mathematics substantially, whilst retaining most of the basic dynamics, we must generalize the theory to more complicated equations of state in order to model real stars, such as the γ-Doradus variables discussed in the next chapter. We shall do this by first considering how, and to what extent, we can retain the results of chapters 3 and 4, and then by considering how much these results need to be changed.

7.1 GENERALIZATION OF PREVIOUS CHAPTERS

We seek to generalize the TA, which requires the components of the momentum equation to take the form

$$\boldsymbol{F}.(\boldsymbol{\xi}) = \begin{pmatrix} -\frac{1}{h_1}\frac{\partial p'}{\partial x} - \frac{\rho'}{h_1}\frac{\partial V}{\partial x} \\ -\frac{1}{h_2}\frac{\partial p'}{\partial \eta} \\ -\frac{1}{h_3}\frac{\partial p'}{\partial \phi} \end{pmatrix}, \tag{7.1}$$

which then allows p' and ρ' to have the same angular form, as is suggested by the relation

$$\frac{p'}{p} = \gamma_1 \left(\frac{\rho'}{\rho} + (\boldsymbol{\xi} \cdot \nabla) A \right) . \tag{7.2}$$

The requirement on the lhs of the momentum equation requires the oblate co-ordinate system to follow the surfaces of constant V. We know that the surfaces of ρ, p and T do not follow the same distortion for a non-barotropic equation of state (in fact, they have been listed in terms of decreasing oblateness of surfaces for a given rotation rate); but how does the surface of constant V relate to these?

7.1.1 HYDROSTATICS FOR A CONSERVATIVE ROTATION LAW

If we look at a general conservative rotation law (i.e. one for which the centrifugal force can be expressed as the gradient of a potential: $\mathbf{F}_{\rm rot} = \nabla\chi$ for some χ), then we can absorb this rotation into a modified potential $V \equiv \Phi + \chi$. Then, searching for putative hydrostatics, we arrive at

$$\nabla p = -\rho \nabla V , \tag{7.3}$$

giving that our surfaces of constant V and constant p must coincide[1]. Physically, we see that this is what we would expect to avoid unbalanced forces on the fluid.

This obviously neglects the Eddington-Sweet flow; if we were to investigate the size of the meridional circulation[2], neglecting inertial terms, $(\boldsymbol{u}.\nabla)\boldsymbol{u}$, and viscous friction, we would arrive at

$$|u_r| = f^2 \frac{LR^2}{GM^2} \left(\alpha_0 + \beta_0 \frac{\bar{\rho}}{\rho} \frac{\Delta\Omega}{\Omega_0} \right) , \tag{7.4}$$

[1]This is due, in part, to the fact, mentioned in chapter 4, that the metric factors h_i come in as identical multiplicative factors on both sides.

[2]A good summary is available in the book by Tassoul (2000).

where α_0 and β_0 are constants of order unity, $\bar{\rho}$ is the mean density, and $\Delta\Omega$ is a measure of the prescribed nonuniform rotation rate; thus the magnitude of Eddington-Sweet flow is very small indeed. It is also worth noting that the Eddington-Sweet flow will advect angular momentum and destroy the irrotational nature of the centrifugal force, causing a small perturbation to the background state.

Once this neglection of E-S flow is accepted, then, by equation (7.3) and a mathematically consistent distortion of other stellar parameters[3], a consistent non-rotating stellar model of (p, ρ, Φ) will be a consistent rotating stellar model of (p, ρ, V), although **not** for the same overall stellar parameters[4]. Then the modified Poisson equation,

$$\nabla^2 V = 4\pi G\rho + \nabla^2\chi \,, \tag{7.5}$$

once ∇^2 is expanded in terms of the metric coefficients (equations (3.8) to (3.10)) gives us formulae for the distortion mapping (equations (3.1) and (3.2)) as in chapter 3, and we can continue, to this order, as in chapter 4 for the distortions.

The two immediate questions arising from this theory are then those of how do we avoid Von-Zeipel's paradox arising from equation (7.3), and where is the surface of a rotating star?

7.1.2 VON-ZEIPEL'S PARADOX REVISITED

Taking the curl of equation (7.3) gives

$$\nabla\rho \times \nabla V = 0 \,, \tag{7.6}$$

forcing the surfaces of constant ρ to coincide with the surfaces

[3]For example the temperature distribution that will be touched upon in the next subsection.

[4]See, for example, the mass alteration section of chapter 3.

of constant V and p. The question then arises of how do we consistently avoid Von-Zeipel's paradox of this reasoning arriving at needing the energy generation to explicitly depend upon rotation?

To do this consistently, we simply require that $\nabla \boldsymbol{X} \neq \mathbf{0}$; then we are not allowed to say that the equation of state gives the surfaces of constant temperature (and hence opacity, then heat flux) to coincide again with surfaces of constant V, p and ρ.

In fact, to maintain mathematical consistency, what is needed for the behaviour of $\boldsymbol{X}$ is, e.g. for a gas pressure equation of state,

$$T = \left(\frac{p}{\mathcal{R}\rho}\right)\mu \,, \tag{7.7}$$

where μ is the mean molecular weight (not to be confused with $\cos\theta$). Thus we need the surfaces of constant μ and constant T to coincide (as the surfaces of constant p and ρ do in our artificial state).

From researches into the lithium depletion (Théado and Vauclair (2003a)) we know that the Eddington-Sweet flow will bend μ gradients in a suitable way to cause this. However, the timescale to create the initial μ gradients in an initially homogeneous star (outside of the core) is that of gravitational settling, which is prohibitively long. Thus it is important to note that this neglection of E-S flow is not what we expect to happen, but is at least a **mathematically consistent starting point**.

For the model to be fully consistent, we need $\nabla \cdot \boldsymbol{F} = 0$ (where $\boldsymbol{F}$ is the heat flux), which gives the required T distortion for a given basis choice, using the formula $\boldsymbol{F} = \kappa \nabla T$. Hence, for an electron-scattering opacity:

$$\kappa \nabla^2 T = 0 \;\Rightarrow\; \nabla^2 T = 0 \,, \tag{7.8}$$

and for Kramer's opacity:

$$\rho\nabla^2 T + \left(\nabla\rho\cdot\nabla T - 3.5\frac{\rho}{T}|\nabla T|^2\right) = 0 \ , \tag{7.9}$$

which we use to define the shape of $T(x,\eta)$, which it is convenient to express as

$$T(x,\eta) = T(x) + \sum_{l\geq 0,\ a\geq 1} f^{2a} T_{a,l} P_{2l}(\eta) \ . \tag{7.10}$$

7.1.3 THE SURFACE OF THE STAR

We have justified carrying across a non-rotating $(p,\ \rho,\ \Phi)$ profile as a consistent starting $(p,\ \rho,\ V)$ profile in a rotating star, but we do not have surfaces of temperature T and mean molecular weight μ coinciding with these $(p,\ \rho,\ V)$ surfaces. Thus we should take some time to consider where the surface of our rotating star is.

We can define the surface of a star by using a grey-atmosphere approximation:

$$\tau \equiv \int_{x_s}^{\infty} \kappa\rho \mathrm{d}x = \frac{2}{3} \ , \tag{7.11}$$

where x_s is denoting the surface of the star, and we know that in this basis

$$p = \int_{x_s}^{\infty} \rho\nabla V \mathrm{d}x = \frac{GM_0}{x_s^2}\int_{x_s}^{\infty} \rho \ \mathrm{d}x \ , \tag{7.12}$$

in which V is a vacuum solution. Here, M_0 is the mass that the star would have if it where not rotating, having the given $(p,\ \rho,\ \Phi)$ profile. This gives the equivalent grey-atmosphere condition as

$$p = \frac{2}{3}\frac{GM_0}{X^2}\frac{1}{\bar{\kappa}} \ , \tag{7.13}$$

which is the same as for a non-rotating star, except that the

mass used is not the true mass of the star (as just discussed, we are using M_0 instead of M), and $\bar{\kappa}$ is an opacity average *at a specific* η. Whilst this slight alteration in the lower limit of integration might cause us some worry, we note that the seismic surface and photosphere do not have to be in the same place, and hence we view the adoption of a non-rotating (p, ρ, Φ) profile as a consistent starting (p, ρ, V) profile in a rotating star as valid, as the alteration introduced here is negligable.

7.2 STRUCTURE FROM MILD NON-CONSERVATIVE ROTATION LAWS

7.2.1 MOTIVATION

Whilst conservative rotation laws are easily tractable mathematically, an Eddington-Sweet flow will cause an angular-momentum and temperature flux through the star, causing the rotation law to become non-conservative. For instance, an approximate rotation law for the Sun is given by:

$$\Omega(r,\theta) = \Omega_{\rm c} + \frac{1}{2}\left[1+\mathrm{erf}(\Delta)\right]\left(\Omega_{\rm s}(\theta)-\Omega_{\rm c}\right) , \tag{7.14}$$

$$\Omega_{\rm s} = \Omega_{\rm eq}(1-\alpha_2\mu^2-\alpha_4\mu^4),\ \Delta = \frac{r-r_{\rm c}}{w} , \tag{7.15}$$

in which $r_{\rm c} = 0.713\ {\rm R}_\odot$ is the radius at the bottom of the convective zone and $w = 0.025\ {\rm R}_\odot$ is the tachocline thickness; $\Omega_{\rm s}(\mu)$ is the surface angular velocity, which is parametrized in terms of the equatorial angular velocity $\Omega_{\rm eq}$ and the coefficients α_2 and α_4 whose values are 0.14 and 0.16, and $\Omega_{\rm c} = 0.93\Omega_{\rm eq}$ is the angular velocity of the core.

For other stars, direct starspot tracking (Collier Cameron et al., 2002) gives a best-fit surface rotation rate of

$$\Omega(\theta) = \Omega_{\rm eq} - \Omega_{\rm b} \sin^2\theta \ , \tag{7.16}$$

with $\Omega_{\rm eq} = 12.2434$ rad day^{-1} and $\Omega_{\rm b} = 0.0564$ rad day^{-1}.

Moving from G-type stars to A- and F-type, it has been found (Reiners and Royer, 2004; Reiners and Schmitt, 2003) that fitting a rotation law of the type

$$\Omega(\theta) = \Omega_{\rm Equator}(1 - \alpha \sin^2\theta) \tag{7.17}$$

to broadening profiles (presumably) caused by the rotation, that there are stars for which the fit is not consistent with $\alpha = 0$. Hence we need to explore deviations from a conservative rotation law. However, it is also worth noting that in all these examples, α never exceeds $1/3$, and is often much smaller. This encourages us to view the magnitude of differential rotation, $\Delta\Omega$, as significantly smaller than the magnitude of solid body rotation, Ω. The fact that for modest-to-rapid rotation the differential rotation is not strong is also found in numerical simulations – for example Kueker and Ruediger (2004).

7.2.2 FORMULATION OF THE PROBLEM

Motivated by this, we will look at rotation laws of the form

$$\boldsymbol{\Omega} = \boldsymbol{\Omega}_{\rm c} + \epsilon \boldsymbol{\Omega}_{\rm nc} \ , \tag{7.18}$$

with $\boldsymbol{\Omega}_{\rm c}$ and $\boldsymbol{\Omega}_{\rm nc}$ denoting the conservative and non-conservative parts of rotation respectively. We consider these two components of rotation to be co-axial and of the same magnitude, with ϵ small enough to be viewed as a perturbative parameter. Thus we can write

$$\boldsymbol{\Omega} = \boldsymbol{\Omega}_{\rm c}(1 + \epsilon b) \ , \tag{7.19}$$

with b a function of x and η.

7.2 Structure from mild non-conservative rotation laws

In the distorted co-ordinate basis given by the conservative part of rotation, we have to order f^4, after scaling:

$$\begin{aligned} \nabla\tilde{p} &= -\tilde{\rho}\nabla\tilde{V} + \epsilon f^2\tilde{\rho}(2+\epsilon b)(\sqrt{1-\eta^2}\mathbf{e}_x - \eta\mathbf{e}_\eta) \ , & (7.20)\\ \nabla^2\tilde{V} &= \tilde{\rho} + \nabla^2\tilde{\chi} \ , & (7.21) \end{aligned}$$

with $\tilde{\chi} \propto f^2$. We can then deal with ϵ in a perturbative manner; expanding

$$\tilde{p} = \tilde{p}_0(x) + f^2\epsilon\tilde{p}_1(x,\eta) + f^2\epsilon^2\tilde{p}_2(x,\eta) + \dots \ , \qquad (7.22)$$

and other variables likewise, we have, to order $f^2\epsilon$,

$$\begin{aligned} \nabla_0\tilde{p}_1 &= -\tilde{\rho}_1\nabla_0\tilde{V}_0 - \tilde{\rho}_0\nabla_0\tilde{V}_1 \\ &+ 2\tilde{\rho}_0(\sqrt{1-\eta^2}\mathbf{e}_x - \eta\mathbf{e}_\eta)b \ , & (7.23)\\ \nabla_0^2\tilde{V}_1 &= \tilde{\rho}_1 \ , & (7.24) \end{aligned}$$

with the operator ∇_0 being the ∇ operator correct to $O(f^0)$; this is because the distortion to the metric coefficients due to our change of basis contains no terms in $f^2\epsilon$.

Then, motivated by the form of the centrifugal force, we further expand $\tilde{p}_1(x,\eta)$ (and the other variables) in terms of Legendre polynomials:

$$\tilde{p}_1(x,\eta) = \sum_{s\geq 0}\tilde{p}_{1,s}(x)P_{2s}(\eta) \ , \qquad (7.25)$$

and then substitute in the equations of motion, equating coefficients of these Legendre polynomials to give

$$\frac{\partial \tilde{p}_{1,s}}{\partial x} = -\left(\tilde{\rho}_{1,s}\frac{\partial \tilde{V}_0}{\partial x} + \tilde{\rho}_0\frac{\partial \tilde{V}_{1,s}}{\partial x}\right)$$

$$+\tilde{\rho}_0(4s+1)\int_{-1}^{1} b \quad \sqrt{1-\eta^2}P_{2s}(\eta)\mathrm{d}\eta \ , \tag{7.26}$$

$$\left(\frac{1}{x^2}\frac{\partial}{\partial x}\left(x^2\frac{\partial}{\partial x}\right) - 2s(2s+1)\right)\tilde{V}_{1,s} = \tilde{\rho}_{1,s} \ , \tag{7.27}$$

$$(1-\delta_{s,0})\tilde{p}_{1,s} = (1-\delta_{s,0})\tilde{\rho}_0\tilde{V}_{1,s}$$

$$-\tilde{\rho}\frac{(4s+1)}{2s(2s+1)}\int_{-1}^{1} b \quad (1-\eta^2)\eta P'_{2s}(\eta)\mathrm{d}\eta \ . \tag{7.28}$$

Likewise, to order $f^2\epsilon^2$,

$$\frac{\partial \tilde{p}_{2,s}}{\partial x} = -\left(\tilde{\rho}_{2,s}\frac{\partial \tilde{V}_0}{\partial x} + \tilde{\rho}_0\frac{\partial \tilde{V}_{2,s}}{\partial x}\right)$$

$$+\tilde{\rho}_0\frac{4s+1}{2}\int_{-1}^{1} b^2 \quad \sqrt{1-\eta^2}P_{2s}(\eta)\mathrm{d}\eta \ , \tag{7.29}$$

$$\left(\frac{1}{x^2}\frac{\partial}{\partial x}\left(x^2\frac{\partial}{\partial x}\right) - 2s(2s+1)\right)\tilde{V}_{2,s} = \tilde{\rho}_{2,s} \ , \tag{7.30}$$

$$(1-\delta_{s,0})\tilde{p}_{2,s} = (1-\delta_{s,0})\tilde{\rho}_0\tilde{V}_{2,s}$$

$$-\tilde{\rho}\frac{(4s+1)}{4s(2s+1)}\int_{-1}^{1} b^2 \quad (1-\eta^2)\eta P'_{2s}(\eta)\mathrm{d}\eta \ . \tag{7.31}$$

These equations can then be combined to yield second-order differential equations for $\tilde{V}_{i,s}$ for non-zero s, giving

$$\left(\frac{\partial \tilde{V}_0}{\partial x}\left(\frac{1}{x^2}\frac{\partial}{\partial x}\left(x^2\frac{\partial}{\partial x}\right) - 2s(2s+1)\right) - \frac{\partial \tilde{\rho}}{\partial x}\right)\tilde{V}_{1,s}$$

$$
\begin{aligned}
&= -\int_{-1}^{1}\left\{\tilde{\rho}_0 b\frac{\partial\tilde{V}_0}{\partial x}(4s+1)P_{2s}(\eta)\right.\\
&\left.+\frac{4s+1}{2s(4s+1)}(1-\eta^2)P'_{2s}(\eta)\frac{\partial}{\partial x}(\tilde{\rho}_0 b)\right\}\mathrm{d}\eta\ , \qquad (7.32)\\
&\left(\frac{\partial\tilde{V}_0}{\partial x}\left(\frac{1}{x^2}\frac{\partial}{\partial x}\left(x^2\frac{\partial}{\partial x}\right)-2s(2s+1)\right)-\frac{\partial\tilde{\rho}}{\partial x}\right)\tilde{V}_{2,s}\\
&= -\frac{1}{2}\int_{-1}^{1}\left\{\tilde{\rho}_0 b^2\frac{\partial\tilde{V}_0}{\partial x}(4s+1)P_{2s}(\eta)\right.\\
&\left.+\frac{4s+1}{2s(4s+1)}(1-\eta^2)P'_{2s}(\eta)\frac{\partial}{\partial x}(\tilde{\rho}_0 b^2)\right\}\mathrm{d}\eta\ . \qquad (7.33)
\end{aligned}
$$

For boundary conditions, physically we see that we have a choice of the central value of the potential alteration which can be absorbed into setting the potential at infinity to zero, and also that the potential must match onto a vacuum solution at the surface of the star. Mathematically, these translate to

$$
\begin{aligned}
\tilde{V}_{i,s}(0) &= 0\ , \qquad (7.34)\\
\frac{\partial}{\partial x}\tilde{V}_{i,s}(x_s) &= -\frac{2s+1}{X}\tilde{V}_{i,s}(x_s)\ , \qquad (7.35)
\end{aligned}
$$

where $x = x_s$ is the surface of the star.

7.2.3 SPHERICALLY SYMMETRIC DISTORTION

To calculate the spherically symmetric component of the distortion of the background state due to non-conservative rotation laws, we have equations (7.26) and (7.27) (and their $O(f^2\epsilon^2)$ equivalents), but both sides of equation (7.28) are identically zero, so this equation cannot close the mathematical system. We are left with a number of ways to proceed.

Gough and Thompson (1990), when considering a very similar problem concerning the effect of rotation in the Sun, took a two-region model and perturbed the structure equations in the outer region due to the force generated by a quadrapole toroidal magnetic field

$$\boldsymbol{B} = \left[0,\ 0,\ a(r)\frac{d}{d\theta}P_k(\cos\theta)\right] , \tag{7.36}$$

and perturbed the hydrogen abundance and mixing-length parameter, α, to calibrate their model to solar luminosity and radius. However, for other stars, we do not have the accuracy of these parameters that we do for the Sun. Owing to this lack of accuracy of data, there is a large amount of freedom with how we may choose to close our mathematical system. Exploiting this freedom, and in order to avoid the possibility of the correction to N^2 being larger than the value of N^2 at any point in the star, we fix the radial profiles of $-gN^2$ and γ_1 to calculate $\tilde{p}_{1,0}$ and $\tilde{\rho}_{1,0}$, and use the definition of $-gN^2$ to close the system, so

$$-gN^2 \equiv \frac{\partial \ln \rho}{\partial x} - \frac{1}{\gamma_1}\frac{\partial \ln p}{\partial x} , \tag{7.37}$$

$$\Rightarrow\ \tilde{\rho}_{1,0}\frac{\partial \tilde{p}_0}{\partial x} + \tilde{\rho}_0\frac{\partial \tilde{p}_{1,0}}{\partial x} = \gamma_1\left(\tilde{p}_0\left(\frac{\partial \tilde{\rho}_{1,0}}{\partial x} - \tilde{\rho}_{1,0}A\right) + \tilde{p}_{1,0}\left(\frac{\partial \tilde{\rho}_0}{\partial x} - \tilde{\rho}_0 A\right)\right) , \tag{7.38}$$

which closes the system. It is no longer sensible to eliminate $\tilde{\rho}_{1,0}$ and $\tilde{p}_{1,0}$ in favour of $\tilde{V}_{1,0}$, so we instead eliminate $\tilde{V}_{1,0}$ and $\tilde{p}_{1,0}$ in favour of $\tilde{\rho}_{1,0}$. For the outer boundary condition, we enforce $\tilde{\rho}_{1,0} = 0$ at the surface.

The perturbations to order $f^2\epsilon^2$ are calculated similarly.

7.3 CORRECTING THE FREQUENCIES

This alteration to the structure changes the frequencies to a greater level than $O(f^4)$, which we should therefore consider. Again, we can exploit the variational principle formulation of the equations for oscillations in a distorted star to calculate this.

7.3.1 BACKGROUND FLOW

Unlike in chapter 4, we may now have a background flow, which we shall denote $\mathbf{u}_0$, so some of the equations (4.10) to (4.18) have to be changed to

$$\begin{aligned} \mathbf{B}.(\boldsymbol{\xi}) &= 2\mathrm{i}\rho_0\boldsymbol{\Omega}\times\boldsymbol{\xi} + 2\mathrm{i}\rho_0(\mathbf{u}_0\cdot\nabla)\boldsymbol{\xi}\ , &(7.39)\\ \mathbf{T}.(\boldsymbol{\xi}) &= \rho_0(\mathbf{u}_0\cdot\nabla)(\mathbf{u}_0\cdot\nabla)\boldsymbol{\xi} + 2\rho_0\boldsymbol{\Omega}\times((\mathbf{u}_0\cdot\nabla)\boldsymbol{\xi}) \\ &+ \rho_0\boldsymbol{\Omega}\times(\boldsymbol{\Omega}\times\boldsymbol{\xi})\ . &(7.40)\end{aligned}$$

We absorb all of the solid-body rotation into the rotation $\boldsymbol{\Omega}_\mathrm{s}$ of our co-ordinate system and therefore set[5]

$$\mathbf{u}_0 \equiv (\boldsymbol{\Omega}-\boldsymbol{\Omega}_\mathrm{s})\times\mathbf{r}\ . \tag{7.41}$$

Therefore we have to view $\mathbf{B}.(\boldsymbol{\xi})$ (or $\mathbf{B}_{\mathrm{TA}}.(\boldsymbol{\xi})$) and $\mathbf{T}.(\boldsymbol{\xi})$ in equation as being perturbed to, for example,

$$\mathbf{B}.(\boldsymbol{\xi}) \rightarrow \mathbf{B}.(\boldsymbol{\xi}) + \Delta_{\mathrm{flow}}\mathbf{B}.(\boldsymbol{\xi}) \tag{7.42}$$

with

$$\begin{aligned} \Delta_{\mathrm{flow}}\mathbf{B}.(\boldsymbol{\xi}) &= 2\mathrm{i}\rho_0(\mathbf{u}_0\cdot\nabla)\boldsymbol{\xi}\ , &(7.43)\\ \Delta_{\mathrm{flow}}\mathbf{T}.(\boldsymbol{\xi}) &= \rho_0(\mathbf{u}_0\cdot\nabla)(\mathbf{u}_0\cdot\nabla)\boldsymbol{\xi}\end{aligned}$$

[5]We have neglected, owing to timescale, the direct effect of Eddington-Sweet flow on the pulsation, as given earlier in the chapter.

$$+ \quad 2\rho_0 \boldsymbol{\Omega} \times ((\mathbf{u}_0 \cdot \nabla)\boldsymbol{\xi}) \; . \tag{7.44}$$

These terms have a directional derivative $\mathbf{u}_0 \cdot \nabla$ in them. Owing to the definition of $\mathbf{u}_0$, and the choice of axis, we can say that

$$\begin{aligned} \mathbf{u}_0 &\equiv u_0 \mathbf{e}_\phi \; , & (7.45) \\ \Rightarrow \mathbf{u}_0 \cdot \nabla &= \frac{u_0}{h_3} \frac{\partial}{\partial \phi} \; , & (7.46) \\ &= \frac{\mathrm{i}m u_0}{h_3} \; , & (7.47) \end{aligned}$$

assuming an $e^{\mathrm{i}m\phi}$ dependence to arrive at equation (7.47), which assumption of ϕ dependence we shall adopt. Therefore, the size of this term can be easily considered as

$$\begin{aligned} |\mathbf{u}_0 \cdot \nabla| &\sim \frac{|\mathrm{i}m u_0|}{|h_3|} \; , & (7.48) \\ &= \frac{|m| \; |\boldsymbol{\Omega} - \boldsymbol{\Omega}_\mathrm{s}|}{\left|(x\sqrt{1-\eta^2})^{-1} h_3\right|} \; , & (7.49) \end{aligned}$$

We can see from equation (3.10) that $|h_3| \approx |x\sqrt{1-\eta^2}|$, so we must be certain that $|\boldsymbol{\Omega} - \boldsymbol{\Omega}_\mathrm{s}|$ is small enough for this term to be viewed as a perturbation. We can investigate this by looking at the first-order change in frequencies that this alteration causes, by using

$$\begin{aligned} (\omega_0 + \Delta_\mathrm{flow}\omega)^2 \mathbf{A}.(\boldsymbol{\xi}) \; &+ \; (\omega_0 + \Delta_\mathrm{flow}\omega)(\mathbf{B}_\mathrm{TA} + \Delta_\mathrm{flow}\mathbf{B}).(\boldsymbol{\xi}) \\ &+ \; \mathbf{C}.(\boldsymbol{\xi}) \; = 0 \; , \end{aligned} \tag{7.50}$$

which gives to first order in Δ_flow,

$$\langle \boldsymbol{\xi}, \Delta_{\text{flow}}\omega(2\omega_0\mathbf{A}+\mathbf{B}).(\boldsymbol{\xi})\rangle + \omega_0\langle \boldsymbol{\xi}, \Delta_{\text{flow}}\mathbf{B}.(\boldsymbol{\xi})\rangle = 0 \ , \quad (7.51)$$

$$\Rightarrow \Delta_{\text{flow}}\omega = -\frac{\langle \boldsymbol{\xi}, \Delta_{\text{flow}}\mathbf{B}.(\boldsymbol{\xi})\rangle}{2\langle \boldsymbol{\xi}, \rho\boldsymbol{\xi}\rangle} \ , \quad (7.52)$$

the form of which equation should not surprise us: equation (7.52) simply says that the change that non-solid-body rotation causes to the frequency is a weighted mean (via the size of u_0) of the deviation from solid-body rotation around areas where $|\boldsymbol{\xi}|$ is large, as we would expect physically.

7.3.2 DISTORTION OF THE BACKGROUND STATE

We also need to take account of the background distortion of the star in the calculation of frequencies. This distortion is of orders $f^2\epsilon$ and $f^2\epsilon^2$, so, as we have said, ϵ is small: thus, we do not have to calculate any variation to the eigenfunction to correct the frequencies up to $\mathrm{O}(f^4)$ as these corrections will only affect the frequencies at order $O(f^4\epsilon^2)$. We shall denote the changes to orders ϵ and ϵ^2 as Δ_ϵ and Δ_{ϵ^2} respectively.

Also, owing to the fact that ϵ is small, the combination of perturbed structure along with structure/eigenfunction perturbations (for instance, $\tilde{\rho}_{1,s}\delta\boldsymbol{\xi}$) are also too small to produce changes at the level at which we are looking, greatly simplifying the problem. Likewise we do not have to consider $\Delta_\epsilon\mathbf{T}.(\boldsymbol{\xi})$ or $\Delta_{\epsilon^2}\mathbf{T}.(\boldsymbol{\xi})$ as $\mathbf{T}.(\boldsymbol{\xi})$ is already of order f^2.

Therefore the perturbations to the operators that we need to consider are

$$\Delta_\epsilon\mathbf{A} = \sum_l \rho_{1,l}P_{2l}(\eta)\mathbf{I} \ , \quad (7.53)$$

$$\Delta_\epsilon \mathbf{B}.(\boldsymbol{\xi}) = \sum_l \Big(2\mathrm{i}\rho_{1,l} P_{2l}(\eta) \boldsymbol{\Omega} \times \boldsymbol{\xi} + 2\mathrm{i}\rho_{1,l} P_{2l}(\eta)(\mathbf{u}_0 \cdot \nabla)\boldsymbol{\xi} \Big) , \tag{7.54}$$

$$\Delta_\epsilon \mathbf{P}.(\boldsymbol{\xi}) = \sum_l P_{2l}(\eta) \Big(\nabla_s \left[(1-\gamma_1) p_{1,l} \nabla_s . \boldsymbol{\xi} \right] - p_{1,l} \nabla_s (\nabla_s . \boldsymbol{\xi}) - \nabla_s \left[(\boldsymbol{\xi} . \nabla_s) p_{1,l} \right] + (\boldsymbol{\xi} . \nabla_s) \nabla_s p_{1,l} \Big) , \tag{7.55}$$

$$\Delta_\epsilon \mathbf{V}.(\boldsymbol{\xi}) = \sum_l \left(\rho_0 (\boldsymbol{\xi} . \nabla_s) \nabla_s V_{1,l} + \rho_{1,l} (\boldsymbol{\xi} . \nabla_s) \nabla_s V_0 \right) . \tag{7.56}$$

The importance of the second term in $\Delta_\epsilon \mathbf{B}.(\boldsymbol{\xi})$ can vary in importance, as discussed in the previous subsection.

These perturbations to the operators give

$$\Delta_\epsilon = -\frac{\langle \boldsymbol{\xi}, \left(\omega_0^2 \Delta_\epsilon \mathbf{A} + \omega_0 \Delta_\epsilon \mathbf{B} + \Delta_\epsilon \mathbf{C} \right) . (\boldsymbol{\xi}) \rangle}{2\omega_0 \langle \boldsymbol{\xi}, \rho_0 \boldsymbol{\xi} \rangle} , \tag{7.57}$$

and similarly for Δ_{ϵ^2}.

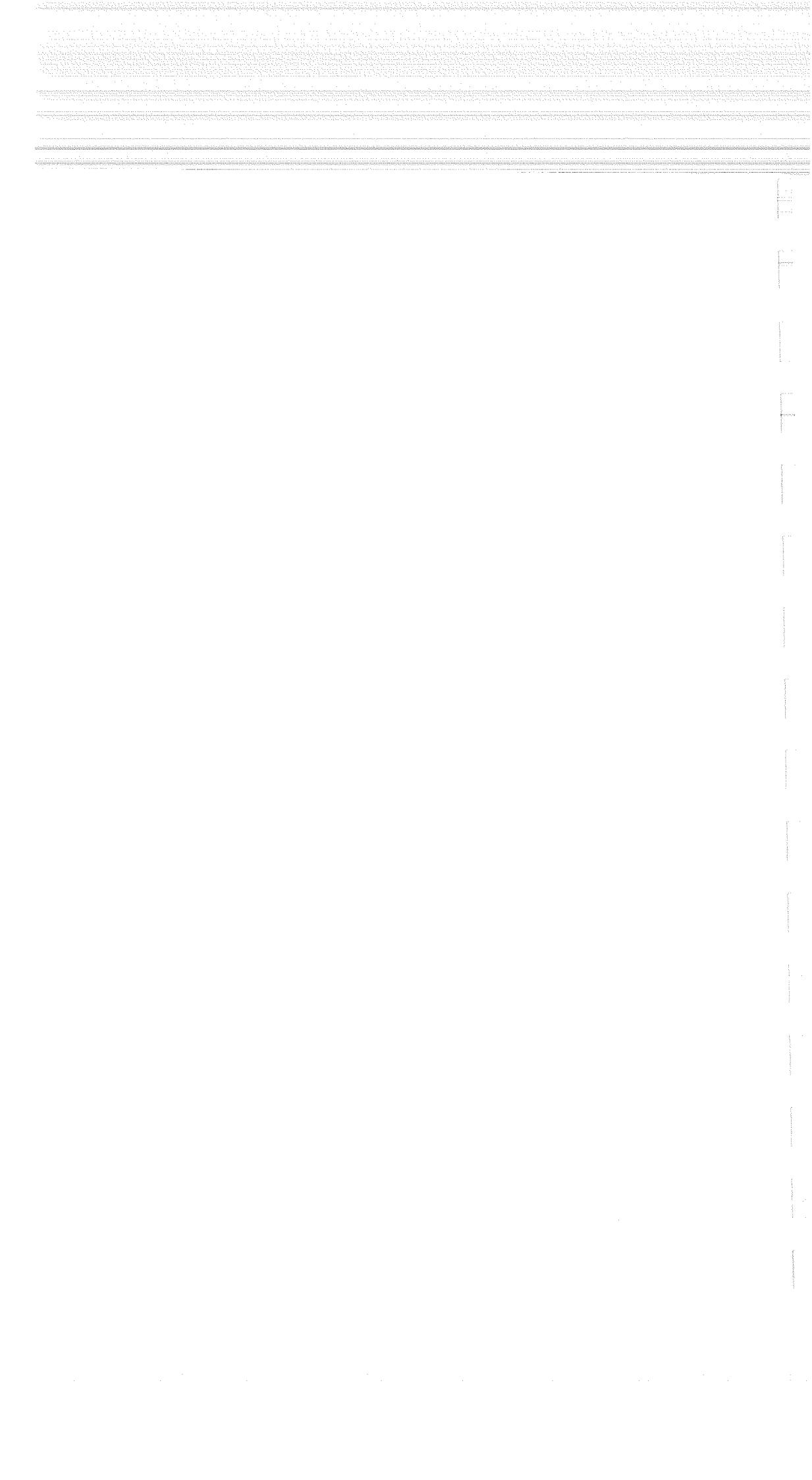

Chapter 8
γ-Doradus Stars

"He determines the number of the stars and calls them each by name." – Psalm 147, verse 4

8.1 An introduction to γ-Doradus Stars

8.1.1 Their discovery and their pulsations

The class of γ-Doradus stars is made up of g-mode pulsators occupying a small region of the H-R diagram (see figure 1.1; and figure 8.1 for a magnitude verses colour diagram) just above the Sun on the main sequence. They are of a spectral type around F0, they have pulsational periods of the order of 1 day and amplitudes of variability in the V band of the order of a few tens of millimagnitudes.

As was mentioned in the introduction, γ-Doradus stars as a group of pulsators are relatively recently discovered. Many of these discoveries were serendipitous, as the general region that we now know them to occupy (figure 8.1) was outside known instability strips, and therefore many of these stars were picked for use as comparison stars[1], and only then found to be variable.

The identification of these variable stars as a class of pulsators largely post-dates[2] the discovery of many of the individual stars

[1]For example, HD 164615, mentioned later, was picked for use as a comparison star for the Ap star HD 165474.

[2]In fact, as can be seen by the name of the star after which this class of star is named, the discovery of the individual star and the discovery of the nature of its pulsations can differ by millennia!

that we now know to be variable. Abt et al. (1983) discovered the variability of HD 164165, but attributed the variability to the star being spotted. Such a hypothesis existed for many stars, until it was realized (Balona et al. (1994b) for γ Doradus itself) that large overlapping spots and incredibly strong differential rotation would be required to be consistent with the observed light and colour amplitudes. Kaye and Strassmeier (1998) looked for signatures of strong magnetic activity, which would support the starspot hypothesis, in the Ca II H & K lines, and found none, further suggesting the identification of γ-Doradus variables as (non-radial) pulsators.

After it was realized that the variability was due to pulsation, models quickly showed that the pulsations must be high-radial-order g-mode pulsations, because of the low values of the observed periods. Exact radial orders have not been determined, although fitting of the spherical harmonic degrees (l, m) has been attempted, for example by Balona et al. (1996) for γ Doradus itself.[3]

After the classification of these stars as a separate group of pulsators, systematic searches have begun. For instance, Handler (1999) examined the *Hipparcos* database for variables with spectral types of A-G, periods between 0.3 and 10 days, amplitudes of pulsation less the 0.2 mmag, and brighter than $H_p = 8.5$ mag at minimum, which were not classified as supergiants. After this refinement, individual lightcurves were examined and obvious non-γ-Doradus stars (for example, eclipsing binaries, low-amplitude Cepheids) were removed from the data set.

Subsequently a period search was performed, looking for variations on a time-scale longer than that of the period of the funda-

[3]This identification was based upon a first order expansion in Ω/ω for spherical harmonics. It was noted that with $\Omega/\omega > 0.55$, this was not expect to be a good fit, but thought that the "original" spherical harmonic would still be dominant. For more on this, see chapter 9.

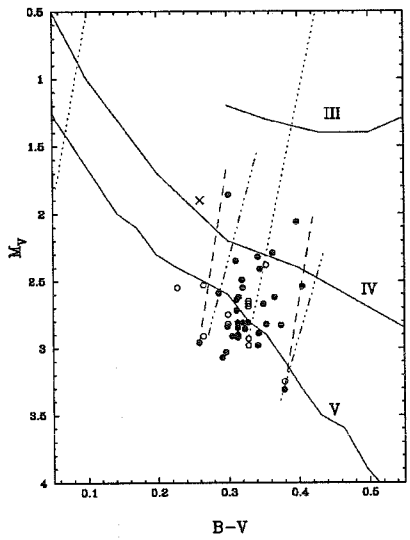

Figure 8.1: Location of 42 confirmed γ-Doradus stars (and binary components for three of them) in the H-R diagram. Filled circles denote stars with well determined locations, and other stars are marked as open circles. HD 209295 is marked as the cross. The dotted lines indicate the boundaries of the δ-Scuti instability strip, dashed lines the observed domain of γ-Doradus stars, and triple-dot-dashed lines the theoretical domain of γ-Doradus stars, from Warner et al. (2003) (taken from Henry and Fekel, 2003).

mental radial mode. This further refinement of the data set left 70 candidates which were further sub-divided into "prime" and "other" candidates, according to whether the stars were multi-periodic, with clearly separated, unambiguous, periods, or not. The resulting list, and further updates[4], can be found at the following URL: www.astro.univie.ac.at/~gerald/gdorlist.html .

It is on the stars in this list (occasionally with some additions) that follow-up observations are often carried out, such as those by Henry and Fekel (2003). In these searches, after reliably obtaining magnitude readings in B and V filters, a least-squares fitting of sinusoids was performed. The frequency fit achieved was derived iteratively. At each iteration only previously detected frequencies were specified, and the mean brightness, a trial frequency, all amplitudes and all phases were fitted. The fractional reduction of the variance versus trial frequency was plotted at each iteration to determine the next frequency. This method proves very good at detecting multiple frequencies without pre-whitening, proving an advantage, especially in the low-frequency domain.

The results of an example of this analysis can be seen in figure 8.2 for the star HD 152896, which will be discussed later in more detail.

8.1.2 The overlap of γ-Doradus and δ-Scuti classes

The region of parameter space occupied by γ-Doradus variables overlaps with that occupied by δ-Scuti stars (which are evolved low-radial-order p-mode pulsators), as can be seen in figure 8.1. Because of this overlap, at least one careful search (by Handler and Shobbrook, 2002) has been made to find stars exhibiting both types of pulsation; apart from the star HD 209295, which is peculiar in the sense that it is a close binary (and therefore the

[4]Note that list is no longer (from 25th September 2002) updated.

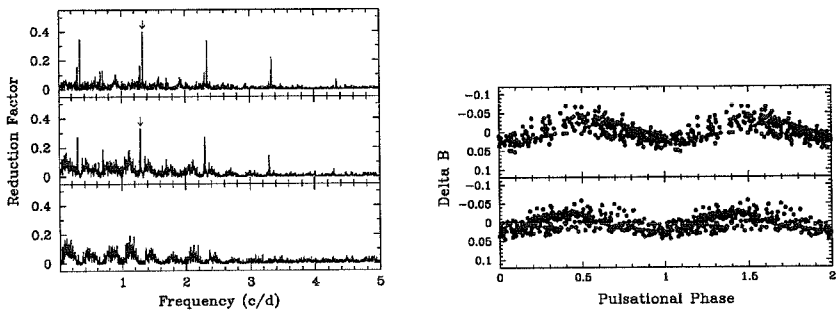

Figure 8.2: Left panel: Least-squares spectra of HD 152896 (Johnson B data set), showing the results of progressively fixing detected frequencies (denoted by the arrows). Right panel: Johnson B photometric data for HD 152896, phased with the frequencies from the left-hand panel; for each graph, the data have been pre-whitened to remove the other known frequency (taken from Henry and Fekel, 2003).

"γ-Doradus pulsations" might well be tidally excited oscillations), none have been found.

The authors showed also that, although the pulsation periods of the longest-period δ-Scuti stars are very close to those of the shortest-period γ-Doradus stars, the two types of pulsations (and hence pulsators) can be quite clearly separated if instead the pulsation constant Q, calculated as[5]

$$\log Q_i = 0.5 \log g + 0.1 M_{\rm bol} + \log T_{\rm eff} + \log P_i - 6.456 \ , \quad (8.1)$$

[5]Equation (8.1) is simply from the equation $Q = P(\bar{\rho}/\bar{\rho}_\odot)^{1/2}$ (i.e. what the period would be for the Sun undergoing such a pulsation) using the relations $\bar{\rho} \propto g/R$, $L \propto R^2 T_{\rm eff}^4$, and $M_{\rm bol} = -2.5 \log(L) + C$, to obtain an observationally tractable form. Hence the constant -6.456 is chosen such that the equation collapses to $\log Q = \log P$ for the Sun.

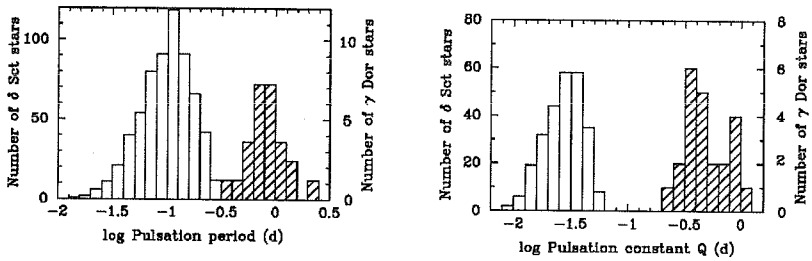

Figure 8.3: The number (known at the time of publication) of δ-Scuti stars (open histogram bars) and γ-Doradus stars against pulsation period (left panel) and pulsation constant, Q (right panel) (taken from Handler and Shobbrook, 2002).

is used. This fact is shown in figure 8.3, and is as would be expected due to the differing nature of the two types of pulsations, and allows us to define γ-Doradus pulsations quite clearly.

8.1.3 Their Driving

As may be expected, the driving mechanisms for these two groups of stars differ; whilst δ-Scuti stars are driven by the κ mechanism, models of γ-Doradus stars are found computationally (as proposed by Guzik et al., 2000) to be driven by what is known as "convective blocking". For this driving mechanism, the local convective timescale is large enough compared to the pulsational period that the convection cannot adjust completely to the change in luminosity due to the pulsation at the base of the convection zone, resulting in driving of the pulsation. This is seen to occur in computer codes modelling stars, but remains in question as to the exact physics that is going on.

This driving of computational models provides predictions of the edges of the instability region that can be tested; although

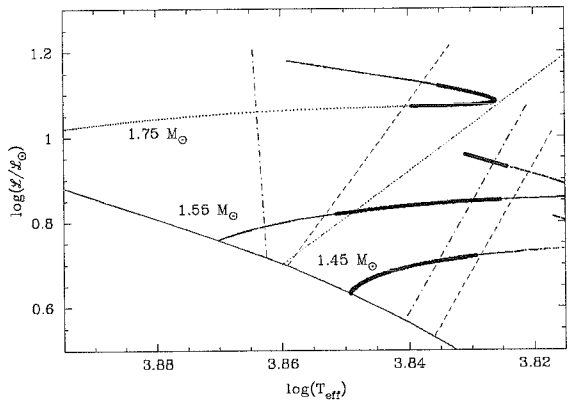

Figure 8.4: H-R diagram showing theoretical (dashed lines) and observed (dot-dash lines) regions in which models of stars are unstable to γ-Doradus pulsations. The red edge of the δ-Scuti instability strip is show by the triple-dot-dash line. Evolutionary tracks for 1.45, 1.55 and 1.75 $M_\odot$ stars are shown by the dotted lines, with models that are unstable to $l = 1$ pulsation driving shown in bold (taken from Warner et al., 2003).

the number of γ-Doradus stars is reasonably small (42), it is in rough agreement with the current data, as is shown in figure 8.1. To calculate this theoretical instability region, Warner et al. (2003) calculated approximately 15,000 models, and investigated which models had growth rates (ΔKE/KE per period) greater than 10^{-7} per period for modes in the period 0.3-3 days (for l in $\{0,1,2,3,4,5\}$). The theoretical and observed instability regions are again displayed in figure 8.4, with evolutionary tracks for 1.45, 1.55, and 1.75 $M_\odot$ stars (for a solar composition of Y=0.28, Z=0.02).

As can be seen, stars of non-negligible range of masses will pass through the theoretical instability strip during some early

era of their evolution. This result is in fairly good concordance with the observations of γ-Doradus stars as young stars of the required mass range. However, for the exact placement of the theoretical instability strip, we should note that these results have all been obtained using the solar composition of Y=0.28 and Z=0.02. A changing of the metallicity would cause the red and blue edges to shift slightly.

8.1.4 The challenge

Some γ-Doradus stars, along with their values of the parameter ν, were displayed in chapter 1; it is the modelling of this type of fast-rotating, low-frequency, g-mode pulsator that has been driving the investigation of pulsations for which ν is not small enough to be treated as a perturbative parameter. Owing to the fact that the pulsations of γ-Doradus stars are fairly-high-order g modes, the modelling of these modes is exactly where we would expect the realm of validity of the generalized TA to be.

We shall therefore proceed to give an example of the implications of the theory developed in previous chapters to a model of a γ-Doradus star.

8.1.5 A closer look at an individual star

In order to both examine an individual star and construct a model of it, we must, arbitrarily select a star. HD 152896 ($\equiv$ V645 Her), an F1 variable star of V-band magnitude around 7.6, was chosen (from the paper by Henry and Fekel, 2003), as it is a single star exhibiting more than one mode of pulsation, with no cited possible confusion over aliasing. The properties of this star are displayed in table 8.1.

As can be seen from table 8.1, the data are of very high precision; from now on, we shall adopt the B-band frequencies for the fifth significant figure to calculate parameters displayed and

Parameter	Value
$R/R_\odot$	1.5
$L/L_\odot$	5.6
ω_1 (V band, day^{-1})	1.3384 $\pm$0.0002
ω_2 (V band, day^{-1})	1.2972 $\pm$0.0002
ω_1 (B band, day^{-1})	1.3385 $\pm$0.0002
ω_2 (B band, day^{-1})	1.2971 $\pm$0.0003
$v \sin i$	50 km s^{-1}

Table 8.1: Table of derived properties of HD 152896.

for the sake of brevity we shall drop the errors. As can be seen from figure 8.2, after the two frequencies have been fitted, there is a strong indication of further periodicities at low frequencies, but without any obvious period(s). This suggestion of further variability is confirmed by the fact that the rms of the residual variation after the two periods given in table 8.1 have been removed is 0.016 mag. However, we shall not postulate about further frequencies.

The stellar parameter fit mentioned in subsection 8.2.1 gave the star a mass of $M = 1.55$ M$_\odot$,[6] giving a natural frequency of $\sqrt{GM/R^3} = 4.25 \times 10^{-4}\ s^{-1} = 36.7$ day^{-1}. Thus, depending on the inclination angle, i, values of the parameters f and ν_k are shown in table 8.2. The choice of the B-band values, with this natural frequency, gives the scaled[7] frequencies as $\bar{\omega}$=(3.6436, 3.5309) $\times 10^{-2}$, in the non-rotating frame.

However, should we have $m = 1$, then the frequencies in the rotating frame (the natural frame of the star) would be those given in table 8.3.

[6]Note that a star of this mass value spends a relatively long time in the γ-Doradus instability strip given in figure 8.4.

[7]Scaled by the natural frequency.

i	$v(\mathrm{km\ s^{-1}})$	$\Omega(\mathrm{d^{-1}})$	f	ν_1	ν_2
10	288	3.793	0.103	5.67	5.85
20	146	1.925	0.052	2.88	2.97
30	100	1.317	0.036	1.97	2.03
40	77.8	1.025	0.028	1.53	1.58
50	65.3	0.860	0.023	1.28	1.33
60	57.7	0.760	0.021	1.14	1.17
70	53.2	0.701	0.019	1.05	1.08
80	50.8	0.669	0.018	1.00	1.04
90	50.0	0.659	0.018	0.98	1.02

Table 8.2: Non-dimensional rotation parameters of HD 152896 for various inclination angles, i, assuming $m = 0$.

As can be seen from tables 8.2 and 8.3, the values of ν_k are much too large, for any value of inclination angle i, for an expansion in Ω/ω to be valid, regardless of a chosen (plausible) value of m. We shall therefore proceed with a numerical model of this star.

8.2 NUMERICAL MODEL USED

8.2.1 INITIAL FIT

To select the stellar parameters for our model, a star was picked from the twelve γ-Doradus discovered by Henry and Fekel (2003), already mentioned, and then, from published L and R, a fit was carried out using the STARS code[8] to extract masses, helium abundances, ages, and so forth.

[8]Using the updated opacities published by Eldridge and Tout (2004). For this search, models were calculated using 499 mesh points, which proved sufficient not to introduce large inaccuracy. The author thanks J. Eldridge for help with this search.

i	f	ω_1	ω_2	ν_1	ν_2
10	0.103	0.134	0.139	1.48	1.49
20	0.052	0.089	0.088	1.18	1.20
30	0.036	0.072	0.071	0.99	1.01
40	0.028	0.064	0.063	0.87	0.88
50	0.023	0.060	0.059	0.78	0.80
60	0.021	0.057	0.056	0.72	0.74
70	0.019	0.056	0.054	0.69	0.70
80	0.018	0.055	0.054	0.67	0.68
90	0.018	0.054	0.053	0.66	0.67

Table 8.3: Non-dimensional rotation parameters of HD 152896 for various inclination angles, i, assuming $m = 1$.

There is an excess of parameters in this fit, which was tightened considerably by assuming a solar metallicity, for ease of opacity calculations. Since the two lists of γ-Doradus variables mentioned above include only $L/\mathrm{L}_\odot$ and $R/\mathrm{R}_\odot$, the model given by the STARS code provides a satisfactory fit[9] (i.e. within the error bounds that this precision allows) to the data; by reducing the metallicity slightly, it is expected that a more precise fit could be obtained. However, it is important to note that the model was selected only as an example; therefore the fit provided by the STARS code is adequate for our purposes.

8.2.1.1 The Cambridge Stellar Evolution Code, STARS

The STARS code is a short (less than 2000 lines of Fortran 77) code to model the evolution of stars. It was originally written by Eggleton (1971), with a large update by Pols et al. (1995), and further minor refinements such as expanded opacity tables.

[9]The model star given by the fit has $L/\mathrm{L}_\odot = 5.595$ and $R/\mathrm{R}_\odot = 1.549$

8.2 Numerical model used

In common with many stellar evolution codes, it replaces the equations governing stellar evolution (for example, equations (1.1)-(1.10)) by appropriate difference equations and solves by relaxation. The boundary conditions at the surface are of conservation of mass, black body emission and a grey atmosphere (optical depth of $\frac{2}{3}$), which are mathematically[10]

$$\frac{\mathrm{d}m}{\mathrm{d}t} = \dot{M}_{\mathrm{wind}} + \dot{M}_{\mathrm{binary}} \ , \tag{8.2}$$

$$L = 4\pi R^2 \sigma T_{\mathrm{eff}}^4 \ , \tag{8.3}$$

$$P_{\mathrm{gas}} = \frac{2}{3}\frac{g}{\kappa}\left(1 - \frac{L}{L_{\mathrm{Edd}}}\right) \ . \tag{8.4}$$

The centre of the star is modelled as an uniform spherical region (as opposed to an infinitesimal point), using mass conservation, the radius-density-mass relation, and the central luminosity, translating to

$$m = -\frac{\mathrm{d}m}{\mathrm{d}k} \ , \tag{8.5}$$

$$m = \frac{4}{3}\pi r^3 \rho \ , \tag{8.6}$$

$$L = (\epsilon - T\dot{S})m \ , \tag{8.7}$$

therefore it does not treat the (co-ordinate) singularity accurately.

The properties that make the STARS code unique amongst stellar evolution code are:

- the use of a self-adaptive non-Lagrangian mesh (Gough et al., 1975),

[10]Most symbols are as defined in chapter 1; L_{Edd}, k, S denote the Eddington luminosity, mesh point number and entropy respectively.

- the treatment of both convective and semi-convective mixing as a diffusion process (although it is not obvious that this is correct), and
- the simultaneous and implicit solution of both the stellar structure equations and the diffusion equations for chemical composition; this both increases stability and means that little or no human intervention is required to evolve a star.

8.2.1.2 Assumptions of the STARS code

It should be noted that, in common with almost all stellar evolution codes, makes following assumptions are made:

- the star is spherically symmetric; this property is assumed in order to reduce the problem to one-dimension; a major part of this thesis is devoted to finding ways to make this assumption appropriately applicable when it would not classically be so, i.e., the case of rapid rotation;
- the star is in local thermodynamic equilibrium; this assumption does occasionally break down (for instance, in the atmosphere of Wolf-Rayet stars), but should not do so for the modelling we are dealing with here;
- the star is in hydrostatic equilibrium; again, this constraint can be broken (for example, during rapid mass loss, $\dot{M} > 0.01 M_{\odot}$ yr^{-1}, or in burning in degenerate regions), but such an event should not occur during the evolution modelled in the search outlined above.

8.2.2 Final Model

The output of the STARS code is not adequate for pulsation calculations (for instance, in its treatment of the centre of the

star, where consistency of the second derivatives pressure, temperature and the H and ^{3}He abundances matter for pulsation calculations); because of this, the values found in this fit were taken and placed into another stellar evolution code, written by Jørgen Christensen-Dalsgaard[11], which was written in such a way as to compute models which were adequate for pulsational calculations.[12] This code also has an adaptive mesh, but importantly uses $\log(m/M)$ as the independent variable (as opposed to mass, which is used by the STARS code; here m is the mass interior to the mesh-point, and M is the total mass), with a resulting alteration of the exact equations of stellar evolution and structure. The inner boundary conditions are set by matching expansions of m and L in p, T, X and X_3 (the abundance of ^{3}He) to the values of these variables. The outer boundary conditions are that of black-body emission and matching the pressure to the pressure obtained by integrating the equations of hydrostatic support in the atmosphere, in the Eddington approximation, assuming gravity to be constant.

The second stellar evolution code also outputs the variables[13]

$$x = r/R\,, \tag{8.8}$$

$$c_1 = \frac{m/M}{x^3}\,, \tag{8.9}$$

$$\gamma_1 = \left(\frac{\mathrm{d}\ln p}{\mathrm{d}\ln \rho}\right)_{ad}\,, \tag{8.10}$$

[11]For more details than given here, see Christensen-Dalsgaard (1982). For the sake of brevity, this stellar evolution code will be referred to as the "second" stellar evolution code from now on.

[12]This is the code that produced the well-known model S in the paper by Christensen-Dalsgaard et al. (1996). The author thanks G. Houdek for providing the final model.

[13]Reproduced here for convenience.

$$V_g = \frac{V_h}{\gamma_1}, \tag{8.11}$$

$$A = \frac{\mathrm{d}\ln\rho}{\mathrm{d}r} - \frac{1}{\gamma_1}\frac{\mathrm{d}\ln p}{\mathrm{d}r}, \tag{8.12}$$

$$U = \frac{\mathrm{d}\ln m}{\mathrm{d}\ln r}, \tag{8.13}$$

which are exactly what are used for the pulsational calculations, as shown by equations (2.17) and (2.18).

Graphs of the pressure, density and temperature of the model provided by the second stellar evolution code are shown in figure 8.5. The full properties of the model are displayed in table 8.4, which can be seen to be very close to the original stellar parameter values for HD 152896 given by the observers.

Parameter	Value
$R/R_\odot$	1.500
$M/M_\odot$	1.550
$L/L_\odot$	5.630
(X, Z)	(0.7017,0.02)
T_{eff}	7257 K
Age	1.98×10^8 yr

Table 8.4: Properties of the final model of HD 152896.

The stellar parameter values of the model calculated using the second stellar evolution code is closer than those of the model calculated using the STARS code, which used updated opacity tables; however, as the second stellar evolution code uses very similar input tables and equations to those used by the observers to obtain their predictions of (and hence the relation between) $R/R_\odot$ & $L/L_\odot$, this is to be expected.

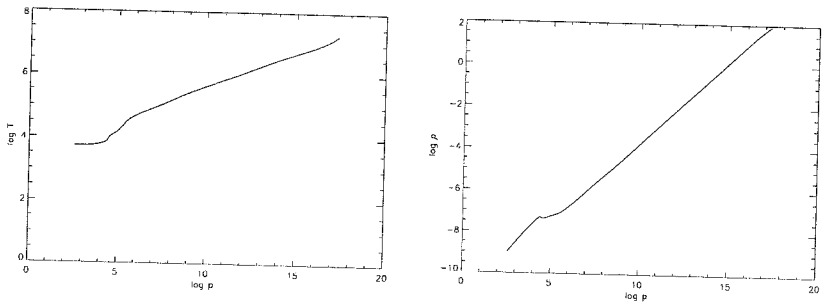

Figure 8.5: Graphs of $\log T$ (left), and $\log \rho$ (right) against $\log p$ for final model of HD 152896.

8.3 EIGENFREQUENCIES - TA

Now that we have our model of HD 152986, we can investigate the effect of rotation on its pulsations. This investigation is accomplished using the same formalism as adopted in chapter 5, using equations (2.17) and (2.18) for the "radial" components of the pulsation, and equations (2.12) and (2.13) for the horizontal components, resulting in four coupled first-order differential equations that we replace by difference equations (with second-order accuracy centred differences used to represent derivatives, and the differential equations represented midway between the mesh points) and solve by relaxation, as outlined in appendix E. The input functions for the structure of the star are given by equations (8.8) to (8.13). To show the general behaviour of the eigenfrequencies with rotation, figures 8.6 and 8.7 follow the progress variation of modes with frequencies around 0.035 and 0.05 as rotation rate increases, for various m and L^2 values.

It can be seen immediately that the qualitative behaviour of these modes is identical to those for a polytrope, as displayed in figure 5.2, and as discussed in chapter 5. We shall therefore proceed to generalize the TA to rotationally distorted co-ordinate

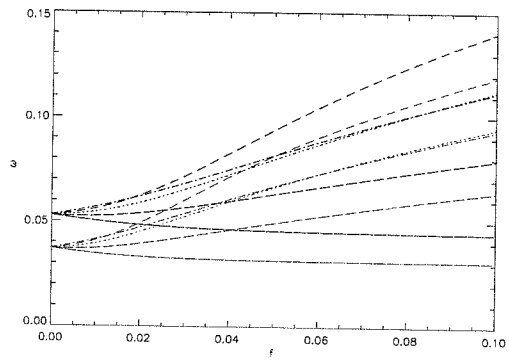

Figure 8.6: Graph of the frequency, under the Traditional Approximation, of two g modes that start as $l = 2$ against scaled rotation rate, f. Black is for radial order, k, equal to 71; red is for $k = 92$. $m = \{-2, -1, 0, 1, 2\}$ are denoted by dash dot-, dashed-, dotted-, dash dot dot dot- and long dashed- lines respectively.

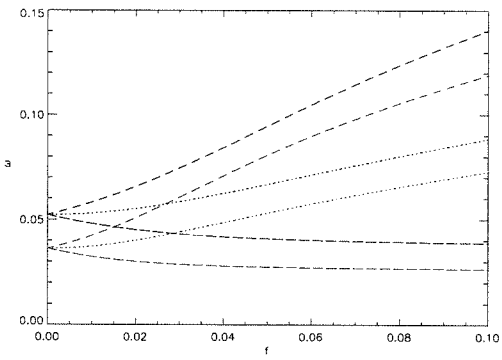

Figure 8.7: Graph of the frequency, under the Traditional Approximation, of two g modes that start as $l = 1$ against scaled rotation rate, f. Black is for radial order, k, equal to 46; green is for $k = 62$. $m = \{-1, 0, 1\}$ are denoted by dashed-, dotted- and long dashed- lines respectively.

systems, but first we must test the approximation. The methods of doing this testing are those given in chapter 2; as the rotation rates considered are much too large for a comparison with a perturbation formalism, we shall do this by means of the χ_i given by equations (2.55) to (2.57). A graph of χ_1 and χ_2, for a given mode, against rotation rate is displayed in figure 8.8. From the values of the χ_i in this graph, we see that we can indeed adopt the TA in this case, as long as the rotation rate does not get too high (beyond $v = 150 - 200\text{km s}^{-1}$, equivalent to the rotation rate inferred from having inclination angle $i \leqslant 20$). This is in keeping with our predictions, and the findings in chapter 2, that the TA breaks down for very large ν.

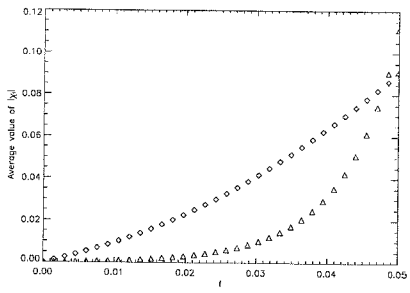

Figure 8.8: Graphs of χ_1 (triangles) and χ_2 (diamonds) for the $(k, m) = (62, 1)$ mode, starting as $l = 1$, against f.

8.4 ASPHERICITY

Now we have examined the un-generalized TA, and its validity, in γ-Doradus stars, we can employ the generalized TA and look at the effects of asphericity. The first step in this endeavour is of course to quantify the centrifugal distortion of the star. This is accomplished via calculating the $\lambda_{l,a}(x)$ and $t_{l,a}(x)$, given by the equations (3.18) and (3.19), reproduced here:

$$\begin{aligned} &\lambda''_{l,1}(x\tilde{V}') + \lambda'_{l,1}(2x\tilde{V}'' + 4\tilde{V}') \\ +\lambda_{l,1}&\left(\frac{\tilde{V}'}{x}(4 - 2l(2l+1)) + 2\tilde{V}''\right) = \delta_{l,0}\left(2\frac{\tilde{V}}{V}\frac{\Omega^2}{f^2}\right) , \quad (8.14) \\ &\lambda''_{l,2}(x\tilde{V}') + \lambda'_{l,2}(2x\tilde{V}'' + 4\tilde{V}') \\ +\lambda_{l,2}&\left(\frac{\tilde{V}'}{x}(4 - 2l(2l+1)) + 2\tilde{V}''\right) = -B_l , \quad (8.15) \end{aligned}$$

with $\tilde{V}$ as a suitably scaled V. It is expedient thus to scale all our variables (x, ρ, p, V) governing hydrostatics. From these equations, we can see the expedient choice is also to rescale our

length co-ordinate to $(0, 1)$, according to

$$\left(\frac{\tilde{V}}{V}\frac{\Omega^2}{f^2}\right) = \frac{1}{R_*^2} \; . \tag{8.16}$$

Following this through, straightforward algebra yields

$$\begin{aligned}
V &= \frac{GM_*}{R_*}\tilde{V} \; , && (8.17)\\
\nabla^2 V &= 4\pi G\rho \; , && (8.18)\\
\Rightarrow \tilde{\nabla}^2\tilde{V} &= 4\pi\frac{R_*^3}{M_*}\rho \equiv 4\pi\tilde{\rho} \; , && (8.19)\\
\& \; \tilde{V}' &= \frac{m/M_*}{(r/R_*)^2} \; , && (8.20)\\
\Rightarrow \tilde{V}'' &= 4\pi\tilde{\rho} - 2\frac{m/M_*}{(r/R_*)^3} \; . && (8.21)
\end{aligned}$$

This allows us to obtain $\lambda_{l,a}$ just as in chapter 5. The main change to the boundary conditions from the polytropic case is that

$$a_l = -\tilde{V}'|_{x=1} \; \delta_{l,0} = -\delta_{l,0} \; . \tag{8.22}$$

The results for the centrifugal distortion are displayed in figure 8.9. For the calculation of $\delta\boldsymbol{C}$ and $\delta_2\boldsymbol{C}$, it is also useful to notice that

$$\begin{aligned}
\tilde{\nabla}p &= -\rho\tilde{\nabla}\tilde{V}\frac{GM_*^2}{R_*^4} \; , && (8.23)\\
\Rightarrow \tilde{p} &\equiv \frac{R_*^4}{GM_*^2}p \; . && (8.24)\\
& && (8.25)
\end{aligned}$$

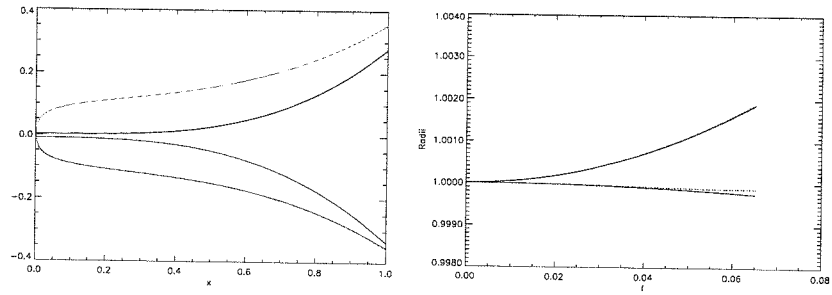

Figure 8.9: Left: Graph of first order rescaling functions for model of HD 152896; $\lambda_{0,1}$ (black), $\lambda_{1,1}$ (red), $t_{0,1}$ (green) and $t_{1,1}$ (blue). Right: Graphs of equatorial and polar radii against scaled rotation rate, f; solid lines are with f^2 corrections only, dotted lines are with f^2 and f^4 corrections included.

Graphs of the scaled values (of $\tilde{\rho}$, $\tilde{p}$, $\tilde{V}'$, $\tilde{V}''$) are shown in figure 8.10. The coefficients governing the change in (scaled) mass given by values displayed in table 8.4 are

Parameter	Value
M_0	1.
M_1	0.032569
M_2	-0.067830

The general form of these results is similar to the polytropic case. However, there are two main differences: the size of the distortion, and the behaviour near the centre of the star.

The first of these is a result of two effects. Firstly, the magnitude of the scalings differs largely: for the polytropic case, the forcing for $\lambda_{l,1}$ was $\propto \xi_0^2$, whereas for the case of HD 152896, we have chosen our scalings such that the forcing is independent of R_*. For an $n = 3$ polytrope, $\xi_0^2 \approx 50$; given that the scalings

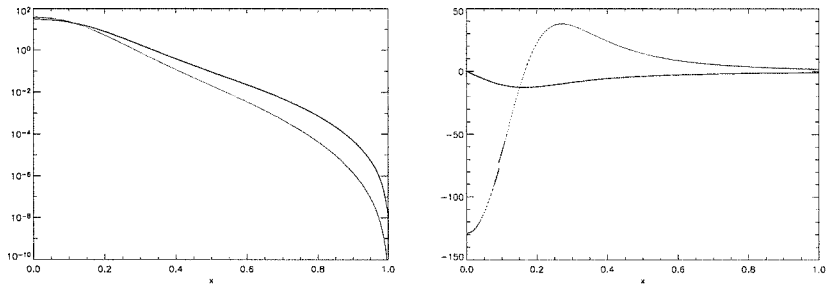

Figure 8.10: Graphs of scaled values against x. Left: $\tilde{\rho}$ and $\tilde{p}$ marked by black and red lines respectively. Right: $\tilde{V}'$ and $\tilde{V}''$ also marked by black and red respectively.

differ by a factor of this order of magnitude, this scaling factor bring the two results much closer into line. The second fact that contributes to the magnitude of distortion functions being different between the two main examples (an $n = 3$ polytrope and our model of HD 152896) is that an $n = 3$ polytrope describes a highly compressible equation of state, so we would expect the distortion for such a polytrope to be larger than for a realistic stellar model, as indeed we do find.

Also worth noting is that equation (3.18) requires both $\lim_{x\to 0} \lambda_{1,1} = 0$ and $\lim_{x\to 0} \lambda'_{1,1} = 0$ to keep $\lambda''_{1,1}$ regular as x tends to zero. The model given does not have a mesh point at zero, and indeed has a substantial gap between the first mesh point (which is placed very close to zero) and the remaining ones; to achieve $\lim_{x\to 0} \lambda'_{1,1} = 0$ requires $\lim_{x\to 0} \lambda_{1,1}$ non-zero; this is most evident in the $t_{l,1}$, due to the formula

$$t'_{l,1} = 2\frac{\lambda_{1,1}}{x} \times (-\delta_{l,0} + \delta_{l,1}) \ , \tag{8.26}$$

so departure of $\lambda_{1,1}$ from zero results in large gradients in the $t_{l,1}$. It is the case that the value of $\lim_{x\to 0} \lambda_{1,1}$ thus derived is small

(-0.0104) and does not affect the solution (enforcing a reduction the limit by a factor of 10^{20} does not produce discernible change in the tabulated 12 significant figures of $\lambda_{1,1}$ and $\lambda'_{1,1}$ at $x = 1$, and a change in the surface value of the $t_{l,1}$ of the order of 10^{-4}). Whilst this non-zero limit (and the knock-on fractionally-non-zero limits of the B_l) is not ideal, and owing to fractional numerical error, we do not foresee the slight error changing the results for the asphericity to the accuracy required.

8.4.1 EIGENFREQUENCIES FROM ASPHERICITY

Now that we have obtained our distortion coefficients, we can use the generalized TA in the orthogonal curvilinear co-ordinate formalism from chapters 3, 4 and 7 to obtain predictions of frequencies, some results of which are shown in figure 8.11.

Although this figure is only an example, it is interesting to note that, as for the polytropic case, the largest centrifugal influence is for the $|m| = 1$ modes. The other modes experience what can become a large alteration to their eigenfrequencies, with the exception of the prograde mode with the largest $|m|$, which is by far the most stable eigenfrequency to the effects of rotation.

8.5 FREQUENCY FIT FOR HD 152896

To investigate fits of the actual pulsational frequencies of HD 152896, frequencies correct to $O(f^2)$ (in order to not be prohibitive in terms of computational requirements) were calculated for values of inclination angle, i, such that

$$i = 90^\circ \left(1 - \frac{n}{180}\right) \ , \ n\epsilon\{0, ..., 90\} \ ; \qquad (8.27)$$

and the scaled frequencies compared to those of HD 152896[14]

[14]Scaled by $\sqrt{GM/R^3}$, so $\bar{\omega}$=(3.6436, 3.5309) $\times 10^{-2}$.

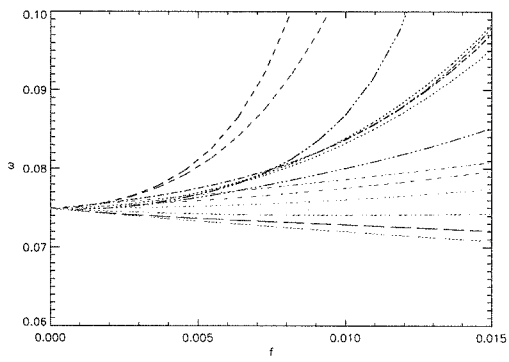

Figure 8.11: Graph of the frequency (in the rotating frame) of a $k = 54$, g mode that starts as $l = 2$ against scaled rotation rate, f. Green is with just the TA effects taken into account, red is with f^2 corrections also included, and black is with f^4 corrections as well; $m = \{2, 1, 0, -1, -2\}$ are denoted by long dashed, dash-dot-dot-dotted, dotted, dashed and dash-dotted lines respectively, as in figure 5.5.

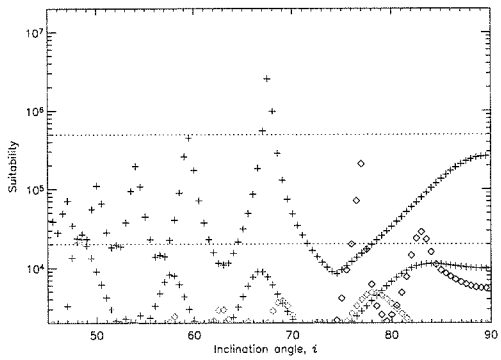

Figure 8.12: Graph of suitability (given by equation (8.28)) for various inclination angles, i; black, red and green symbols represent $m = 0$, $m = 1$ and $m = 2$ respectively, crosses are for modes that start as $l = 1$, diamonds for modes that start as $l = 2$. The graph is cut off at 5×10^3, equivalent to both frequencies being fit to 1% accuracy (hence some points, especially for higher $|m|$ and $|l|$, are not displayed); the red and blue lines are equivalent to both frequencies being fit to 0.2% and 0.1% respectively.

according to a suitability formula

$$F = \left(\sum_i \frac{(\omega_{i,obs} - \omega_{i,predicted})^2}{\omega_{i,obs}^2} \right)^{-1}, \qquad (8.28)$$

as in chapter 6. A graph of F for various inclination angles, and values of m and $L^2(m, \nu)$ is shown in figure 8.12.

The form of these results is very much as would be expected; if we view the spectrum of frequencies evolving with increasing rotation rate, the spectrum both moves and the spacing between adjacent frequencies evolves as the rotation rate increases. The closeness of fit will therefore increase as two frequencies become

8.5 Frequency fit for HD 152896

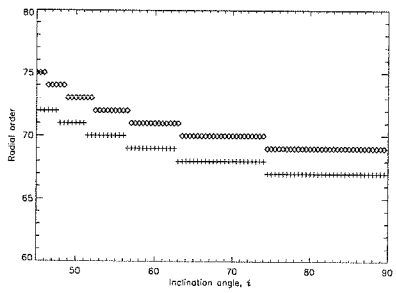

Figure 8.13: Graph of "radial" order, k, of the $m = 0$ mode which starts as $l = 1$ which best fits $\bar{\omega} = 3.6436 \times 10^{-2}$ (diamonds) and $\bar{\omega} = 3.5309 \times 10^{-2}$ (squares), plotted against inclination angle, i.

close to the observed frequencies we are trying to match, then decrease as they move past, then eventually be replaced by other frequencies as the "closest fit", which will cause the closeness of fit to again increase until another maximum, and so on; this is clearly the behaviour seen in figure 8.12 (the "radial" order of the best fitting modes are shown in figure 8.13). One of the major constraints on the goodness of fit actually achieved is the spacing of successive frequencies, so we would expect the peaks for various (L^2, m) values to be of greatly differing heights, as indeed is seen in figure 8.12.

The best fit found for HD 152896 is that with $m = 0$ modes which start as $l = 1$, with the parameters

ω_1	0.036424
ω_2	0.035328
i	67.5°
f	0.01934

Whilst this fit is good, it is still not within the errors of the data. This fact should not surprise us, as there are many factors that have not been taken into account, such as non-conservative rotation laws and magnetic fields, in addition to the fact that we have only considered one model, with a modest number of mesh points (of the order of 700) for HD 152896. However, this search demonstrates the need for non-perturbative theory in the modelling of the effects of rotation on the structure and pulsations of stars, and of the results achievable through the method outlined in this thesis.

8.6 Conclusions

Having developed the presented rotation formalism, and tested it on barotropic equations of state, with assuring quantifiable results, we have now generalized the theory to real equations of state, and tested it on a model of a γ-Doradus star. Again this has produced results in qualitative agreement with what we may expect and be hoping for.

We have also investigated the class of γ-Doradus stars, and seen that pulsators in this class are exactly those that the theory models best. This, as will be expounded upon in the next chapter, opens up these stars to a far deeper level of asteroseismic probing.

Chapter 9

Future Work and Conclusions

"Doroga k Zvjozdam Otkrita" (The way to the stars is open) – Sergei Korolev

9.1 Future Work

Whilst effort has been made to point to many of the applications of this method, there are three[1] areas that would benefit further investigation:

- Line profile variations. These have been used to identify modes via the values of (l, m); whilst the effects of moderate rotation have often been included in these calculations, this work allows much higher rotation rates to be considered. For example, Balona et al. (1996) noted that the full effects of rotation had not been taken into account in their identification of (l, m) for the pulsational modes of γ Doradus. Work in this direction has been started, mainly by R. H. D. Townsend (Townsend, 1997, 2003a), but it has yet to be fully adopted.

[1] At least!

9.1 Future Work

- Genetic algorithms with full stellar models. With much high-accuracy data soon to arrive from the asteroseismic satellites, we need algorithms in place for fitting the data. Whilst chapter 6 touched upon a possible way to achieve this, the models used were polytropes, unlike the example in chapter 8. This matter is currently being approached for standard perturbative theory with rotation (see Metcalfe et al., 2004a).

- The full effects of rotation on stellar structure and evolution. Whilst the rotating stellar models that this work presents have mathematical consistency, they are not exact; nor has the alteration that rotation may have had upon their prior evolution been taken into account. This remains a huge unanswered question in stellar astronomy, and one that needs an answer before we can truly claim to understand stars. Work on this has been started most promisingly, in the author's opinion, by M. Rieutord in Toulouse, using a tensor formalism similar to that used in general relativity, but this work is still in its early stages. The Toulouse group (Dintrans and Rieutord, 2000) has also numerically modelled individual perturbation frequencies in an individual star (a $1.5M_{\odot}$ ZAMS star ignoring centrifugal distortion), under the anelastic approximation and for high l values, finding some periodic orbits that are focused towards calculable attractors for certain parameter ranges, as well as ergodic orbits that are easily associated with the distorted gravity modes that are looked at in this thesis in detail. Combining these two numerical fields, as long as it is not prohibitive in terms of computational demands, could provide huge insights into the oscillations of individual stars.

9.2 Conclusions

In this thesis, a method of dealing with extreme rotation has been presented. Past studies have pushed the limits of completely perturbative methods close to a logical extreme. Some of the first works dealt with expanding in just Ω; however, Soufi et al. (1998) noted, as others had before, that the crucial parameter can well be the ratio of rotation rate to pulsational frequency[2]. As that ratio is increased perturbative methods will eventually break down, as chapter 1 showed the case for γ-Doradus stars.[3]

To deal with some of these cases with larger ν, the study presented in this thesis represents a new approach, developed from the geophysical Traditional Approximation and the rescaling suggested by Gough and Thompson (1990). In this method, oblate orthogonal co-ordinates are found which form the natural physical basis for the rotating star, and a generalization of the Traditional Approximation is created, formally allowing any value of the parameter ν to be considered. Once this is adopted, distortion of the star can be dealt with in a standard perturbative way, which is also outlined here.

The procedure allows us to explore many areas of seismology in rapidly rotating stars, such as the alteration to eigenfrequencies, the alteration to eigenfunctions, and mode trapping. Examples of the uses of this method have been presented for polytropes and a model of the γ-Doradus variable HD 152896.

Some of the issues outstanding in seeking to fit asteroseismic data by the newly popular genetic algorithms have been touched upon, and investigated, to help our fitting of data that will be shortly available through space missions such as MOST

[2]Their expansion parameter was $\epsilon \equiv \Omega/\omega \equiv \nu/2$; however, they do include an equivalent of f to the same order without treating it separately.

[3]Soufi et al. (1998) , cite the accuracy of their method as one part in 10^3, for the δ-Scuti variables they were seeking to model, with ϵ up to approximately 0.1.

and COROT.

This research opens up a new realm of stars to accurate asteroseismic probing, further enhancing our ability to study stars, as put by Eddington: "*by awaiting and interpreting the messages dispatched to us by the objects of nature*".

Appendix A

A LIST OF NOTATION USED

It may be useful to the reader to have the following notation grouped into one place:

Symbol	Meaning	Definition
f	Scaled rotation rate	$\Omega/\sqrt{GM/R^3}$
ν	Ratio of rotation rate to pulsational frequency	$2\Omega/\omega$
A	–	$(\mathrm{d}(\ln\rho)/\mathrm{d}r)$ $-(1/\gamma_1)(\mathrm{d}(\ln p)/\mathrm{d}r)$
V_h	–	$-\mathrm{d}(\ln p)/\mathrm{d}(\ln r)$
m	Mass interior to a given radius r	–
U	–	$\mathrm{d}(\ln m)/\mathrm{d}(\ln r)$
V	Scaled Potential	Varies
γ_1	Adiabatic Exponent	$(\partial(\ln p)/\partial(\ln\rho))_{ad}$
c_1	–	$(r/R)^3/(m/M)$
$\bar{\omega}$	Scaled frequency	$\omega/\sqrt{GM/R^3}$
$\lambda_{l,a}$	Scaling of r in a spherical basis in terms of the r-like co-ordinate in the new, rotating, basis	See below
$t_{l,a}$	Likewise, but for μ and the μ-like co-ordinates	"
h_i	Metric coefficients	See appendix C

A A LIST OF NOTATION USED

A, $V_{\rm h}$, U, γ_1 and c_1 are functions of the stellar structure that prove useful in the pulsational equations.

The $\lambda_{l,a}(x)$ and $t_{l,a}(x)$ are defined by

$$r = x\left(1+\sum_{l\geq 0,a>1} f^{2a}P_{2l}(\eta)\lambda_{l,a}(x)\right) , \qquad (A.1)$$

$$\mu = \eta\left(1+\sum_{l\geq 0,a>1} f^{2a}P_{2l}(\eta)t_{l,a}(x)\right) . \qquad (A.2)$$

A.0.1 MODE CLASSIFICATION

It has been noted by a number of authors (Townsend, 2003b; Lee and Saio, 1997) that the classification of Hough functions by (l,m) indices, although clearly identifying their non-rotating progenitors, does not allow classification of the other modes (such as r modes) described by Laplace's Tidal Equation. These authors have created good, holistic, classification schemes which describe all the modes. However, because of the cases considered in this thesis, the (l,m) index classification is retained to emphasise the analogies to the non-rotating modes.

Appendix B

Definition of the Principal Variational-Principle functions

For using the variational principle in chapter 4, we have looked at the equation:

$$-\omega^2 \mathbf{A}.\boldsymbol{\xi} + \omega \mathbf{B}.(\boldsymbol{\xi}) + \mathbf{C}.(\boldsymbol{\xi}) \ = 0 \ , \tag{B.1}$$

with

$$\begin{aligned}
\mathbf{A} &= \rho_0 \mathbf{I} \ , & \text{(B.2)} \\
\mathbf{B}.(\boldsymbol{\xi}) &= 2\mathrm{i}\rho_0 \boldsymbol{\Omega} \times \boldsymbol{\xi} \ , & \text{(B.3)} \\
\mathbf{C}.(\boldsymbol{\xi}) &= \mathbf{P}.(\boldsymbol{\xi}) + \tilde{\mathbf{V}}.(\boldsymbol{\xi}) \ , & \text{(B.4)} \\
\mathbf{P}.(\boldsymbol{\xi}) &= \nabla \left[(1-\gamma_1) p_0 \nabla.\boldsymbol{\xi} \right] - p_0 \nabla (\nabla.\boldsymbol{\xi}) \\
&- \nabla \left[(\boldsymbol{\xi}.\nabla) p_0 \right] + (\boldsymbol{\xi}.\nabla) \nabla p_0 \ , & \text{(B.5)} \\
\tilde{\mathbf{V}}.(\boldsymbol{\xi}) &= \rho_0 (\boldsymbol{\xi}.\nabla) \nabla V_0 \ . & \text{(B.6)}
\end{aligned}$$

All the terms in this equation are Hermitian. Under the Traditional Approximation, the horizontal parts of the rotation vector are ignored; thus $\mathbf{B}$ becomes

$$\mathbf{B}_{\mathrm{TA}} \equiv 2\mathrm{i}\rho_0 \begin{pmatrix} 0 & 0 & 0 \\ 0 & 0 & -\boldsymbol{\Omega}.\mathbf{e}_\eta \\ 0 & \boldsymbol{\Omega}.\mathbf{e}_\eta & 0 \end{pmatrix}$$

B Definition of the Principal Variational-Principle functions

$$= \mathrm{i}\omega\nu\rho_0 \begin{pmatrix} 0 & 0 & 0 \\ 0 & 0 & -\hat{\mathbf{\Omega}}.\mathbf{e}_\eta \\ 0 & \hat{\mathbf{\Omega}}.\mathbf{e}_\eta & 0 \end{pmatrix} . \qquad \text{(B.7)}$$

It is important to note that this second form is different from the simplification given in chapter 4, which is conceptually slightly easier, and is the form with which to calculate ω_0. But this second form will prove to admit perturbation solutions in much more straightforward manner here.

We now have:

$$\omega^2(\mathbf{A} - \mathbf{B}_{\mathrm{TA}}).(\boldsymbol{\xi}) = \mathbf{C}.(\boldsymbol{\xi}) , \qquad \text{(B.8)}$$

with all of $\mathbf{A}$, $\mathbf{B}_{\mathrm{TA}}$ and $\mathbf{C}$ being Hermitian. Therefore, with the inner product

$$\langle \tilde{\boldsymbol{\xi}}, \boldsymbol{\xi} \rangle \equiv \int \tilde{\boldsymbol{\xi}}^* \boldsymbol{\xi} \mathrm{d}^3\mathbf{x} , \qquad \text{(B.9)}$$

we can easily show that these operators ($\mathbf{A}$, $\mathbf{B}_{\mathrm{TA}}$ and $\mathbf{C}$) are self-adjoint. We also define

$$\langle\ ,\ \rangle = \langle\ ,\ \rangle_0 + f^2\langle\ ,\ \rangle_2 + f^4\langle\ ,\ \rangle_4 \qquad \text{(B.10)}$$

in a natural way. Note that $\langle \boldsymbol{\xi}, \mathbf{B}_{\mathrm{TA}}.(\boldsymbol{\xi}) \rangle = 0$. Thus, the zeroth-order equation admits

$$\left(\omega^2(\mathbf{A} - \mathbf{B}_{\mathrm{TA}}) - \mathbf{C}\right).(\boldsymbol{\xi}) = 0 \qquad \text{(B.11)}$$

$$\Rightarrow \langle \tilde{\boldsymbol{\xi}}, (\omega^2\rho_0 - \mathbf{C})\boldsymbol{\xi} \rangle_i = 0 , \ \forall i . \qquad \text{(B.12)}$$

And the first-order part of the inner product of $\boldsymbol{\xi}$ with equation (B.8) is

$$2\omega\delta\omega\langle\boldsymbol{\xi},\rho_0\boldsymbol{\xi}\rangle_0 = \omega^2\left(\langle\boldsymbol{\xi},\delta.\mathbf{B}_{\mathrm{TA}}(\boldsymbol{\xi})\rangle_0 - \langle\boldsymbol{\xi},\rho_0\boldsymbol{\xi}\rangle_2\right) + \langle\boldsymbol{\xi},\mathbf{C}.(\boldsymbol{\xi})\rangle_2 + \langle\boldsymbol{\xi},\boldsymbol{\delta C}.(\boldsymbol{\xi})\rangle_0 \,, \tag{B.13}$$

which becomes[1]

$$\delta\omega = \frac{\langle\boldsymbol{\xi},(\boldsymbol{\delta C}).(\boldsymbol{\xi})\rangle_0}{2\omega\langle\boldsymbol{\xi},\rho_0\boldsymbol{\xi}\rangle_0} \,. \tag{B.14}$$

Likewise using the antisymmetry of $\delta\boldsymbol{B}_{\mathrm{TA}}$ and equation (B.12) on the second-order terms yields

$$\begin{aligned}((\delta\omega)^2 + 2\omega\delta_2\omega)\langle\boldsymbol{\xi},\rho_0\boldsymbol{\xi}\rangle_0 &= \omega^2\langle\boldsymbol{\xi},\delta\boldsymbol{B}_{\mathrm{TA}}.(\delta\boldsymbol{\xi})\rangle_0 \\ - 2\omega\delta\omega\langle\boldsymbol{\xi},\rho_0\boldsymbol{\xi}\rangle_2 &+ \langle\boldsymbol{\xi},\delta\boldsymbol{C}.(\boldsymbol{\xi})\rangle_2 \\ + \langle\boldsymbol{\xi},\delta_2\boldsymbol{C}.(\boldsymbol{\xi})\rangle_0 &+ \langle\boldsymbol{\xi},\delta\boldsymbol{C}.(\delta\boldsymbol{\xi})\rangle_0 \,,\end{aligned} \tag{B.15}$$

which, by using equation (B.14), becomes

$$\delta_2\omega = \frac{\omega^2\langle\boldsymbol{\xi},\delta\boldsymbol{B}_{\mathrm{TA}}.(\delta\boldsymbol{\xi})\rangle_0 + \langle\boldsymbol{\xi},\delta_2\boldsymbol{C}.(\boldsymbol{\xi})\rangle_0 + \langle\boldsymbol{\xi},\delta\boldsymbol{C}.(\delta\boldsymbol{\xi})\rangle_0}{2\omega\langle\boldsymbol{\xi},\rho_0\boldsymbol{\xi}\rangle_0} - \frac{(\delta\omega)^2}{2\omega} \,. \tag{B.16}$$

It is important to point out at this point that the perturbations to the displacement vectors have now been chosen to be orthogonal to $(\mathbf{A}+\mathbf{B}_{\mathrm{TA}}).(\boldsymbol{\xi})$ (and $(\mathbf{A}+\mathbf{B}_{\mathrm{TA}}).(\delta\boldsymbol{\xi})$ for the second-order displacement). We can see that, owing to the antisymmetry of $\mathbf{B}_{\mathrm{TA}}$, these retain the orthonormality of the $\boldsymbol{\xi}$. Also $\mathbf{B}_{\mathrm{TA}}.(\boldsymbol{\xi})$ contains no ξ_x term, so we do not need to concern ourselves with the possibility that picking our eigenfunction pertur-

[1] Also using the fact that, like $\boldsymbol{B}_{\mathrm{TA}}$, $\delta\boldsymbol{B}_{\mathrm{TA}}$ is antisymmetric.

bations to be orthogonal to $(\mathbf{A}+\mathbf{B}_{\mathrm{TA}}).(\boldsymbol{\xi})$ rather than orthogonal to $\mathbf{A}.(\boldsymbol{\xi})$ will cause loss of completeness of the $\boldsymbol{\xi}$ as a basis over which to expand the perturbations.

Appendix C
Some useful mathematical results

It may prove useful to the reader to have the following mathematical results, reproduced from Gradshteyn and Ryzhik (1994), Abramowitz and Stegun (1972) and the appendix of Acheson (1990), listed here.

C.1 Legendre Polynomials

The Legendre polynomial of order l is defined as:

$$P_l(\mu) \equiv \frac{1}{2^l l!}\frac{d^l}{d\mu^l}(\mu^2-1)^l \ , \tag{C.1}$$

making it a solution to the following Sturm-Liouville problem:

$$\frac{\partial}{\partial\mu}\left((1-\mu^2)\frac{\partial}{\partial\mu}P_l(\mu)\right) = -l(l+1)P_l(\mu) \ . \tag{C.2}$$

Equations (C.1) and (C.2) allow us to arrive at

$$P_l' = \sum_{k=0}^{l-2k-1\geq 0}(2l-4k-1)P_{l-2k-1} \ , \tag{C.3}$$

$$(2l+1)\mu P_l = (l+1)P_{l+1} + lP_{l-1} \ , \tag{C.4}$$

$$\int_{-1}^{1} P_l P_{l'} d\mu = \delta_{l,l'} \ , \tag{C.5}$$

and, for $m \leq l$,

$$P_l P_m = \sum_{k=0}^{k=m} \frac{a_{m-k} a_k a_{l-k}}{a_{m+l-k}} \left(\frac{2l + 2m - 4k + 1}{2l + 2m - 2k + 1} \right) P_{l+m-2k} \ , \quad \text{(C.6)}$$

$$a_k = \frac{(2k-1)!!}{k!} \ (k \neq 0 \ , \ a_0 = 1) \ . \quad \text{(C.7)}$$

C.1.1 Some low-l expressions

There are some formulae that will be written explicitly here, as they are used often.

$$P_0 = 1 \ , \quad \text{(C.8)}$$

$$P_1 = \mu \ , \quad \text{(C.9)}$$

$$P_2 = \frac{1}{2}(3\mu^2 - 1) \ , \quad \text{(C.10)}$$

$$\Leftrightarrow \ 1 - \mu^2 = \frac{2}{3}(1 - P_2) \ , \quad \text{(C.11)}$$

$$P_3 = \frac{5}{2}\mu^3 - \frac{3}{2}\mu \ , \quad \text{(C.12)}$$

$$P_4 = \frac{1}{8}(35\mu^4 - 30\mu^2 + 3) \ , \quad \text{(C.13)}$$

$$P_2 P_2 = \frac{18}{35} P_4 + \frac{2}{7} P_2 + \frac{1}{5} P_0 \ . \quad \text{(C.14)}$$

It is also worth noting from the definition of P_2 that

$$\frac{P_2(\mu) - P_0(\mu)}{1 - \mu^2} = \frac{-3}{2} \ , \quad \text{(C.15)}$$

which allows us to simplify greatly the $\sum_{l \geq 0} (1-\eta^2)^{-1} P_{2l}(\eta) t_{l,1}(x)$ terms in our metric coefficients, once we have established that

$t_{0,1}(x) = -t_{1,1}(x)\ \forall\, x$ and that the other $t_{l,1}$ are zero. A similar simplification exists for the $t_{l,2}$.

C.2 ASSOCIATED LEGENDRE FUNCTIONS

Having defined $P_l(\mu)$, we can define associated Legendre functions $P_l^m(\mu)$, and normalized spherical harmonics $Y_l^m(\mu, \phi)$, according to

$$P_l^m \equiv (-1)^m (1-\mu^2)^{m/2} \frac{d^m}{d\mu^m} P_l \ , \tag{C.16}$$

$$Y_l^m \equiv (-1)^m \left[\frac{2l+1}{4\pi}\frac{(l-m)!}{(l+m)!}\right]^{1/2} P_l^m e^{\mathrm{i}m\phi}, \tag{C.17}$$

$$\Rightarrow \int_0^{2\pi}\int_{-1}^{1} Y_l^m Y_{l'}^{m'} d\mu d\phi = \delta_{l,l'}\delta_{m,m'} \ . \tag{C.18}$$

It is also useful to note, for $m \neq 0$,

$$\int_0^{2\pi}\int_{-1}^{1} (\frac{\partial}{\partial\theta} Y_l^m)^* Y_l^m \frac{\cos\theta}{\sin\theta} d\mu d\phi \ = \frac{1}{2} \ . \tag{C.19}$$

From Gradshteyn and Ryzhik,

$$\int_0^1 \frac{[P_l^m]^2}{1-\mu^2} d\mu \ = \frac{1}{2m}\frac{(l+m)!}{(l-m)!} \ , \tag{C.20}$$

$$\int_{-1}^{1} P_l^m P_{l'}^m d\mu \ = \frac{1}{2(l+1)}\frac{(l+m)!}{(l-m)!}\delta_{l,l'} \ , \tag{C.21}$$

$$P_{l-1}^m - \mu P_l^m \ = (l-m+1)(1-\mu^2)^{1/2} P_l^{m-1} \ ; \tag{C.22}$$

which equations allow us to derive

$$\mu Y_l^m = A_{lm} Y_{l+1}^m + B_{lm} Y_{l-1}^m \,, \tag{C.23}$$

$$\Rightarrow P_2 Y_l^m = \frac{3}{2}\left(A_{lm} A_{l+1,m} Y_{l+2}^m + B_{lm} B_{l-1,m} Y_{l-2}^m\right) + \frac{l^2+l-m^2}{(2l-1)(2l+3)} Y_l^m \,, \tag{C.24}$$

$$(\mu^2-1)\frac{d}{d\mu} Y_l^m = l A_{lm} Y_{l+1}^m - (l+1) B_{lm} Y_{l-1}^m \,, \tag{C.25}$$

with

$$A_{lm} \equiv \sqrt{\frac{(l+1)^2-m^2}{(2l+1)(2l+3)}} \,, \; B_{lm} \equiv \sqrt{\frac{l^2-m^2}{(2l+1)(2l-1)}} \,. \tag{C.26}$$

C.3 Vector Identities

The following vector identities will prove useful.

$$\nabla \cdot (\phi \mathbf{F}) = \phi \nabla \cdot \mathbf{F} + \mathbf{F} \cdot \nabla \phi \,, \tag{C.27}$$

$$\nabla \times (\phi \mathbf{F}) = \phi \nabla \times \mathbf{F} + (\nabla \phi) \times \mathbf{F} \,, \tag{C.28}$$

$$\nabla \times (\mathbf{F} \times \mathbf{G}) = (\mathbf{G} \cdot \nabla)\mathbf{F} - (\mathbf{F} \cdot \nabla)\mathbf{G} + \mathbf{F}(\nabla \cdot \mathbf{G}) - \mathbf{G}(\nabla \cdot \mathbf{F}) \,. \tag{C.29}$$

C.4 Orthogonal Curvilinear Coordinates

Let u, v, and w denote a set of orthogonal curvilinear coordinates, and let $\mathbf{e}_u$, $\mathbf{e}_v$ and $\mathbf{e}_w$ be the basis for this orthogonal coordinate system. Then

$$\mathbf{e}_u = \mathbf{e}_v \times \mathbf{e}_w \,, \tag{C.30}$$

and similar equations hold for $\mathbf{e}_v$ and $\mathbf{e}_w$. The equation

$$\delta\mathbf{x} = h_1\delta u\mathbf{e}_u + h_2\delta v\mathbf{e}_v + h_3\delta w\mathbf{e}_w \tag{C.31}$$

defines the metric coefficients h_i, e.g.

$$h_1 = \left|\frac{\partial\mathbf{x}}{\partial u}\right| . \tag{C.32}$$

These give

$$\nabla\phi = \frac{1}{h_1}\frac{\partial\phi}{\partial u}\mathbf{e}_u + \frac{1}{h_2}\frac{\partial\phi}{\partial v}\mathbf{e}_v + \frac{1}{h_3}\frac{\partial\phi}{\partial w}\mathbf{e}_w , \tag{C.33}$$

$$\nabla\cdot\mathbf{F} = \frac{1}{h_1h_2h_3}\left[\frac{\partial}{\partial u}(h_2h_3F_u) + \frac{\partial}{\partial v}(h_1h_3F_v) + \frac{\partial}{\partial w}(h_2h_1F_w)\right] , \tag{C.34}$$

$$\nabla\times\mathbf{F} = \frac{1}{h_1h_2h_3}\begin{vmatrix} h_1\mathbf{e}_u & h_2\mathbf{e}_v & h_3\mathbf{e}_w \\ \frac{\partial}{\partial u} & \frac{\partial}{\partial v} & \frac{\partial}{\partial w} \\ h_1F_u & h_2F_v & h_3F_w \end{vmatrix} , \tag{C.35}$$

which can then be used to obtain, for example, $\delta\boldsymbol{C}$ given in appendix B; this is demonstrated in appendix D.

Appendix D

Perturbations to the Pulsational Operators in terms of the metric coefficients

In appendix B, **A**, **B** and **C** where written in a co-ordinate-independent way by use of the ∇ operator. However, for calculation, it is necessary to expand these, for which the following formulae may prove useful.

We have defined

$$\begin{aligned} \mathbf{P}.(\boldsymbol{\xi}) &= \nabla\left[(1-\gamma_1)p_0\nabla.\boldsymbol{\xi}\right] - p_0\nabla(\nabla.\boldsymbol{\xi}) \\ &- \nabla\left[(\boldsymbol{\xi}.\nabla)p_0\right] + (\boldsymbol{\xi}.\nabla)\nabla p_0 \ , \qquad \text{(D.1)} \\ \tilde{\mathbf{V}}.(\boldsymbol{\xi}) &= \rho_0(\boldsymbol{\xi}.\nabla)\nabla V_0 \ . \qquad \text{(D.2)} \end{aligned}$$

It is useful to note that, owing to the choice of basis,

$$\nabla p_0 = \frac{1}{h_1}\frac{\partial p_0}{\partial x}\mathbf{e}_x \ , \qquad \text{(D.3)}$$

$$(\boldsymbol{\xi}.\nabla)\, p_0 = \frac{\xi_x}{h_1}\frac{\partial p_0}{\partial x} \ , \qquad \text{(D.4)}$$

and similarly for V_0. Thus

D Perturbations to the Pulsational Operators in terms of the metric coefficients

$$\begin{aligned}\nabla\left[(\boldsymbol{\xi}.\nabla)p_0\right] &= \mathbf{e}_x\frac{1}{h_1}\frac{\partial}{\partial x}\left(\frac{\xi_x}{h_1}\frac{\partial p_0}{\partial x}\right)+\mathbf{e}_\eta\frac{1}{h_2}\frac{\partial}{\partial \eta}\left(\frac{\xi_x}{h_1}\frac{\partial p_0}{\partial x}\right)\\ &+ \mathbf{e}_\phi\frac{1}{h_3}\frac{\partial}{\partial \phi}\left(\frac{\xi_x}{h_1}\frac{\partial p_0}{\partial x}\right) \qquad \text{(D.5)}\\ &= \mathbf{e}_x\frac{1}{h_1}\frac{\partial}{\partial x}\left(\frac{\xi_x}{h_1}\frac{\partial p_0}{\partial x}\right)+\mathbf{e}_\eta\frac{1}{h_2}\frac{\partial}{\partial \eta}\left(\frac{\xi_x}{h_1}\frac{\partial p_0}{\partial x}\right)\\ &+ \mathbf{e}_\phi\frac{im\xi_x}{h_1h_3}\frac{\partial p_0}{\partial x}\ , \qquad \text{(D.6)}\end{aligned}$$

and

$$(\boldsymbol{\xi}.\nabla)\nabla p_0 = \left[(\boldsymbol{\xi}.\nabla)\left(\frac{1}{h_1}\frac{\partial p_0}{\partial x}\right)\right]\mathbf{e}_x+\frac{1}{h_1}\frac{\partial p_0}{\partial x}\left[(\boldsymbol{\xi}.\nabla)\mathbf{e}_x\right]\ , \qquad \text{(D.7)}$$

although it is worth noting that

$$\begin{aligned}\nabla p_0 &= -\rho_0\nabla V_0\ , \qquad \text{(D.8)}\\ \Rightarrow\ (\boldsymbol{\xi}.\nabla)\nabla p_0+\rho_0(\boldsymbol{\xi}.\nabla)\nabla V_0 &= \nabla V_0(\boldsymbol{\xi}.\nabla)\rho_0\\ &= \frac{\xi_x}{h_1^2}\frac{\partial V_0}{\partial x}\frac{\partial \rho_0}{\partial x}\mathbf{e}_x\ , \qquad \text{(D.9)}\end{aligned}$$

which may prove to be an easier form. Note that

$$\begin{aligned}\nabla\left[(1-\gamma_1)p_0\nabla.\boldsymbol{\xi}\right]-p_0\nabla(\nabla.\boldsymbol{\xi}) &= -\gamma_1 p_0\nabla(\nabla.\boldsymbol{\xi})\\ +(\nabla\cdot\boldsymbol{\xi})\frac{1}{h_1}\mathbf{e}_x&\left((1-\gamma_1)\frac{\partial p_0}{\partial x}-p_0\frac{\partial \gamma_1}{\partial x}\right)\ , \qquad \text{(D.10)}\end{aligned}$$

and also

Perturbations to the Pulsational Operators in terms of the metric coefficients

$$\nabla \cdot \boldsymbol{\xi} = \frac{1}{h_1 h_2 h_3}\left[\frac{\partial}{\partial x}\left(h_2 h_3 \xi_x\right) + \frac{\partial}{\partial \eta}\left(h_1 h_3 \xi_\eta\right)\right] + \frac{\mathrm{i}m\xi_\phi}{h_3}\ , \quad \text{(D.11)}$$

with the predictable formula for $\nabla(\nabla \cdot \boldsymbol{\xi})$:

$$\begin{aligned}
\nabla(\nabla \cdot \boldsymbol{\xi}) &= \frac{1}{h_1}\mathbf{e}_x \frac{\partial}{\partial x}\left(\frac{\mathrm{i}m\xi_\phi}{h_3}\right. \\
&+ \frac{1}{h_1 h_2 h_3}\left[\frac{\partial}{\partial x}\left(h_2 h_3 \xi_x\right) + \frac{\partial}{\partial \eta}\left(h_1 h_3 \xi_\eta\right)\right]\Bigg) \\
&+ \frac{1}{h_2}\mathbf{e}_\eta \frac{\partial}{\partial \eta}\left(\frac{\mathrm{i}m\xi_\phi}{h_3}\right. \\
&+ \frac{1}{h_1 h_2 h_3}\left[\frac{\partial}{\partial x}\left(h_2 h_3 \xi_x\right) + \frac{\partial}{\partial \eta}\left(h_1 h_3 \xi_\eta\right)\right]\Bigg) \\
&+ \frac{\mathrm{i}m}{h_3}\mathbf{e}_\phi\left(\frac{\mathrm{i}m\xi_\phi}{h_3}\right. \\
&+ \frac{1}{h_1 h_2 h_3}\left[\frac{\partial}{\partial x}\left(h_2 h_3 \xi_x\right) + \frac{\partial}{\partial \eta}\left(h_1 h_3 \xi_\eta\right)\right]\Bigg)\ . \quad \text{(D.12)}
\end{aligned}$$

Thus

$$\begin{aligned}
\mathbf{C}.(\boldsymbol{\xi}) &= \mathbf{e}_x \frac{1}{h_1}\Bigg\{ - \frac{\partial}{\partial x}\left(\frac{\xi_x}{h_1}\frac{\partial p_0}{\partial x}\right) - \gamma_1 p_0 \frac{\partial}{\partial x}\left(\frac{\mathrm{i}m\xi_\phi}{h_3}\right. \\
&+ \frac{1}{h_1 h_2 h_3}\left[\frac{\partial}{\partial x}\left(h_2 h_3 \xi_x\right) + \frac{\partial}{\partial \eta}\left(h_1 h_3 \xi_\eta\right)\right]\Bigg) \\
&+ \frac{\xi_x}{h_1}\frac{\partial V_0}{\partial x}\frac{\partial \rho_0}{\partial x} + \left((1-\gamma_1)\frac{\partial p_0}{\partial x} - p_0 \frac{\partial \gamma_1}{\partial x}\right) \times \left(\frac{\mathrm{i}m\xi_\phi}{h_3}\right. \\
&+ \frac{1}{h_1 h_2 h_3}\left[\frac{\partial}{\partial x}\left(h_2 h_3 \xi_x\right) + \frac{\partial}{\partial \eta}\left(h_1 h_3 \xi_\eta\right)\right]\Bigg)\Bigg\}
\end{aligned}$$

$$
\begin{aligned}
&+\mathbf{e}_\eta \frac{1}{h_2}\Bigg\{ -\frac{\partial}{\partial\eta}\left(\frac{\xi_x}{h_1}\frac{\partial p_0}{\partial x}\right) - \gamma_1 p_0 \frac{\partial}{\partial\eta}\Bigg(\frac{\mathrm{i}m\xi_\phi}{h_3} \\
&+\frac{1}{h_1h_2h_3}\left[\frac{\partial}{\partial x}\left(h_2h_3\xi_x\right)+\frac{\partial}{\partial\eta}\left(h_1h_3\xi_\eta\right)\right]\Bigg)\Bigg\} \\
&+\mathbf{e}_\phi \frac{\mathrm{i}m}{h_3}\Bigg\{ -\frac{\xi_x}{h_1}\frac{\partial p_0}{\partial x} - \gamma_1 p_0\Bigg(\frac{\mathrm{i}m\xi_\phi}{h_3} \\
&+\frac{1}{h_1h_2h_3}\left[\frac{\partial}{\partial x}\left(h_2h_3\xi_x\right)+\frac{\partial}{\partial\eta}\left(h_1h_3\xi_\eta\right)\right]\Bigg)\Bigg\} . \qquad \text{(D.13)}
\end{aligned}
$$

It is into this formula that the metric coefficients

$$
\begin{aligned}
h_1 \;=1+f^2\sum_{l\geq 0} P_{2l}\left(x\lambda_{l,1}\right)' + f^4\Bigg[\sum_{l\geq 0} P_{2l}\left(x\lambda_{l,2}\right)' \\
+\sum_{l,m\,\geq 0}\left(3P_{2l}P_{2m}\left(x\lambda_{l,1}\right)'\left(x\lambda_{m,1}\right)'\right. \\
\left.-(1-\eta^2)P'_{2l}P'_{2m}\lambda_{l,1}\lambda_{m,1}\right)\Bigg] , \qquad \text{(D.14)}
\end{aligned}
$$

$$
\begin{aligned}
h_2 \;=\frac{x}{\sqrt{1-\eta^2}}\Bigg\{1 \\
+f^2\sum_{l\,\geq 0}\left((P_1P_{2l})'t_{l,1}+P_{2l}\left(\lambda_{l,1}+\frac{\eta^2 t_{l,1}}{1-\eta^2}\right)\right) \\
+f^4\Bigg[\sum_{l\,\geq 0}\left((P_1P_{2l})'t_{l,2}+P_{2l}\left(\lambda_{l,2}+\frac{\eta^2 t_{l,2}}{1-\eta^2}\right)\right) \\
+\sum_{l,m\,\geq 0}\Big(P_{2l}(P_1P_{2m})'\lambda_{l,1}t_{m,1}-3(1-\eta^2)P'_{2l}P'_{2m}\lambda_{l,1}\lambda_{m,1} \\
+2P_{2l}P_{2m}\left(x\lambda_{l,1}\right)'\left(x\lambda_{m,1}\right)'
\end{aligned}
$$

$$+\frac{\eta^2 t_{l,1}t_{m,1}}{1-\eta^2}\left(P_{2l}(P_1P_{2m})' + P_{2l}P_{2m}\right)\Big]\Big\}\ , \quad \text{(D.15)}$$

$$\begin{aligned} h_3 \ = x\sqrt{1-\eta^2}\Bigg(1 &+ f^2\sum_{l\geq 0} P_{2l}\left(\lambda_{l,1} - \frac{\eta^2 t_{l,1}}{1-\eta^2}\right) \\ &+ f^4\sum_{l\geq 0} P_{2l}\left(\lambda_{l,2} - \frac{\eta^2 t_{l,2}}{1-\eta^2}\right) \\ + f^4\sum_{l,m\geq 0}\frac{\eta^2 t_{l,1}}{1-\eta^2}P_{2l}P_{2m}&\left(\lambda_{m,1} - \frac{t_{m,1}}{1-\eta^2}\right)\Bigg)\ , \end{aligned} \quad \text{(D.16)}$$

are inserted to obtain $\delta\boldsymbol{C}$ and $\delta_2\boldsymbol{C}$.

To obtain $\delta\boldsymbol{B}_{\rm TA}$ and $\delta_2\boldsymbol{B}_{\rm TA}$, recall from appendix B that

$$\mathbf{B}_{\rm TA} \ = \mathrm{i}\omega\nu\rho_0\hat{\mathbf{\Omega}}.\mathbf{e}_\eta\begin{pmatrix} 0 & 0 & 0 \\ 0 & 0 & -1 \\ 0 & 1 & 0 \end{pmatrix}\ . \quad \text{(D.17)}$$

Using the procedure outlined in chapter 3, we can obtain

$$\begin{aligned} \hat{\mathbf{\Omega}}.\mathbf{e}_\eta \ = \sqrt{1-\eta^2}\Bigg[&-1 + f^2\sum_{l\geq 0}\left(\lambda_{l,1}\eta P'_{2l} + \frac{\eta^2 t_{l,1}}{1-\eta^2}P_{2l}\right) \\ &+ f^4\sum_{l\geq 0}\left(\lambda_{l,2}\eta P'_{2l} + \frac{\eta^2 t_{l,2}}{1-\eta^2}P_{2l}\right) \\ + f^4\sum_{l,m\geq 0}\Bigg(&2(1-\eta^2)P'_{2l}P'_{2m}\lambda_{l,1}\lambda_{m,1} + \frac{\eta^2 t_{l,1}t_{m,1}}{(1-\eta^2)^2}P_{2l}P_{2m} \\ &+\frac{\eta^2 t_{l,1}}{1-\eta^2}P_{2l}P_{2m}(x\lambda_{m,1})' - 3P_{2l}P_{2m}(x\lambda_{l,1})'(x\lambda_{m,1})' \end{aligned}$$

$$-\lambda_{l,1}\eta P'_{2l}\left(\left(\lambda_{m,1}P_{2m}+\frac{\eta^2 t_{m,1}}{1-\eta^2}P_{2m}\right)+t_{m,1}\eta P'_{2m}\right)\Bigg)\Bigg]\,, \quad \text{(D.18)}$$

from which equations ((D.17) and (D.18)) $\delta\boldsymbol{B}_{\rm TA}$ and $\delta_2\boldsymbol{B}_{\rm TA}$ are straightforwardly constructed.

Appendix E

Searching for Eigenvalues and Eigenfunctions

Throughout the thesis, solutions have been found to coupled first-order differential equations, satisfying suitable boundary conditions. This was done by relaxation, adapting a code called NRK, provided by D. O. Gough, to calculate successive frequencies and eigenfunctions of a oscillating string. As this is the only code that has not written from scratch by the author, and relaxation can be misunderstood, both the method of relaxation, and the algorithm for searching for trial solutions will be expanded upon in this appendix.

E.1 Relaxation

Many systems of equations, including all those described in this thesis, can be reduced into a system of coupled first order equations. Writing the variables that are functions of the independent variable[1] as a single vector $\mathbf{y}(x)$ and denoting the N eigenvalues as λ_i, this system of coupled first order equations can be written in vector form as

$$\frac{\partial}{\partial x}\mathbf{D}(\mathbf{y}, \lambda_1, ..., \lambda_N) + \mathbf{F}(\mathbf{y}, \lambda_1, ..., \lambda_N) = 0 \ , \qquad \text{(E.1)}$$

[1]The independent variable can be x or η, but we shall denote by x in this appendix. Due to our scaling of the "radial" coordinate, both x and η vary over $[0, 1]$.

with $\mathbf{D}$ and $\mathbf{F}$ being vectors of dimension M. Physically our system will also be subject to constraints, which in this thesis take the form of boundary conditions. As mentioned in chapter 2, the differential equations are represented by finite difference equations upon a mesh $(x_1, ..., x_I)$ of the independent variable, with second-order accuracy centred differences used to represent derivatives, and the differential equations represented midway between the mesh points; this representation, defining

$$\mathbf{y}_{i+1} \equiv \mathbf{y}(x_{i+1}) \tag{E.2}$$

gives

$$\frac{\mathbf{D}(\mathbf{y}_{i+1}, \lambda_1, ..., \lambda_N) - \mathbf{D}(\mathbf{y}_i, \lambda_1 ... \lambda_N)}{x_{i+1} - x_i} + \frac{1}{2}\left(\mathbf{F}(\mathbf{y}_{i+1}, \lambda_1, ..., \lambda_N) - \mathbf{F}(\mathbf{y}_i, \lambda_1, ..., \lambda_N)\right) = 0 \ , \tag{E.3}$$

subject to boundary conditions at the inner and outer mesh points of the model

$$\mathbf{G}(\mathbf{y}_1, \lambda_1, ..., \lambda_N) = 0 \ , \tag{E.4}$$

$$\mathbf{H}(\mathbf{y}_I, \lambda_1, ..., \lambda_N) = 0 \ . \tag{E.5}$$

Motivated by this representation of the system by FDEs, we can define, for any trial solution, $\mathbf{y}^{(t)}$, an "error" vector $\boldsymbol{E}_i$, at the mesh point x_i, by

$$\boldsymbol{E}_i(\mathbf{y}^{(t)}, \lambda_1, ..., \lambda_N) = \frac{\mathbf{D}(\mathbf{y}^{(t)}_{i+1}, \lambda_1, ..., \lambda_N) - \mathbf{D}(\mathbf{y}^{(t)}_i, \lambda_1 ... \lambda_N)}{x_{i+1} - x_i} + \frac{1}{2}\left(\mathbf{F}(\mathbf{y}^{(t)}_{i+1}, \lambda_1, ..., \lambda_N) - \mathbf{F}(\mathbf{y}^{(t)}_i, \lambda_1, ..., \lambda_N)\right) \ . \tag{E.6}$$

for $1 \geq i \geq I-1$, and

$$\boldsymbol{E}_0(\mathbf{y}^{(t)}, \lambda_1, ..., \lambda_N) = \mathbf{G}(\mathbf{y}_1^{(t)}, \lambda_1, ..., \lambda_N) \ , \tag{E.7}$$

$$\boldsymbol{E}_I(\mathbf{y}^{(t)}, \lambda_1, ..., \lambda_N) = \mathbf{H}(\mathbf{y}_I^{(t)}, \lambda_1, ..., \lambda_N) \ . \tag{E.8}$$

This, having defined[2]

$$\mathbf{E}_{\mathrm{T}} \equiv \begin{pmatrix} \boldsymbol{E}_0 \\ \boldsymbol{E}_1 \\ \vdots \\ \boldsymbol{E}_I \end{pmatrix} \ , \tag{E.9}$$

$$\mathbf{Y} \equiv \begin{pmatrix} \mathbf{y}_1 \\ \vdots \\ \mathbf{y}_I \\ \lambda_1 \\ \vdots \\ \lambda_N \end{pmatrix} \ , \tag{E.10}$$

this notation causes us to rewrite our system of equations as

$$\mathbf{E}_{\mathrm{T}}(\mathbf{Y}) = \mathbf{0} \ . \tag{E.11}$$

Were we to consider a trial solution, $\mathbf{Y}^{(t)}$ in equation (E.11), then a Taylor series would give

[2]It is worth briefly examining the dimensions of many of these matrices thus defined. For a system of M coupled first order equations (for the system in chapter 2, $M = 4$), $\dim(\boldsymbol{E}_i)=M$ gives $\dim(\mathbf{E})=M(I-1)+\dim(\boldsymbol{E}_0)+\dim(\boldsymbol{E}_I)$. $\dim(\mathbf{y}_i)=M$, giving $\dim(\mathbf{Y})=MI+N$. Thus for the system to not be over-determined, we require $\dim(\boldsymbol{E}_0)+\dim(\boldsymbol{E}_I)=M+N$.

$$\mathbf{E}_\alpha(\mathbf{y}^{(t)} + \delta\mathbf{Y}^{(t)}) = \mathbf{E}_\alpha(\mathbf{Y}^{(t)}) + \sum_\beta \frac{\partial \mathbf{E}_\alpha}{\partial Y_\beta}\delta Y_\beta^{(t)} + \ldots . \qquad \text{(E.12)}$$

For notational convenience, we shall define the matrix

$$S_{\alpha,\beta} \equiv \frac{\partial \mathbf{E}_\alpha}{\partial Y_\beta} . \qquad \text{(E.13)}$$

Equation E.12 suggests a "corrected" trial solution given by the equation

$$Y_\beta^{(t+1)} = Y_\beta^{(t)} - \sum_\alpha [S_{\alpha,\beta}]^{-1}\,\mathbf{E}_\alpha . \qquad \text{(E.14)}$$

If the initial trial solution is close to a true solution of equation (E.11), then this "corrected" trial solution will be closer still, providing a way to iterate (with extremely rapid convergence) until a fit closer[3] than a pre-selected cutoff value is reached, provided that the function derivative matrices, $S_{\alpha,\beta}$, are known. These are derived analytically for the problems considered in this thesis.

E.2 Obtaining a good trial solution

The method given in the previous section works well once initial trial solutions close to a true solution are provided; to obtain these "good" initial solutions, a method similar to shooting is employed. The outer boundary conditions are "relaxed" with only $\dim(\boldsymbol{E}_I)-j$ $(j \leq N)$ being used; a trial solution using guesses of λ_n $(N - j \leq n \leq N)$ is integrated outwards, and the value of $\mathbf{y}_I$ recorded. If the outer boundary conditions are nearly met,

[3] In NRK, the fit is judged by the absolute value of the relative corrections to the trial function.

then the solution is placed into the relaxation code with the full boundary conditions.

As a judge of the boundary conditions being "nearly met", after a given calculation of $\mathbf{y}_I$ for guesses of λ_n, guesses of λ_n are advanced a step, and the relaxed integration repeated, with the new value of $\mathbf{y}_I$ being compared to the previous one. If the sign of the relaxed parts of $\boldsymbol{E}_m$ changes, the trial solution is close to a true solution of the full problem.[4]

One issue that may arise is that of choice of step size for the advancement of the λ_n. This is especially important for higher-order g-modes, as the spectrum of eigenfrequencies becomes more dense with increasing radial order. Thus we might have a concern that our predicted spectrum of eigenfrequencies is incomplete. There are two things that we can do to address this concern; the first is to make the advancement dependent upon the previous frequency, and the second is to take account of the radial orders of the eigenfunctions found by our search, which allows for an easy check of the completeness of our predicted spectrum.

[4]The easiest example of this is for the problem of the oscillating string, where the outer boundary condition is that $y_I = 0$, so we look for when y_I changes sign between guesses. For the pulsational problem, the sign of the fractional Lagrangian pressure perturbation is employed to judge between the successive $\mathbf{y}_I$.

Bibliography

Abramowitz, M. and Stegun, I. A. (1972). *Handbook of Mathematical Functions.* Dover.

Abt, H. A., Bollinger, G., and Burke, E. W. (1983). HD 164615 - A probable spotted single F type star. *ApJ*, 272:196–201.

Acheson, D. J. (1990). *Elementary Fluid Dynamics.* Oxford University Press.

Aerts, C., Cuypers, J., De Cat, P., Dupret, M. A., De Ridder, J., Eyer, L., Scuflaire, R., and Waelkens, C. (2004). Long-term multicolour photometry and high-resolution spectroscopy of the two γ Doradus stars HD 12901 and HD 48501. *AAP*, 415:1079–1088.

Anand, S. P. S. (1968). The Equilibrium Structure of Rapidly Rotating Gaseous Polytropes and Completely Degenerate Systems. *ApJ*, 153:135.

Baglin, A., Auvergne, M., Catala, C., Michel, E., and COROT Team (2001). Asteroseismology with the space mission COROT: photometric performances targets and mission profile. In *ESA SP-464: SOHO 10/GONG 2000 Workshop: Helio- and Asteroseismology at the Dawn of the Millennium*, page 395.

Balona, L. A., Bohm, T., Foing, B. H., Ghosh, K. K., Janot-Pacheco, E., Krisciunas, K., Lagrange, A.-M., Lawson, W. A., James, S. D., Baudrand, J., Catala, C., Dreux, M., Felenbok,

P., and Hearnshaw, J. B. (1996). Line profile variations in gamma Doradus. *MNRAS*, 281:1315–1325.

Balona, L. A., Hearnshaw, J. B., Koen, C., Collier, A., Machi, I., Mkhosi, M., and Steenberg, C. (1994a). Photometry and Line Profile Variations of the Peculiar Variable Gamma-Doradus. *MNRAS*, 267:103.

Balona, L. A., Krisciunas, K., and Cousins, A. W. J. (1994b). Gamma-Doradus - Evidence for a New Class of Pulsating Star. *MNRAS*, 270:905.

Berthomieu, G., Gonczi, G., Graff, P., Provost, J., and Rocca, A. (1978). Low-frequency Gravity Modes of a Rotating Star. *AAP*, 70:597.

Bildsten, L., Cumming, A., Ushomirsky, G., and Cutler, C. (1998). Oceanography of Accreting Neutron Stars: Nonradial Oscillations and Periodic X-ray Variability. In *A Half Century of Stellar Pulsation Interpretation: A Tribute to Arthur N. Cox, edited by Paul A. Bradley and Joyce A. Guzik, Proceedings of a Conference held in Los Alamos, NM 16-20 June 1997, ASP Conference Series #135, p. 437.*, page 437.

Bildsten, L., Ushomirsky, G., and Cutler, C. (1996). Ocean g-Modes on Rotating Neutron Stars. *ApJ*, 460:827.

Billéres, M., Fontaine, G., Brassard, P., Charpinet, S., Liebert, J., and Saffer, R. A. (2000). Detection of p-Mode Pulsations and Possible Ellipsoidal Luminosity Variations in the Hot Subdwarf B Star KPD 1930+2752. *ApJ*, 530:441–453.

Brassard, P., Fontaine, G., Billères, M., Charpinet, S., Liebert, J., and Saffer, R. A. (2001). Discovery and Asteroseismological Analysis of the Pulsating sdB Star PG 0014+067. *ApJ*, 563:1013–1030.

BIBLIOGRAPHY

Breger, M., Handler, G., Garrido, R., Audard, N., Beichbuchner, F., Zima, W., Paparo, M., Li, Z.-P., Jiang, S.-Y., Liu, Z.-L., Zhou, A.-Y., Pikall, H., Stankov, A., Guzik, J. A., Sperl, M., Krzesinski, J., Ogloza, W., Pajdosz, G., Zola, S., Serkowitsch, E., Reegen, P., Rumpf, T., and Schmalwieser, A. (1997). The variability of a newly discovered γ-Doradus star, HD 108100. *AAP*, 324:566–572.

Bruntt, H., Catala, C., Garrido, R., Rodríguez, E., Stütz, C., Knoglinger, P., Mittermayer, P., Bouret, J., Hua, T., Lignières, F., Charpinet, S., Van't Veer-Menneret, C., and Ballereau, D. (2002). Abundance analysis of targets for the COROT / MONS asteroseismology missions. I. Semi-automatic abundance analysis of the gamma Dor star HD 49434. *AAP*, 389:345–354.

Bryan, G. H. (1899). The Waves on a Rotating Liquid Spheroid of Finite Ellipticity. *Proceedings of the Physical Society of London. A*, 180:187–219.

Chandrasekhar, S. and Lebovitz, N. R. (1962). On the Oscillations and the Stability of Rotating Gaseous Masses. III. The Distorted Polytropes. *ApJ*, 136:1082.

Chapman, S. and Lindzen, R. (1970). *Atmospheric tides. Thermal and gravitational.* Dordrecht: Reidel, 1970.

Charbonneau, P. (1995). Genetic Algorithms in Astronomy and Astrophysics. *ApJs*, 101:309.

Charbonneau, P., Christensen-Dalsgaard, J., Henning, R., Larsen, R. M., Schou, J., Thompson, M. J., and Tomczyk, S. (1999). Helioseismic Constraints on the Structure of the Solar Tachocline. *ApJ*, 527:445–460.

BIBLIOGRAPHY

Charbonneau, P., Tomczyk, S., Schou, J., and Thompson, M. J. (1998). The rotation of the solar core inferred by genetic forward modeling. *ApJ*, 496:1015+.

Christensen-Dalsgaard, J. (1982). On solar models and their periods of oscillation. *MNRAS*, 199:735–761.

Christensen-Dalsgaard, J. (1993). On the asteroseismic hr diagram. In *ASP Conf. Ser. 42: GONG 1992. Seismic Investigation of the Sun and Stars*, pages 347+.

Christensen-Dalsgaard, J. (1998). Probing stellar interiors with mons. In *The First MONS Workshop: Science with a Small Space Telescope, held in Aarhus, Denmark, June 29 - 30, 1998, Eds.: H. Kjeldsen, T.R. Bedding, Aarhus Universitet, p. 17.*, pages 17+.

Christensen-Dalsgaard, J. (2003). Lecture notes on stellar oscillations.

Christensen-Dalsgaard, J., Däppen, W., Ajukov, S. V., Anderson, E. R., Antia, H. M., Basu, S., Baturin, V. A., Berthomieu, G. Chaboyer, B., Chitre, S. M., Cox, A. N., Demarque, P., Donatowicz, J., Dziembowski, W. A., Gabriel, M., Gough, D. O., Guenther, D. B., Guzik, J. A., Harvey, J. W., Hill, F., Houdek, G., Iglesias, C. A., Kosovichev, A. G., Leibacher, J. W., Morel, P., Proffitt, C. R., Provost, J., Reiter, J., Rhodes Jr., E. J., Rogers, F. J., Roxburgh, I. W., Thompson, M. J., and Ulrich, R. K. (1996). The current state of solar modeling. *Science*, 272:1286–1292.

Christensen-Dalsgaard, J. and Mullan, D. J. (1994). Accurate frequencies of polytropic models. *MNRAS*, 270:921+.

BIBLIOGRAPHY

Christensen-Dalsgaard, J. and Thompson, M. J. (1999). A note on Saio's estimate of second-order effects of rotation on stellar oscillation frequencies. *AAP*, 350:852–854.

Collier Cameron, A., Donati, J.-F., and Semel, M. (2002). Stellar differential rotation from direct star-spot tracking. *MNRAS*, 330:699–706.

Cousins, A. W. J. (1992). Gamma Doradus. *The Observatory*, 112:53–56.

Cowling, T. G. (1941). The non-radial oscillations of polytropic stars. *MNRAS*, 101:367+.

Dintrans, B. and Rieutord, M. (2000). Oscillations of a rotating star: a non-perturbative theory. *AAP*, 354:86–98.

Dreizler, S., Koester, D., and Heber, U. (2000). Time-Resolved Spectroscopy of BPM 37093 and PG 1336-018. *Baltic Astronomy*, 9:113–118.

Dyson, J. and Schutz, B. F. (1979). Perturbations and stability of rotating stars. I - Completeness of normal modes. *Royal Society of London Proceedings Series A*, 368:389–410.

Dzhalilov, N. S. and Staude, J. (2004). Eigenoscillations of the differentially rotating Sun. II. Generalization of the Laplace tidal equation. *AAP*, 421:305–322.

Dziembowski, W. A. (1971). Nonradial oscillations of evolved stars. I. Quasiadiabatic approximation. *Acta Astronomica*, 21:289–306.

Dziembowski, W. A. and Goode, P. R. (1992). Effects of differential rotation on stellar oscillations - a second-order theory. *ApJ*, 394:670–687.

BIBLIOGRAPHY

Eckart, C. (1960). *Hydrodynamics of Oceans and Atmosphere.* Pergamon.

Eggleton, P. P. (1971). The evolution of low mass stars. *MNRAS*, 151:351+.

Eldridge, J. J. and Tout, C. A. (2004). A more detailed look at the opacities for enriched carbon and oxygen mixtures. *MNRAS*, 348:201–206.

Eyer, L. and Aerts, C. (2000). A search for new gamma Doradus stars in the Geneva photometric database. *AAP*, 361:201–206.

Gough, D., Merryfield, W. J., and Toomre, J. (1998). Phase Inversion: Inferring Solar Subphotospheric Flow and Other Asphericity from the Distortion of Acoustic Waves. *ApJ*, 501:882.

Gough, D. O. (1993). Course 7. linear adiabatic stellar pulsation. In Zahn, J. P. and Zinn-Justin, J., editors, *Astrophyscial fluid dynamics, Les Houches Session XLVII*, pages 399–560. Elsevier.

Gough, D. O. (1996). Astereoasteroseismology. *The Observatory*, 116:313–315.

Gough, D. O., Spiegel, E. A., and Toomre, J. (1975). Highly stretched meshes as functionals of solutions. *Lecture Notes in Physics, Berlin Springer Verlag*, 35:191–196.

Gough, D. O. and Thompson, M. J. (1990). The effect of rotation and a buried magnetic field on stellar oscillations. *MNRAS*, 242:25–55.

Goupil, M. J., Samadi, R., Lochard, J., Dziembowski, W. A., and Pamyatnykh, A. (2004). Inferring information about rotation

from stellar oscillations. In *Second Eddington Workshop: Stellar structure and habitable planet finding, 9 - 11 April 2003, Palermo, Italy. Edited by F. Favata, S. Aigrain and A. Wilson. ESA SP-538, Noordwijk: ESA Publications Division, ISBN 92-9092-848-4, 2004, p. 133 - 140*, page 133.

Gradshteyn, I. S. and Ryzhik, I. M. (1994). *Table of Integrals, Series, and Products.* Academic Press, fifth edition.

Gray, R. O. and Kaye, A. B. (1999). HR 8799: A Link between γ-Doradus Variables and λ-Bootis Stars. *AJ*, 118:2993–2996.

Guzik, J. A., Kaye, A. B., Bradley, P. A., Cox, A. N., and Neuforge, C. (2000). Driving the Gravity-Mode Pulsations in γ Doradus Variables. *ApJl*, 542:L57–L60.

Handler, G. (1999). The domain of γ-Doradus variables in the H-R diagram. *MNRAS*, 309:L19–L23.

Handler, G., Balona, L., Shobbrook, R., Koen, C., Bruch, A., Romero-Colmenero, E., Pamyatnykh, A., Willems, B., Eyer, L., James, D., Maas, T., and Crause, L. (2002). Asteroseismology and Forced Oscillations of the Simultaneous p-Mode and g-Mode Pulsator HD 209295. In *ASP Conf. Ser. 259: IAU Colloq. 185: Radial and Nonradial Pulsationsn as Probes of Stellar Physics*, page 90.

Handler, G. and Shobbrook, R. R. (2002). On the relationship between the δ-Scuti and γ-Doradus pulsators. *MNRAS*, 333:251–262.

Hatzes, A. P. (1998). Spectral line profile variations in the gamma Doradus variable HD 164615: non-radial pulsations versus starspots. *MNRAS*, 299:403–409.

BIBLIOGRAPHY

Henry, G. W. and Fekel, F. C. (2003). A Dozen New γ Doradus Stars. *AJ*, 126:3058–3075.

Henry, G. W., Fekel, F. C., Kaye, A. B., and Kaul, A. (2001). 10 New γ Doradus and δ Scuti Stars. *AJ*, 122:3383–3395.

James, R. A. (1964). The Structure and Stability of Rotating Gas Masses. *ApJ*, 140:552.

Kaye, A. B., Henry, G. W., Fekel, F. C., Gray, R. O., Rodríguez, E., Martín, S., Gies, D. R., Bagnuolo, W. G., and Hall, D. S. (1999). HD 62454 and HD 68192: Two New γ-Doradus Variables. *AJ*, 118:2997–3005.

Kaye, A. B. and Strassmeier, K. G. (1998). CA II H&K survey of Gamma Doradus candidates. *MNRAS*, 294:L35–L39.

Kennelly, E. J., Walker, G. A. H., Catala, C., Foing, B. H., Huang, L., Jiang, S., Hao, J., Zhai, D., Zhao, F., Neff, J. E., Houdebine, E. R., Ghosh, K. K., and Charbonneau, P. (1996). The oscillation modes of θ^2^ Tauri. Results from the 1992 MUSICOS campaign. *AAP*, 313:571–580.

Kepler, S. O., Nather, R. E., Winget, D. E., Nitta, A., Kleinman, S. J., Metcalfe, T., Sekiguchi, K., Xiaojun, J., Sullivan, D., Sullivan, T., Janulis, R., Meistas, E., Kalytis, R., Krzesinski, J., Ogoza, W., Zola, S., O'Donoghue, D., Romero-Colmenero, E., Martinez, P., Dreizler, S., Deetjen, J., Nagel, T., Schuh, S. L., Vauclair, G., Ning, F., Chevreton, M., Solheim, J.-E., Gonzalez Perez, J. M., Johannessen, F., Kanaan, A., Costa, J. E., Murillo Costa, A. F., Wood, M. A., Silvestri, N., Ahrens, T. J., Jones, A. K., Collins, A. E., Boyer, M., Shaw, J. S., Mukadam, A., Klumpe, E. W., Larrison, J., Kawaler, S., Riddle, R., Ulla, A., and Bradley, P. (2003). The everchanging pulsating white dwarf GD358. *AAP*, 401:639–654.

BIBLIOGRAPHY

Krisciunas, K., Aspin, C., Geballe, T. R., Akazawa, H., Claver, C. F., Guinan, E. F., Landis, H. J., Luedeke, K. D., Ohkura, N., Ohshima, O., and Skillman, D. R. (1993). The 9-AURIGAE System. *MNRAS*, 263:781.

Kueker, M. and Ruediger, G. (2004). Differential rotation of main sequence F stars. *ArXiv Astrophysics e-prints*.

Lamb, H. (1932). *Hydrodynamics*. Hydrodynamics, New York: Dover, 1932.

Lee, U. and Saio, H. (1987). Low-frequency oscillations of uniformly rotating stars. *MNRAS*, 224:513–526.

Lee, U. and Saio, H. (1997). Low-Frequency Nonradial Oscillations in Rotating Stars. I. Angular Dependence. *ApJ*, 491:839.

Lignières, F., Rieutord, M., and Valdettaro, L. (2001). Acoustic modes in spheroidal cavities. In *SF2A-2001: Semaine de l'Astrophysique Francaise*, page 127.

Lynden-Bell, D. and Ostriker, J. P. (1967). On the stability of differentially rotating bodies. *MNRAS*, 136:293.

Maniopoulou, A. and Andersson, N. (2004). The traditional approximation in general relativity. *MNRAS*, 351:1349–1358.

Mantegazza, L., Poretti, E., and Zerbi, F. M. (1994). Unusual Variability among Early F-Type Stars - HD224638 and HD224945. *MNRAS*, 270:439.

Mathias, P., Le Contel, J.-M., Chapellier, E., Jankov, S., Sareyan, J.-P., Poretti, E., Garrido, R., Rodríguez, E., Arellano Ferro, A., Alvarez, M., Parrao, L., Peña, J., Eyer, L., Aerts, C., De Cat, P., Weiss, W. W., and Zhou, A. (2004). Multi-site, multi-technique survey of γ Doradus candidates. I. Spectroscopic results for 59 stars. *AAP*, 417:189–199.

BIBLIOGRAPHY

Metcalfe, T. S. (2003). Seismic Inference using Genetic Algorithms. *APSS*, 284:141–151.

Metcalfe, T. S., Brown, T. M., and Christensen-Dalsgaard, J. (2004a). Asteroseismology of Sun-like Stars - A Proposal. *ArXiv Astrophysics e-prints.*

Metcalfe, T. S., Montgomery, M. H., and Kanaan, A. (2004b). Testing White Dwarf Crystallization Theory with Asteroseismology of the Massive Pulsating DA Star BPM 37093. *ApJl*, 605:L133–L136.

Metcalfe, T. S. and Nather, R. E. (2000). The Asteroseismology Metacomputer. *Baltic Astronomy*, 9:479–483.

Moya, A., Suarez, J. C., Amado, P. J., Martin-Ruiz, S., and Garrido, R. (2004). Frequency ratio method for seismic modeling of Gamma Doradus stars. *ArXiv Astrophysics e-prints.*

Mullan, D. J. (1989). G-mode pulsations in polytropes - High-precision eigenvalues and the approach to asymptotic behavior. *ApJ*, 337:1017–1022.

Odrzywołek, A. (2003). Analytical approximation for the structure of differentially rotating barotropes. *MNRAS*, 345:497–505.

Papaloizou, J. and Pringle, J. E. (1978). Non-radial oscillations of rotating stars and their relevance to the short-period oscillations of cataclysmic variables. *MNRAS*, 182:423–442.

Pols, O. R., Tout, C. A., Eggleton, P. P., and Han, Z. (1995). Approximate input physics for stellar modelling. *MNRAS*, 274:964–974.

BIBLIOGRAPHY

Poretti, E., Koen, C., Martinez, P., Breuer, F., de Alwis, D., and Haupt, H. (1997). Discovery and analysis of Gamma Doradus type pulsations in the F0 IV star HR 2740 ~ QW PUP. *Delta Scuti Star Newsletter*, 11:5.

Press, W. H., Flannery, B. P., Teukolsky, S. A., and Vetterling, W. T. (1993). *Numerical recipes in Fortran 77*. Cambridge University Press, second edition.

Reiners, A. and Royer, F. (2004). First signatures of strong differential rotation in A-type stars. *AAP*, 415:325–329.

Reiners, A. and Schmitt, J. H. M. M. (2003). Differential rotation in rapidly rotating F-stars. *AAP*, 412:813–819.

Rucinski, S., Carroll, K., Kuschnig, R., Matthews, J. M., and Stibrany, P. (2003). MOST (Microvariability & oscillations of stars) Canadian astronomical micro-satellite. *Advances in Space Research*, 31:371–373.

Rucinski, S. M. (1985). IUE observations of HD 164615. *PASP*, 97:657–659.

Saio, H. (1981). Rotational and tidal perturbations of nonradial oscillations in a polytropic star. *ApJ*, 244:299–315.

Saio, H. (2002). The Effects of Rapid Rotation on Pulsation (invited paper). In *ASP Conf. Ser. 259: IAU Colloq. 185: Radial and Nonradial Pulsationsn as Probes of Stellar Physics*, page 177.

Schuh, S., Dreizler, S., Deetjen, J. L., Heber, U., and Geckeler, R. D. (2000). CCD Photometry of Variable Subdwarfs and White Dwarfs at Calar Alto Observatory. *Baltic Astronomy*, 9:395–402.

BIBLIOGRAPHY

Severino, G., Magrì, M., Oliviero, M., Straus, T., and Jefferies, S. M. (2001). The Solar Intensity-Velocity Cross Spectrum: A Powerful Diagnostic for Helioseismology. *ApJ*, 561:444–449.

Smith, B. L. (1976). Strained co-ordinate methods in rotating stars. I - Polytropes. *APSS*, 43:411–424.

Soufi, F., Goupil, M. J., and Dziembowski, W. A. (1998). Effects of moderate rotation on stellar pulsation. i. third order perturbation formalism. *AAP*, 334:911–924.

Tassoul, J. (2000). *Stellar rotation.* Stellar rotation / Jean-Louis Tassoul. Cambridge ; New York : Cambridge University Press, 2000. (Cambridge astrophysics series ; 36).

Tassoul, M. (1980). Asymptotic approximations for stellar non-radial pulsations. *ApJS*, 43:469–490.

Théado, S. and Vauclair, S. (2003a). On the Coupling between Helium Settling and Rotation-induced Mixing in Stellar Radiative Zones. II. Numerical Approach. *ApJ*, 587:784–794.

Théado, S. and Vauclair, S. (2003b). On the Coupling between Helium Settling and Rotation-induced Mixing in Stellar Radiative Zones. III. Applications to Light Elements in Population I Main-Sequence Stars. *ApJ*, 587:795–805.

Thorne, W. A. (2004). Rotation: Distorted Co-Ordinate Systems and a Generalization of the Traditional Approximation. In *Proceedings of the SOHO 14 / GONG 2004 Workshop (ESA SP-559). "Helio- and Asteroseismology: Towards a Golden Future". 12-16 July, 2004. New Haven, Connecticut, USA. Editor: D. Danesy.*, pages 653+.

Townsend, R. H. D. (1997). Spectroscopic modelling of non-radial pulsation in rotating early-type stars. *MNRAS*, 284:839–858.

BIBLIOGRAPHY

Townsend, R. H. D. (2000). Surface trapping and leakage of low-frequency g modes in rotating early-type stars - II. Global analysis. *MNRAS*, 319:289–304.

Townsend, R. H. D. (2003a). A semi-analytical formula for the light variations due to low-frequency g modes in rotating stars. *MNRAS*, 343:125–136.

Townsend, R. H. D. (2003b). Asymptotic expressions for the angular dependence of low-frequency pulsation modes in rotating stars. *MNRAS*, 340:1020–1030.

Unno, W., Osaki, Y., Ando, H., Saio, H., and Shibahashi, H. (1989). *Nonradial oscillations of stars.* Nonradial oscillations of stars, Tokyo: University of Tokyo Press, 1989, 2nd ed.

Vauclair, S. and Théado, S. (2003). On the Coupling between Helium Settling and Rotation-induced Mixing in Stellar Radiative Zones. I. Analytical Approach. *ApJ*, 587:777–783.

Warner, P. B., Kaye, A. B., and Guzik, J. A. (2003). A Theoretical γ Doradus Instability Strip. *ApJ*, 593:1049–1055.

Zerbi, F. M., Rodríguez, E., Garrido, R., Martín, S., Ferro, A. A., Sareyan, J. P., Krisciunas, K., Akan, M. C., Evren, S., Ibanoğlu, C., Keskin, V., Pekunlu, R., Tunca, Z., Luedeke, K., Paparo, M., Nuspl, J., and Guerrero, G. (1999). The γ-DOR variable HR 8799: results from a multisite campaign. *MNRAS*, 303:275–283.